Advanced Solid Biofuel Production via the Integration of Torrefaction and Densification and its Characterization for the Direct Coal Substitution in Energy Intensive Industries

Peter George Gaudet

Thesis submitted to the
Faculty of Graduate and Postdoctoral Studies
In partial fulfillment of the requirements
For the M.A.Sc. degree in Chemical Engineering

Department of Chemical and Biological Engineering
Faculty of Engineering
University of Ottawa

Abstract

The greatest political, scientific, and engineering challenge of the 21st century is finding a viable solution to limit anthropogenic greenhouse gas emissions (CO_2) to curb the effects of global climate change. All sectors of society need to contribute to alleviate this problem, but industrial operations must play a significant leadership role. Some of these industries include: metallurgy, cement, power, agriculture and forestry. In particular, the iron/steel, cement, and power generation industries use coal on account of its high energy density among solid fuels. Coal combustion yields 720 tonne CO_2/GWh, and produces fine particulates, sulphur and nitrous oxides, along with excess CO_2 contributing to climate change. In comparison, biomass (such as agricultural and forestry residues) has a solid fuel rating of 25-100 tonne CO_2/GWh; therefore, biomass fuels are considered more sustainable since the living biomass consumed CO_2 in the early part of its life cycle. However, biomass has significant industrial shortcomings for its use as fuel at large scale, including low energy content, density, and hydrophobicity relative to coal. In short, biomass fuels cannot be substituted without major infrastructure changes which add economic penalties that industry is currently unwilling to absorb.

Biomass upgrading routes were considered in this thesis. These include densification, torrefaction, and integrated torrefaction and densification (ITD). The first half of the methodology involved converting woody biomass (willow residue and poplar bark), agricultural residue (switchgrass plants), and pulp mill waste via a single pellet/briquette press at different densification temperatures and pressures. The second half of the methodology involved product characterization of each batch of pellets and briquettes. In this work, pellets and briquettes were tested for physical characteristics (density and durability), chemical differences (energy content and hydrophobicity), and transport phenomena characteristics (drying profiles).

First, results showed that extrusion of torrefied biomass at 300°C with an estimated pressure of 10 MPa creates partially formed pellets from agricultural residues. Using the concept of ITD (temperature range 220-325°C and pressure range 40 and 215 MPa), the density was found to be 1000-1250 kg/m^3 for pellets and briquettes. The degree of compression from the loose biomass was on the order of 3-10 which corresponds with theoretical expectations. Material density increased with increasing pressure. The solid yield of pellets and briquettes decreased

with increasing temperature, and results aligned with micro-scale thermogravimetric analysis. The larger ITD briquettes (produced at T = 325°C, P = 40 MPa) were evaluated for calorific value and found to fall in the lignite classification (O/C < 0.4 and H/C < 1.2) on a van Krevelen diagram. The resulting ITD pellets and briquettes were found to have a durability similar to commercial materials (durability > 97%), and to be more hydrophobic (8 wt% moisture absorption compared to 35 wt%). The drying time of ITD materials was faster than commercial torrefied briquettes, with an effective diffusivity of 1.5×10^{-6} m^2/s compared to 7.3×10^{-9} m^2/s likely because of a smaller pore volume in ITD briquettes. Further pilot scale studies would help improve the ITD methodology and make the process more appealing for the replacement of coal fuels.

Résumé

Le plus grand défi politique, scientifique et technique commun du XXIe siècle consiste à trouver un moyen de limiter les émissions anthropiques de gaz à effet de serre (CO_2) afin de limiter les effets des changements climatiques. Diverses solutions sont proposées dans différents domaines, mais les activités industrielles doivent jouer un rôle de premier plan. Quelques-unes de ces industries incluent les secteurs de la métallurgie, du ciment, de l'électricité, de l'agriculture et de la foresterie. En particulier, les industries du fer et de l'acier, du ciment et de la production d'énergie utilisent le charbon, en partie grâce à la forte densité énergétique parmi les combustibles solides. Toutefois, la combustion du charbon produit 720 tonnes CO_2/GWh et produit des particules fines, des oxides de soufre et d'azote ainsi qu'un excès de CO_2 contribuant au changement climatique. En comparaison, les combustibles solides provenant de la biomasse (comme les résidus agricoles et forestiers) émettent de 25-100 tonne CO_2/GWh. Par conséquent, les biocarburants sont considérés comme plus durables étant donné que la biomasse vivante consomme du CO2 au début de son cycle de vie. Cependant, l'utilisation de la biomasse comme combustible à grande échelle présente des inconvénients industriels importants, son, notamment pour sa faible teneur en énergie, sa faible densité énergétique et son caractère moins hydrophobe par rapport au charbon. En bref, les biocarburants ne peuvent être remplacés sans des changements d'infrastructure majeurs, ce qui ajoute une pénalité économique que l'industrie ne veut pas absorber pour l'instant.

Certaines voies de valorisation de la biomasse ont été étudiées dans cette thèse, notamment la densification, la torréfaction, et la torréfaction et la densification intégrées (ITD). En premier lieu, la méthodologie consistait à convertir la biomasse ligneuse (résidus de saule et d'écorces de peuplier), les résidus agricoles (plantes de panic érigé) et les résidues d'usines de pâtes et papiers au moyen d'une presse à granulés/briquettes à différentes pressions et températures de densification. En second lieu, la méthodologie considère la caractérisation de chaque lot de granules ou de briquettes. Dans ce travail, les granulés et les briquettes ont été testés pour leurs caractéristiques physiques (densité et durabilité), leurs différences chimiques (teneur en énergie et hydrophobicité) et leurs caractéristiques de transport (profils de séchage).

Premièrement, les résultats montrent que l'extrusion de la biomasse torréfiée à une température de 300°C et une pression de 10 MPa crée des granules partiellement formées à partir de résidus agricoles. Utilisant le concept de l'ITD (plage de température 220-325°C et plage de pression 40 et 215 MPa), la densité était de 1 000 à 1 250 kg/m^3 pour la création des granules et des briquettes dans une plage de pression de 40 à 215 MPa. Le degré de compression de la biomasse était de l'ordre de 3 à 10, ce qui correspond aux attentes théoriques. La densité augmentait avec la pression. Le rendement de masse des granules et des briquettes a diminué avec l'augmentation de la température et les résultats sont corroborés par les analyses thermogravimétriques à petite échelle. Les plus grosses briquettes ITD (produites à T = 325°C, P = 40 MPa) ont été évaluées pour leur valeur calorifique et ont été classées dans la catégorie de la lignite (O / C < 0.4 et H / C < 1.2) sur un diagramme de Van Krevelen. Les granules et les briquettes ITD ainsi produits se sont avérés durables, semblables aux produits commerciaux (durabilité > 97%), et plus hydrophobes (8% d'absorption d'humidité par rapport à 35% en masse). Le séchage des produits ITD est plus rapide que celui des briquettes torréfiées commerciales, avec une diffusivité effective de 1.5×10^{-6} m^2/s par rapport à 7.3×10^{-9} m^2/s, probablement à cause du volume de pores moins importants dans les briquettes ITD. De nouvelles études à l'échelle pilotes permettraient d'explorer plus en profondeur les biocombustibles solides ITD pour le remplacement des combustibles à base de charbon.

Table of Contents

Abstract ii
Résumé iv
Table of Contents vi
List of Figures x
List of Tables xiii
Nomenclature xiv
Acknowledgements xv
Chapter 1. Introduction 1
1.1. Energy Intensive Solid Fuel Usage 2
1.1.1. Iron/Steel Production 2
1.1.2. Cement Production 3
1.1.3. Power Generation 4
1.2. Life Cycle Analysis (LCA) 6
1.2.1. Coal: From Mine to Industry 6
1.2.2. Biomass Sustainability 6
1.3. Biomass Upgrading 8
1.3.1. Physicochemical Properties 9
1.3.2. Thermochemical Conversion 10
1.3.3. Torrefaction 11
1.3.4. Densification 12
1.4. Advanced Solid Biofuel Assessment 14
1.4.1. Product Characterization 15
1.4.1.1. Envelope Density 15
1.4.1.2. Compression Ratio 15
1.4.1.3. Solid Mass Yields 16
1.4.1.4. Durability 16
1.4.1.5. Hydrophobicity 16
1.5. Thesis Objectives 17
1.6. Thesis Outline 19
Chapter 2 20
Abstract 20
2.1. Introduction 21
2.2. Materials and Methods 22
2.2.1. Sample Preparation 23
2.2.1.1. Moisture Content 23
2.2.1.2. Biomass Sieving 23
2.2.1.3. Bulk Density 23
2.2.1.4. Ultimate and Proximate Analysis 24
2.2.1.5. Thermogravimetric Analysis 26
2.2.2. Torrefaction and Densification 27

2.2.3. Pellet and Briquette Formation 28
2.2.4. Durability 29
2.2.5. Hydrophobicity 31
2.2.5.1. Rain Simulation 32
2.2.5.2. Immersion 32
2.2.5.3. Post Weathered Durability 33
2.3. Results 33
2.3.1. Thermogravimetric Analysis 33
2.3.1.1. Non Isothermal: Dry Basis 34
2.3.1.2. Isothermal: Dry Basis 36
2.3.2. Torrefaction and Extrusion 37
2.3.3. Qualitative Densification 38
2.3.3.1. Pelletization 39
2.3.3.2. Briquetting 40
2.3.4. Pelletization and Integrated Torrefaction 41
2.3.4.1. Quantitative Density 42
2.3.4.2. Quantitative Solid Yields 44
2.3.5. Briquetting and Integrated Torrefaction 47
2.3.5.1. Quantitative Densification 48
2.3.5.2. Ultimate/Proximate Analysis 49
2.3.6. Durability Quantification 50
2.3.6.1. Pellet Durability 51
2.3.6.2. Briquette Durability 56
2.3.7. Hydrophobicity Quantification 57
2.3.7.1. Pellet Hydrophobicity 57
2.3.7.2. Briquette Hydrophobicity 64
2.4. Discussion 67
2.4.1. Densification and Moisture Content 67
2.4.2. ITD Process Requirements 68
2.4.3. Macromolecular Cellulose 70
2.5. Conclusions 71
Chapter 3 72
Abstract 72
3.1. Introduction 73
3.2. Materials and Methods 75
3.2.1. Sample Preparation 75
3.2.2. Biofuel Durability 75
3.2.3. Hydrophobicity by Immersion 76
3.2.4. Unsteady State Drying 76
3.2.4.1. Mathematical Models 77
3.3. Results 79
3.3.1. Mechanical Integrity 80

3.3.2. Water Sorptivity 81
3.3.3. Physical Process Changes 83
3.3.4. Feedstock Drying 84
3.3.4.1. Transient Heat Transfer 84
3.3.4.2. Transient Mass Transfer 86
3.4. Discussion 91
3.4.1. Transient Mass Transfer 91
3.4.2. Transient State Heat Transfer 92
3.5. Conclusions 93
Chapter 4. Conclusions and Recommendations 94
4.1. Conclusions 94
4.2. Recommendations 95
Bibliography 96
Appendix A. Calibration Data 105
Appendix B. Protocol Development 105
B.1. Pellet Durability 105
B.2. Briquette Durability 107
B.3. Control Feedstocks 108
B.4. Pellet Hydrophobicity 110
Appendix C. Qualitative Experimental Set-ups 111
C.1. Durability Equipment 111
C.2. Hydrophobicity Equipment 112
C.3. Densification Equipment 113
Appendix D. Sample Raw Data 115
D.1. Material Preparation 115
D.2. Qualitative Densification 117
D.3. Quantitative Compression Ratio 118
D.4. Thermogravimetric Analysis 120
D.5. Transport Phenomena Data 121
Appendix E. Numerical Solutions 124
E.1. VBA Finite Difference Code 126
E.1.1. Nomenclature 126
E.2.1. Subroutine 126
E.2.1.1. Declarations 126
E.2.1.2 Initializations 127
E.3.1. Calculations 127
E.3.1.1. Numerical Stability 127
E.3.1.2. Filling Arrays 127
E.4.1. Finite Differences 128
E.5.1. Print Unsteady State 129
E.5.1.1. Midpoint Method for Numerical Integration 129
E.5.1.2. Cylindrical Coordinate Average 129

E.5.1.3 Printing the Temperature Data 129
E.6.1. User Defined Functions 130
E.6.1.1. Antoine Equation Solver 130
E.6.1.2. Pellet Centre 130
E.6.1.3. Horizon Centre 130
E.6.1.4. Centre Surface M 130
E.6.1.5. Vertic Centre 131
E.6.1.6. Vertic Surface M 131
E.6.1.7. Centre Corner M 131
E.6.1.8. Horizon Surface M 131
E.6.1.9. Corner Surface M 132
E.6.1.10. Pellet Interior 132
E.6.1.11. Centre Surface H 132
E.6.1.12. Vertic Surface H 132
E.6.1.13. Centre Corner H 133
E.6.1.14. Horizon Surface H 133
E.6.1.15. Corner Surface H 133

List of Figures

Figure 1-1: Model blast furnace diagram with major process inputs, outputs and requirements [16]. 3
Figure 1-2: Block flow diagram of a pre-calciner and cement clinker in series [17]. 4
Figure 1-3: Mapping electricity generation from coal to steam generation driving useful work [22–24]. .. 5
Figure 1-4: Goals & ideals for creating a bio-carbon economy while facilitating the transformation [37].. 8
Figure 1-5: Block flow diagram for torrefaction with feed drying and downstream densification [3]..... 11
Figure 1-6: (a) Pelletization by rotating die, and (b) briquetting by extrusion or moving piston. 13
Figure 2-1: Single pellet press schematic with pressure gauge, heating tape and removable cap. 28
Figure 2-2: Non-isothermal TGA (105-700°C), showing the devolatilization rate (dm/dt) as a function of temperature (°C) (at heating rate of 10°C/min), for 6 biomass residues. In addition, the mass loss (wt%) is shown as a function of temperature for (c) hardwood sawdust and (d) switchgrass stem. 35
Figure 2-3: Isothermal switchgrass stem TGA (300°C) for 30 minutes performed in triplicate. A span of five minutes gives a 30 wt% loss by torrefaction (orange). The maximum devolitization rate is in green. The same test was repeated at 260°C in Figure D-5. 36
Figure 2-4: Torrefied switchgrass stem at 250°C (a) & 300°C (b) extruded from the single pellet press with an applied pressure of approximately 10 MPa. 37
Figure 2-5: Qualitative pellet results for 5 biomass materials (woody, agricultural, pulp, and cellulose). (a) Pelletization for wet torrefied willow at 90°C; (b) untreated willow pelletization tested the same as in (a); (c) untreated willow with 2 wt% moisture at 200°C; (d) torrefied willow pellets produced the same as (c); (e) two switchgrass stem pellets at 300°C; (f) sludge pulp residue at 300°C; and pure cellulose produced (g)-(i) at 80, 250, and 300°C respectively. All pellets presented produced at 215 MPa. Additional qualitative results available in Figure D-2. 39
Figure 2-6: Qualitative briquette results for 4 biomass materials (primary and tertiary sources) produced at 45 MPa. Integrated torrefaction and briquetting shown in (a)-(d) and low temperature briquetting (e). (a) Strong and (b) weak willow briquettes, (c) construction and demolition waste, and (d) poplar bark tests ranged from 300-325°C. (e) Poplar briquettes with (bottom) and without (top) tar binder shown at 120°C. 40
Figure 2-7: Pellet densities for 8 biomass residues. Relationships in (a)-(d) for temperature at constant pressure (215 MPa), and (e) for pressure at constant temperature (250°C). 43
Figure 2-8: Dry basis mass loss for 8 biomass residues. Relationships in (a)-(d) for temperature at constant pressure (215 MPa), and (e) for pressure at constant temperature (250°C). 45
Figure 2-9: Results for untreated willow (yellow circle), poplar (green pentagon), and ITD willow and poplar briquettes (red cross and blue trapezoid) plotted on a van Krevelen diagram (adapted from [3]). Additional commercial materials for the industrial evaluation program include: steam explosion pellets (brown triangle), torrefied pellets (pink octagon), and carbonized briquettes (purple diamond). 50
Figure 2-10: Pellet durability for 8 biomass residues as a function of temperature, material, & density compared to the average positive control (solid line) and the standard deviation (dashed line). The measurements in (b) include data at 250°C and 300°C since the means were statistically similar. Pellet durability was generally assayed in triplicate. Durability values less than 90% were tested in replicates. 51
Figure 2-11: Durability results for a three level experimental design including: 1) three blends of switchgrass stem and hardwood sawdust for 40 & 215 MPa at 250 & 300°C; 2) switchgrass stem at 125

MPa & 250°C and at 215 MPa & 150°C; and 3) low quality woodchips at 125 & 215 MPa at 250°C and at 215 MPa & 150°C. 54
Figure 2-12: Qualitative hyrophobicity of pellets produced at 215 MPa. (a)-(c) shower test and (d)-(f) immersion test with the post-weathered Pellet Durability Index (PDI)[1]. Results for (a) willow, (b) cellulose, and (c) knot residue pellets produced at 200-250°C. Results for ITD switchgrass blended pellets (75:25) at two temperatures: (d) 250°C and (e) 300°C and a positive control (f) SE pellets. 58
Figure 2-13: Low severity shower test on pellets produced from 7 biomass sources and controls. (a) Willow produced by densification (145°C, 200°C) and ITD (250°C) shown with mass loss (dry basis). (b) Blends of switchgrass stem (100:0) and hardwood sawdust (0:100) shows better durability at 300°C versus 250°C. (c) Water absorption and mass yield for three pulp residues at 260°C and one trial at 220°C. (d) Select residues compared to positive control samples. 59
Figure 2-14: Immersion of ITD pulp and switchgrass residues compared to torrefied pellets/controls. Hog, knot and sludge fuel tested at 220, 260, and 300°C with the exception of knots (see Figure 2-12). Single switchgrass stem blend (75 wt%) tested at 250 and 300°C. Commercial pellet samples (A1, A5, torrefied; C1, C2 steam explosion) had high water absorption after 1 hour (30-40 wt%). Pre-torrefied willow allowed to cool before densification was hydrophilic. 62
Figure 2-15: Commercial torrefied briquettes and the resulting fines after a 48-hour immersion. 65
Figure 2-16: Time lapse of (a) raw poplar, (b) poplar with 10 wt% tar additive and (c) ITD poplar briquettes immersed in deionized water. Three time points during the immersion were selected: (i) 1 hour, (ii) 8 hours, and (iii) 48 hours. 65
Figure 2-17: Block flow / process flow diagram with heat integration (for drying) and ITD. 69
Figure 2-18: 3D structural formulae of levoglucosan (left) and cellulose (two monomers) (right) 70
Figure 3-1: Process schematic diagram for biomass pellet (represented by brown cylinders) drying by gentle forced convection with air speed of 0.3 m/s and a temperature of 40°C. 77
Figure 3-2: Coupled effect of mass transfer and heat transfer during drying. Experimental results with a stainless steel thermocouple (yellow) and the energy balance model solution (blue) are shown. The unsteady state temperature profile was modeled using the da Silva *et al*. (2013) and finite difference models on the secondary vertical axis (right). Accompanying the heat transfer is the fitted response from three trials of unsteady state mass transfer using the da Silva *et al*. (2013) model. 85
Figure 3-3: Experimental data and finite difference simulated data using the two drying simulation models for the 6 advanced solid biofuels. (a) Commercial steam exploded pellets C1, (b) torrefied briquettes B1, and (c)-(f) torrefied pellets. The plots of the torrefied pellets correspond to samples A1, A3, A4, and A5. 87
Figure 3-4: Drying profiles of (a)-(b) commercial steam exploded and (c)-(d) torrefied pellets using two drying methods. On the left, drying was done in an oven with air flow and bulk fluid temperature of 40°C. On the right, the corresponding sample was dried on an open laboratory bench at 20°C in stagnant air. 89
Figure 3-5: Experimental and simulated drying profiles for (a) poplar tar and (b) ITD briquettes following a 48-h water immersion. Drying was performed in an oven at 40°C with mild air flow rate. 89
Figure B-1: Pellet durability protocol development with commercial samples in the 300 mL tumbler... 106
Figure B-2: 1-hour water average adsorption equilibrium for the burette, faucet, & immersion tests. . 111
Figure C-1: (a) Custom bench scale pellet, (b) commercial pellet, and (c) custom briquette tumbler. ... 112

Figure C-2: (a)-(b) Two versions of the semi-batch shower test and (c)-(d) two versions of the batch immersion test for steam exploded pellet hydrophobicity. In (a), a suspended burette above a Buchner funnel to spread the falling water over the cross sectional area of the micro pellet batch being tested. In (b), a feed tank of deionized water, a pump, and the housing container for a packed bed of pellets. The protocols used for immersion from (c) SECTOR and (d) CanmetENERGY. 113
Figure C-3: Installations of (a) the single pellet press and (b) the briquette press with tar trap. 114
Figure D-1: Forestry, agriculture, & pulp industry biomass residues in various degrees of processing. Forestry residues include (a) willow, (b) torrefied willow, and (c) poplar bark. Agricultural residues include (d) switchgrass stem, (e) switchgrass leaf, and (f) hardwood sawdust. Pulp mill residues include (g) knots, (h) hog, and (i) sludge. 116
Figure D-2: The AAFC blends of switchgrass stem with hardwood sawdust were produced at a pressure of 215 MPa and at temperatures of 300°C (a), (c) and 250°C (b), (d). The pure switchgrass stem pellets (a)-(b) and the pure hardwood sawdust pellets (c)-(d) are representative images. Representative images of the dry willow (e), (g) and torrefied willow (f), (h) pellets produced at 145 (e)-(f) and 200°C (g)-(h) look the same as pellets produced with added moisture (data not shown). Qualitatively, willow torrefaction followed by cooling and pelletization yields similar looking pellets compared to integrated torrefaction and densification (ITD) of the same willow residue (i). Representative images of the knot fuel at three production temperatures 220°C (j), 260°C (k), and 300°C (l), and hog and sludge fuel pellets are depicted for 260°C (m)-(n) respectively. 118
Figure D-3: Pellet compression ratios for 8 biomass residues. Relationships in (a)-(d) for temperature at constant pressure (215 MPa), and (e) for pressure at constant temperature (250°C). 119
Figure D-4: Severity factor as a function of temperature assuming 5 minutes at constant T. 120
Figure D-5: Switchgrass torrefaction simulation at 260°C for 1 hour. 121
Figure D-6: Unsteady state energy balance for eight different pellets and briquettes during drying after immersion. Pellet temperatures rose quickly because of their smaller size whereas briquettes took longer to approach 0 unaccomplished change. 122
Figure D-7: (a)-(c) Pellet drying at room temperature after immersion for 1 hour in 125 mL of deionized water. (d) Pellet drying in a convection oven at 40°C after immersion for 48 hours in 4.5 L of deionized water. Results for (a) Supplier C2, (b) Supplier A1, (c) pulp Hog ITD (260°C and 215 MPa), and (d) Supplier A5 (drying without any other samples). 124

List of Tables

Table 1-1: Potential biomass sources for energy production respecting proposed technologies [3]. 7
Table 1-2: Physicochemical properties of solid fuel alternatives presented on a dry basis (db.). 9
Table 1-3: Process characteristics of varying biomass thermochemical conversion technologies. 10
Table 1-4: Proposed methods to determine the degree of hydrophobicity of advanced solid biofuels and how it relates to questions for industrial operations. 17
Table 2-1: Chemical properties and composition of woody, agricultural, pulp waste and cellulose used for ITD/densification [56,85,86]. 25
Table 2-2: Scope of experimental biomass, temperature, pressure, and sample sizes tested. 29
Table 2-3: Comparison of durability methods for in-house batch products and commercial shipments. . 30
Table 2-4: Differences in hydrophobicity methods for different scales of available material [73]. 31
Table 2-5: Maximum devolatilization rates and optimum pyrolysis temperature by reaction rate. 34
Table 2-6: Micro reactor torrefaction results at 250°C and 300°C for switchgrass stem. 37
Table 2-7: Quantitative densification results for willow and poplar bark in two studies. 48
Table 2-8: Influence of torrefaction on physicochemical properties of fines from ITD briquettes. 49
Table 2-9: Statistical assessment for 5 switchgrass stem concentrations of 14-28 mesh (215 MPa). 55
Table 2-10: Small scale durability of briquettes in commercial scale pellet tumbler. 56
Table 2-11: Evaluation of pre- and post-weathered durability for commercial/in-house materials. 64
Table 2-12: Immersion of torrefied and ITD briquettes compared to thermally untreated poplar. 66
Table 3-1: Boundary conditions for the mass and heat transfer system analysis. 79
Table 3-2: Mechanical integrity of samples for the Industry Evaluation Program of advanced solid biofuels for direct coal substitution. 80
Table 3-3: Severity factor of hydrophobicity test (shower/immersion) on post-weathered durability for the Industry Evaluation Program of advanced solid biofuels. 81
Table 3-4: Analysis of key feedstock parameters for the Industry Evaluation Program of advanced solid biofuels for direct coal substitution. 82
Table 3-5: Results from finite difference solutions to the energy balance resulting from experimental data. 86
Table 3-6: Mathematical modeling results for the drying curves of the seven commercial samples and the two in-house briquettes. 90
Table A-1: Theoretical Currie temperature for some paramagnetic metals and alloys. 105
Table B-1: Dimensions and macroscopic energy calculations experienced during tumbling. 107
Table B-2: Protocol development results for coke and torrefied briquette durability. 108
Table B-3: Initial & final moisture content of two sources (4h oven drying method & 1h immersion). .. 110
Table C-1: Differences for single pellet and briquette press operating conditions. 114
Table D-1: Densification parameters for commercial biomass materials aimed as fuel sources. 117
Table D-2: Physical properties of pellets and briquettes used for the Industry Evaluation Program of advanced solid biofuels for direct coal substitution. 122
Table D-3: Unsteady state heat transfer during convective drying of biomass pellets/briquettes. 123

Nomenclature

Symbol	Meaning	Units
ΔH	Enthalpy of reaction	kJ/mol
Δs	Space step for finite difference solution mesh	cm
CR	Compression ratio	-
D_{AB}	Diffusivity of species A through species B	m^2/s
db	Dry basis	wt%
D_e	Effective diffusivity for tortuous paths in pores	m^2/s
HPI	Hydrophobicity Pellet Index	wt% db
h	Convective heat transfer coefficient in drying	$W/m^2/K$
k	Thermal conductivity of solid biomass & water	W/m/K
k_c	Convective mass transfer coefficient in drying	m/s
L/D	Aspect ratio (length/diameter)	-
m_{loss}	Lost as gases and vapour (for thermal treatments)	wt% db
PDI	Pellet durability index	wt%
Q_{evap}	Energy of water evaporation during drying	W/m^2
RH, or H	Relative humidity in drying air, or humidity	%, kg/kg
r	Cylindrical coordinate along the cylinder radius	cm
SF	Severity factor	-
TWh	Terawatt hour (3.6×10^{15} J)	J
T	Temperature	°C
t	Time	s
wb	Wet basis	wt%
z	Cartesian coordinate along the cylinder length	cm
$\omega'(t)$	Moisture content (dry basis) at time 't'	kg/kg
ω'_{eq}	Equilibrium moisture content after drying	kg/kg
ω'_i	Initial moisture content before drying (0.4-0.6)	kg/kg
α	Thermal diffusivity coefficient heat transfer	m^2/s
ρ	Density of pellet or raw biomass	g/mL
λ_h	Dimensionless thermal diffusivity ($\alpha\Delta t/\Delta s$)	-
λ_m	Dimensionless mass diffusivity ($D_{AB}\Delta t/\Delta s$)	-
ω'	Dry basis moisture content within a solid	kg/kg

Acknowledgements

This work was made possible in part by the efforts of researchers, colleagues and friends. I would like to thank Dr. Mehrani and Dr. Thibault for their insight and guidance as I explored new avenues. I would like to thank Mr. Guy Tourigny for supporting my work in 2013 and 2017-2019 with which I gained skills and experience to conduct engineering research. In addition, I would like to extend my thanks to CanmetENERGY-Ottawa and the Bioenergy Systems Group including, but not limited to, Dr. Sebnem Madrali, Travis Robinson, Guillaume Gagnon-Caya, Lufei Jia, and Keith Ludlow. I would like to thank my fellow graduate students in the Department of Chemical and Biological Engineering including, but not limited to, Fahad Chowdhury, Geraldine Càceres, Emily Cossar, Charbel Atallah, and Dean Kennedy. I would like to thank my family: my parents George and Angela, my brothers Marc and Steven, and Katey Rene de Cotret for their continual support throughout this work – especially for their help in preparing for the Graduate Student Poster Competition (2018), the CSChE Conference in Toronto (2018), and the University of Ottawa 3-MT competition (2019).

Chapter 1. Introduction

Scientific disciplines across a wide spectrum have been building the case for changing climate in the last 40 years. These include, but are not limited to studies in chemistry, physics, earth sciences, meteorology, oceanography, biology, and life sciences [1]. The evidence, taken together, suggests that the anthropogenic addition of CO_2 through combustion of carbon fuels that were long sequestered from the carbon cycle is changing the global heat content. In 2018, Thompson [2] published a review article describing ten models of global carbon dioxide and climate systems. The energy balance of the global system is disrupted with increasing greenhouse gas (GHG) emissions (predominantly CO_2) and shifts towards an equilibrium by heat transfer to the air, soil, and water. The atmosphere exchanges about 90 Gt carbon/year with the oceans, and the ocean capacity for CO_2 by mass is about 50 fold greater than the atmosphere [3]. Ocean carbon dioxide uptake impacts marine life by changing ocean pH.

The global understanding that fossil fuel combustion is a major source of anthropogenic climate change has motivated research into renewable fuel sources. These fossil fuels took millions of years to form and current consumption rates are quite rapid. Fossil fuel sources can be found in three states of matter: coal, crude oil, and natural gas. Biomass fuel is a renewable resource that can also be processed in all three states of matter. For example, biomass supplied as sawdust or charcoal can be used as a solid burning fuel. Biomass can be converted to liquid fuels via fermentation in a microbial process or via pyrolysis in a thermochemical process. Finally, natural gas can be produced by biomass gasification followed by methanation [4]. However, the commercial scale-up of these industries is limited and less competitive than using non-renewable resources at large scale.

Coal usage is not as widespread in the present day compared to historical values (33-40% in the 1960s), although its share still represents 28.1% of the global primary energy consumption [5]. Converting industrial processes to use renewable solid fuels and thus move away from coal has the potential of reducing anthropogenic GHG emissions of carbon dioxide as well as other pollutants like sulphur and nitrous oxides. A viable commercial renewable energy sector would help reduce the 31.25 Gt CO_2 produced from coal assuming that coal generates 720 tonne

CO_2/GWh, and knowing that the 2016 coal usage was 43 403 TWh [6,7]. In comparison, the biomass rating is 25-100 tonne CO_2/GWh depending on the bulk density of the biomass fuel [8].

1.1. Energy Intensive Solid Fuel Usage

Many current mature technologies from the advent of the industrial revolution depend on using coal. Some specific applications include iron and cement manufacturing, and power generation.

1.1.1. Iron/Steel Production

The primary process for obtaining pure iron (Fe) from nature involves mining and refining iron ore. Iron ore, or Fe_2O_3, is a brittle material like many oxides, and the process of converting iron ore into molten iron (Fe) requires pure carbon at elevated temperatures. The combustion of coal generates CO by controlling oxygen input and iron ore reduction creates CO_2. A balanced chemical equation of the process is given in (1-1) [9].

$$Fe_2O_3 + 3CO \rightarrow 2Fe + 3CO_2 \left|\Delta H = -59\frac{kJ}{mol}\right| \quad (1\text{-}1)$$

Iron making is one of several processing steps for steel production, and the blast furnace-basic oxygen furnace (BF-BOF) route also requires some direct carbon [10]. The iron industry provides, in part, its raw material to the steel industry, so all references will be made to the iron/steel industry. Iron/steel production is an energy-intensive process where 70% of GHG emissions originate from the blast furnace iron making process [11]. A schematic diagram of the blast furnace is shown in Figure 1-1. The iron/steel process has high demands for energy sources and reductants, which are predominantly derived from fossil coal to be 1) used for pulverised coal injection (PCI) or 2) transformed into metallurgical coke [12,13]. For PCI, the energy content (MJ/kg) is critical to achieve internal temperatures of ~1800°C and allow for economical fuel transport, respectively [14]. The requirement of coke (or thermally treated coal) can reach as high as 400 kg per tonne of hot metal, where it serves as an iron oxide reducing agent, an energy supply, and a support medium [15].

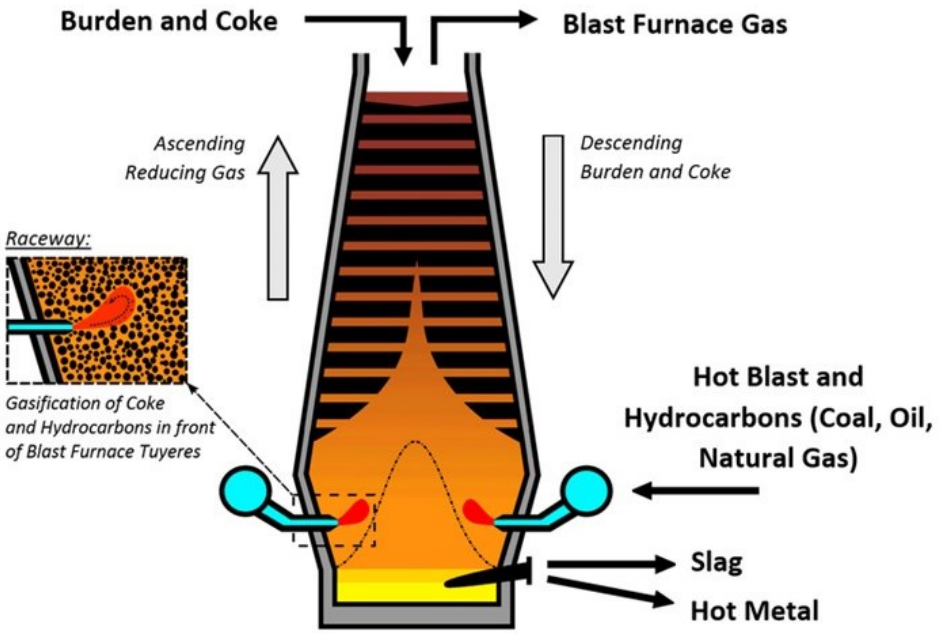

Figure 1-1: Model blast furnace diagram with major process inputs, outputs and requirements [16].

Prior to the industrial revolution, biomass was used as a bed material for iron making, but coal served as a replacement in the 1800s because of its superior properties for scale-up at the time (stronger bed material for large scale production) [11]. In addition, any oxygen and phosphorous impurities used in iron manufacturing typically end up in the final product reducing its strength and value. Finally, a fuel with a lower energy density [MJ/m^3] such as biomass solid fuel leads to a larger fuel volume. As a result, higher transportation shipping costs and higher GHG emissions are associated with biomass. Industry has moved beyond this historical context to use coal, which takes us to the present day and a need to look at the future context.

1.1.2. Cement Production

Similar to the iron/steel industry, the cement industry also requires high temperatures (in the 1400-1500°C range) for the clinker kiln [17,18]. Calcium carbonate, like iron oxide, is a metallic element bound in an oxide form and is typically brittle. Calcium carbonate (or limestone) is an abundant material that can be upgraded to create a strong foundational material (cement). The chemical transformation actually produces CO_2 directly: 70% is derived from the transformation of limestone. The governing process chemistry is given in (1-2) [17].

$$CaCO_3 \rightarrow CaO + CO_2 \quad \left|\Delta H = 178.5 \frac{kJ}{mol}\right| \tag{1-2}$$

The most common sources of fuel in the cement industry are coal, fuel oil, petroleum coke, and natural gas, and the other 30% of CO_2 emissions results from the combustion of these fuels [19]. In this process, calcium carbonate is treated in a pre-calciner at 900°C using air and fuel before moving to the secondary unit (clinker kiln) for cement production. A block flow diagram including a simplified mass balance is shown in Figure 1-2.

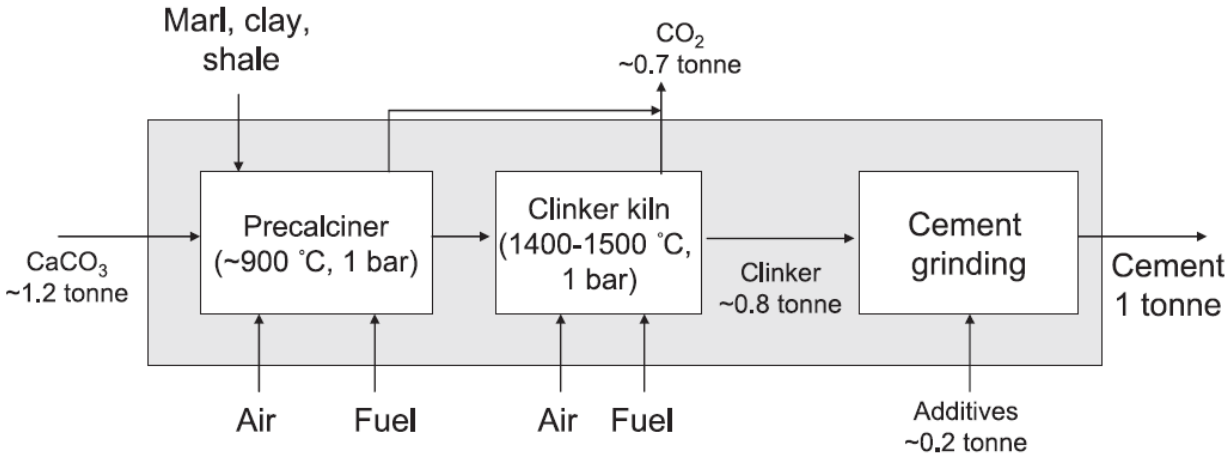

Figure 1-2: Block flow diagram of a pre-calciner and cement clinker in series [17].

The 70% of the CO_2 emissions can only be realistically controlled by advanced carbon capture and storage methods [17]. For example, oxy-combustion with calcium looping or amine scrubbing could isolate CO_2 with high purity. The present day cement industry is relatively energy intensive, uses coal as a major energy source, and emits a large quantity of CO_2 from fuel burning alone [20]. In response, the cement industry started the practice of using alternative fuels in the 1980s including solid fuels such as agricultural and non-agricultural biomass, petroleum waste, miscellaneous waste, chemical waste, and hazardous waste [19]. The critical need in the cement industry to complete the transition is a day-to-day industrially reliable input of biomass fuels [20].

1.1.3. Power Generation

The need for intensive process energy in the power generation field echoes those in metallurgical and cement industries, where process temperatures range from 800-1400°C depending on the specific boiler technology employed [21]. Current mature technologies include pulverized coal combustion (PCC) and fluidized bed coal combustion (FBC). Coal is burned to produce high-pressure steam and the steam enters a turbine which drives the generator for

electricity distribution [22]. Unlike iron and cement production, the thermodynamic Rankine cycle (characterized by physical changes in steam properties) dominates this system shown in Figure 1-3.

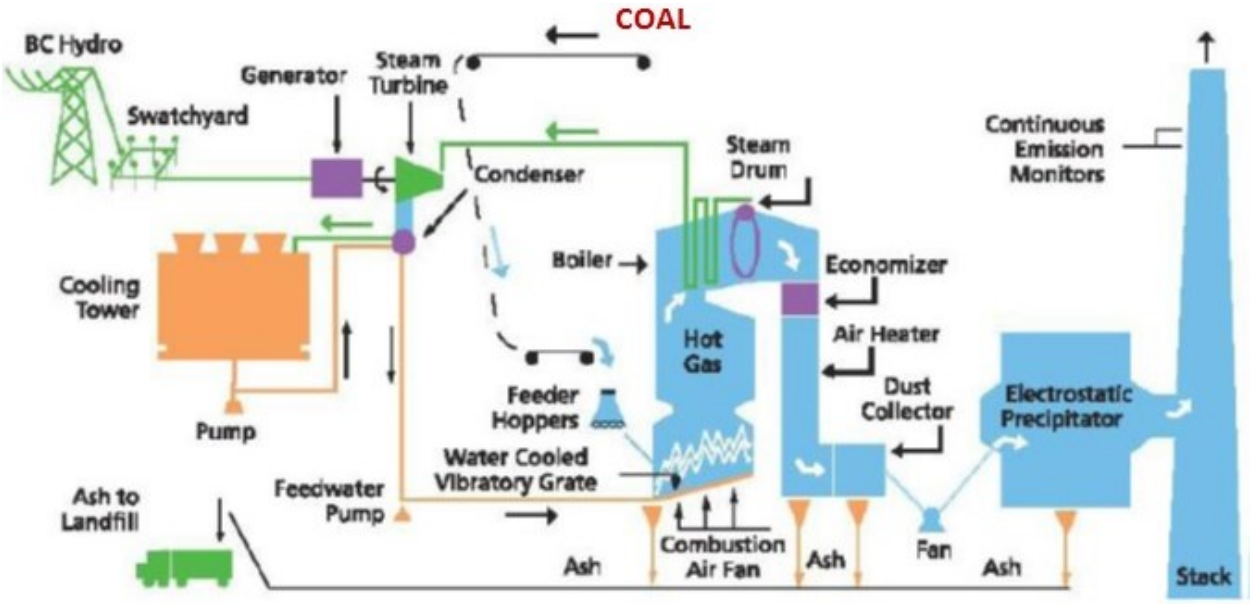

Figure 1-3: Mapping electricity generation from coal to steam generation driving useful work [22–24].

There is great potential for reducing GHG emissions and industrial environmental impacts by transforming fuel consumption in these energy intensive industries. Most power generation facilities across the world still use coal combustion for energy with major investments in place for the current technology. The carbon dioxide emissions from power generation are significant as 39% of the global electricity supply is generated using coal yielding 3200 Mt of CO_2/year [25]. There are some successful significant shifts in the present technical landscape. For example, the Thunder Bay power generating station, operated by Ontario Power Generation (OPG), managed the transition from coal to biomass using pellets imported from Norway. The Norwegian process uses a thermal treatment known as steam explosion (SE) and their product was used effectively between 2014 and 2018, before the power generating station had to close due to inactivity for the provincial electricity grid [26]. Although demonstrations of renewable fuel technologies exist for these sectors, it is important to note that globally this technology is still underdeveloped. Therefore, a global solution is needed to reduce anthropogenic CO_2 emissions.

1.2. Life Cycle Analysis (LCA)

Section 1.1 provided an introduction on some key energy intensive industries dependent on solid fuel usage. This section describes the life cycle of coal and biomass for combustion in industrial operations. Some important metrics include, but are not limited to: 1) sustainability (especially for CO_2 emissions); 2) power density (the magnitude of energy that one can extract per unit land area used); and 3) the sources and sociopolitical impacts of exploitation.

1.2.1. Coal: From Mine to Industry

A typical life cycle for coal from mining to the end-use point includes the following major steps in series: coal mining, transport, storage, conveying, grinding, drying, and combustion [27]. The coal mining step occurs in geological coal mines which are typically found in large rock formations (power density: 1000 W/m^2) [28]. The transportation step can vary considerably based on the distance between coal mines and the power, cement and/or metallurgical industries interested in using coal for process energy. There are other considerations for alternative fuels (biomass) when compared to coal (example hygroscopicity and grindability). Hygroscopicity is the process by which a solid gains moisture content in the form of water vapour via humid air contact. Coal is typically stored in large quantities in a coal yard where different companies apply different stacking techniques and different ranges of coal coverage (from generally used open coal stacking, to covered stack areas, and to the more extreme coal silos for particularly challenging local climates) [29]. Grindability is the metric used in the coal industry to determine the change in pulverizer capacity needed to achieve a desired coal particle fineness [30]. For pulverized coal combustion (PCC), that target is as low as 75 µm compared to mined coal pieces measured in tens of mm [31]. At the end of the process, carbon dioxide emissions from coal fired power generation account for 93% of the total carbon dioxide emissions in the life cycle analysis [32].

1.2.2. Biomass Sustainability

Biomass is composed of three major macromolecules in high concentrations within its structure: hemicellulose, cellulose, and lignin. Global terrestrial biomass can hold anywhere from 600-1000 Gt of carbon converted via photosynthesis taking in CO_2 as a substrate [3]. The first step in the biomass life cycle is very different from coal extraction because woody biomass

occupies wide remote expanses (power density: 0.1-1.0 W/m^2) [28]. Coal is derived from biomass, but the focus is on biological material (forestry and agricultural waste) that hasn't been removed from the carbon cycle across geological time spans. Khan *et al*. [33] list sources of biomass and the corresponding degree of processing and availability as seen in Table 1-1.

Table 1-1: Potential biomass sources for energy production respecting proposed technologies [3].

Category	Primary	Secondary	Tertiary
Degree of Processing	Low	Medium	High
Forestry Products	Logging Residues Stumps	Wood Process By-Products Bark, Chips, Sawdust	Demolition Wood
Agricultural Residues	Straw Vineyard Residues	Bagasse, Molasses, Vinasse Rice, Corn Husks	Domestic Manure
Energy Crops	Sugar beet, sugarcane Miscanthus, switchgrass Poplar, willow, eucalyptus		

The degree of processing influences the next steps in the biomass life cycle: drying (limiting biomass moisture uptake), grinding, and transport. Primary sources have more moisture less uniform particle shapes, and require a higher degree of processing and transport. At the final stage, biomass fuels include low sulphur and nitrogen emissions in comparison to coal. Moreover, biomass combustion CO_2 emissions are highly neutral since the biomass that took up carbon for growth is released in a short term cycle [3]. If biomass sources and wastes are managed optimally, then the process is more sustainable compared to its coal counterpart.

Co-current studies on technical solutions must be done while other parties perform studies to develop life cycle analyses. Some LCA studies on the bioenergy supply chain have been done by Guinee *et al*. [34], Wrisberg *et al*. [35], and Berndes *et al.* [36]. These resource management studies, including plans for different biomass sources, can serve to implement a technical revolution and respect sustainability elements of this change. Members of the European Union such as the Netherlands have provided an outline of biomass sustainability criteria as illustrated in Figure 1-4.

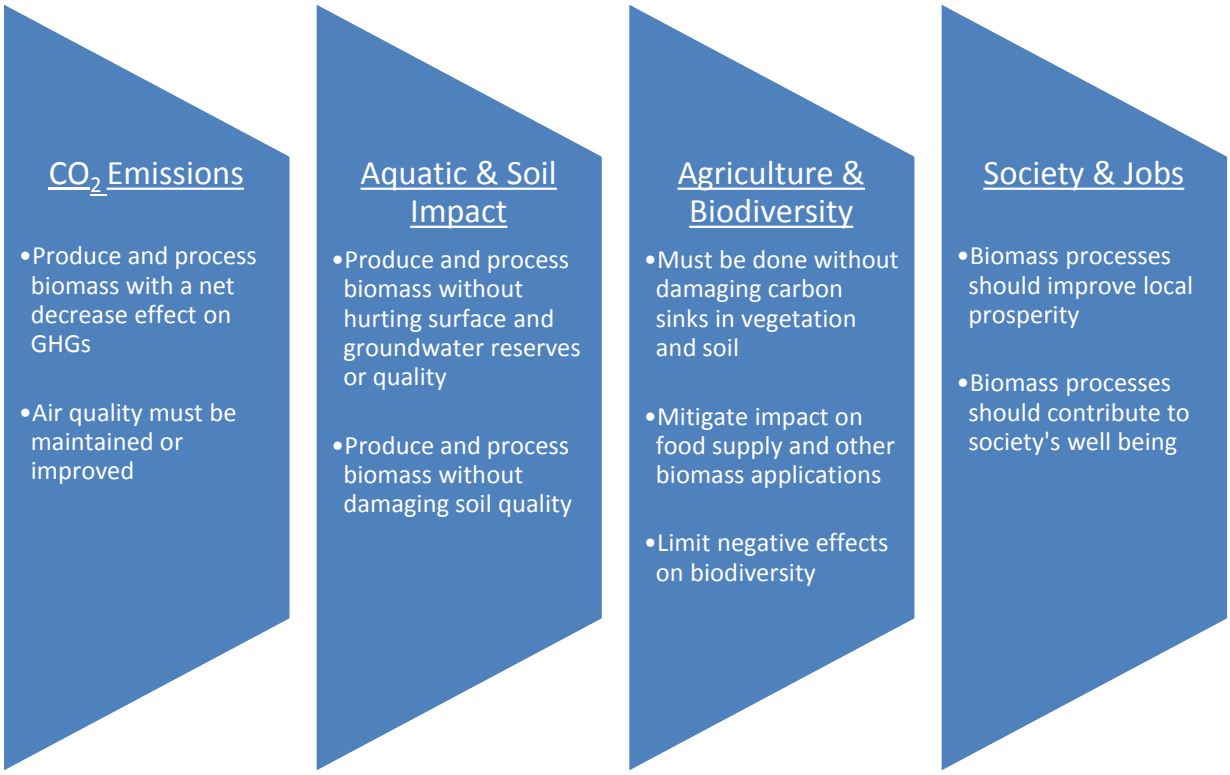

Figure 1-4: Goals & ideals for creating a bio-carbon economy while facilitating the transformation [37].

The direct coal substitution for an improved bio-based product does not necessarily mean sustainability and environmental goals will be realized. Rather, the technology must be developed in ways that meet current global demands while forcing the rate of change of CO_2 levels to be less than or equal to zero in the next 30 years. Some techno-economic analyses have been done to assess solid biofuels including pellets and torrefied biomass [38–42].

In the current socio-political climate, the direct use of biomass is an insufficient solution; it has some inherent disadvantages not seen in coal (for example: energy content, moisture resistance, and mass density). Thus, biomass upgrading, which includes pellet production and biomass torrefaction, must be evaluated.

1.3. Biomass Upgrading

Biomass upgrading is the process of enhancing the characteristics of potential biomass fuels in order to supply a much greater portion of renewable fuels onto the market. By heating the biomass in a lean oxygen environment, volatile organic compounds (VOC) are driven off, turning the biomass solid residue into a carbon/energy rich substance. Depending on the process

conditions, valuable liquid and gaseous products can be collected for their utilization downstream. In this section, 1) an overview of potential physicochemical property changes is presented; 2) the means for upgrading biomass, namely the thermochemical conversion, are discussed; and 3) the main upgrading route, the biomass torrefaction, followed by densification to improve some of the biomass shortcomings are described.

1.3.1. Physicochemical Properties

The industrial motivation to substitute coal for biomass is hindered by shortcomings observed with untreated biomass. The beneficial coal properties (compared to untreated biomass) include: low fouling ash content, as well as high carbon content, energy density, bulk density, grindability, and hydrophobicity. Moreover, biomass is generally more difficult to transport, handle and store compared to coal. The key physicochemical properties of raw biomass (prior to thermal treatment), torrefied biomass (anoxic thermal treatment at 300°C) and coal on a dry basis (db) are listed in Table 1-2.

Table 1-2: Physicochemical properties of solid fuel alternatives presented on a dry basis (db.).

Parameters	Raw Biomass	Torrefied Biomass	Bituminous Coal
Potassium Ash (wt%)	1.0 [43,44]	1.2 [43,45]	0.3 [43,44]
Calcium Ash (wt%)	1.3 [43,44]	1.5 [43,45]	1.3 [43,44]
Fixed Carbon Content (wt%)	15-20 [43]	25-35 [46]	45-55 [43]
Carbon Content (wt%)	45-50 [43]	55-60 [45]	65-80 [43]
Energy Content (MJ/kg)	14-18 [43]	20-23 [46,47]	25-30 [31,43,46]
Material Bulk Density (kg/m^3)	150-450 [47]	300-400 [47]	700-900 [31,46,47]
Hydrophobicity	Low [48]	Medium [47,48]	High [48,49]
Grindability (HGI)	Low [48]	High [48]	High [48]

In general, coal has superior properties as a solid fuel compared to biomass. Although coal (sitting in geological reserves) has a higher ash content than biomass (20 wt% compared to 5 wt%), the problematic species that volatize in the 800-1800°C range (Na, Ca, and K) all have higher concentrations in biomass by factors of 3 to 12 fold [43]. When biomass undergoes a thermal treatment (e.g. torrefaction), the fate of different ash species varies [45]. Some ash species can be concentrated in a torrefied biomass product depending on the process conditions

[50]. Next, untreated biomass would require a higher 1) industrial capacity to achieve the same energy requirements; and 2) transport volume to move the fuel (see Section 1.2). The carbon content and energy density of biomass are lower compared to coal because of the high oxygen content and low envelope density. Biomass is more hydrophilic and has a lower grindability than coal. Biomass transformations that overcome physicochemical property deficiencies could create a final product that can be transported and handled like coal while meeting industry standards, maintaining product quality and operational compatibility.

1.3.2. Thermochemical Conversion

There are biochemical and thermochemical transformation routes used in biomass upgrading. Biochemical conversion is outside the scope of this thesis, and although thermochemical conversion includes combustion, straight combustion does not resolve biomass limitations described in Section 1.3.1. The thermochemical conversion of different biomass sources depends, in large part, on the differences between the major macromolecular constituents. One way to identify differences is by means of thermogravimetric analysis (TGA), which is a continuous assay of devolatilization reactions by mass with respect to temperature and/or time. The key process differences for biomass thermochemical conversion techniques are listed in Table 1-3.

Table 1-3: Process characteristics of varying biomass thermochemical conversion technologies.

Parameters	Torrefaction	Slow Pyrolysis	Fast Pyrolysis	Steam Explosion	Hydrothermal Carbonization
Temperature (°C)	225-325 [3,51]	325-425 [3,46,52]	450-550 [3,46,52]	180-240 [53]	180-250 [54]
Pressure (MPa)	0.1 [3,51]	0.1 [3,52]	0.1 [3,52]	1.0-3.5 [53]	1-5 [54]
Residence Time (min)	10-30 [3,51]	30-120 [46,52]	0.5-5 [46,52]	10-30 [53]	30-360 [54]
Solid Process Yield (wt%)	70 [3,51]	30 [52]	20 [52]	85 [55]	60 [56]
Energy Content (MJ/kg)	20-23 [46,47]	22-26 [57,58]	25-30 [59]	19.5-21.0 [55]	23-28 [56]
Envelope Density (kg/m^3)	600-700 [47,60]	500-550 [57,58,60]	450-500 [52,60]	500-700 [55]	500-600 [61]
Carbon Content (wt%)	55-60 [45]	60-70 [45]	70-80 [59]	50-55 [62]	55-65 [63]
Fixed Carbon (wt%)	25-35 [46]	60-70 [45]	40-50 [59]	20-30 [62]	35-50 [56]

The different thermal conversion processes (torrefaction, slow and fast pyrolysis, hydrothermal carbonisation, and steam explosion) yield fuels that could be used as a substitute for coal. Of these processes, torrefaction has the mildest operating conditions in terms of

temperature and pressure. The torrefaction process is a pre-treatment where a minimal mass fraction is lost as gases (relative to other methods), and a significant solid energy content can still be recovered [64]. The bulk density from torrefaction is comparable to solid products from slow and fast pyrolysis, but the energy content is lower. The remaining solid fraction has a reduced hygroscopicity and improved grindability characteristics. The main process investigated herein is the combination of torrefaction (Section 1.3.3) with densification technologies (Section 1.3.4) to generate an advanced solid biofuel (Section 1.4 ITD). This would allow the use of existing equipment and facilities and thus reduce the conversion cost (Section 1.1).

1.3.3. Torrefaction

The torrefaction heat treatment changes the chemical and physical properties of biomass. A torrefaction process typically reaches its optimum performance for fuel upgrading with a mass loss of about 30 wt% of dry solid matter where the resulting solid contains 90% of the initial energy content, and the condensable and non-condensable gases (or torr-gas) contain the balance [3]. The consequence is a torrefied biomass product with an energy intensification of 0.9/0.7 (or a 28.5% increase). A block flow diagram featuring drying, torrefaction, and densification is given in Figure 1-5.

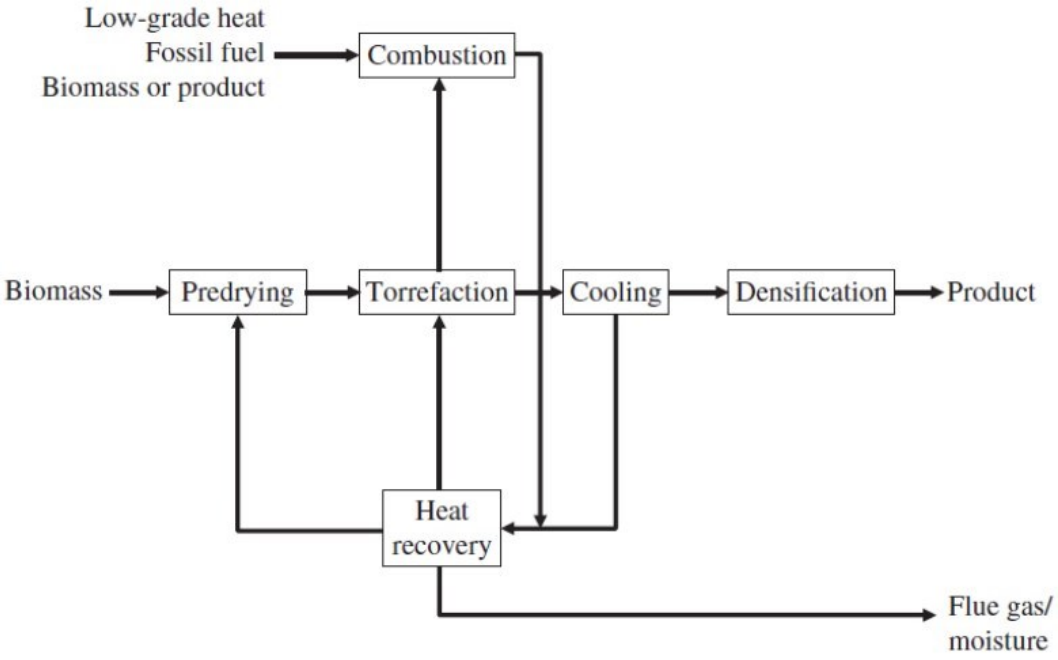

Figure 1-5: Block flow diagram for torrefaction with feed drying and downstream densification [3].

In a typical reactor, the biomass is heated from room temperature. This feed contains some inherent and surface moisture left over from the harvest drying (5-15 wt%), which is considered acceptable for transport and storage considerations. The first stage is the atmospheric heating of the biomass with an increase in the vapour pressure of water resulting in the loss of moisture within the biomass. Very little if any moisture remains as the heating continues above the 100°C point. Once the biomass reaches 225°C, the thermochemical conversion begins in earnest with the decomposition and devolatilization of hemicellulose first and cellulose and lignin reactions happening above 240°C [3]. These volatile species are released as condensable and non-condensable gases with a 30% yield, while 70% of the original biomass remains as the final solid product. Conventional systems will use heat integration to cool the solid product upstream of densification to mitigate the risk of product combustion. Within a torrefaction reactor (purged to low oxygen concentrations < 5 mol%), the risk of combustion is minimal. However, if the torrefied product was moved from the torrefaction chamber to the densification unit at 300°C (oxygen = 21 mol%), the conditions prevail for solid fuel fires.

Current torrefaction technologies have not been demonstrated at the commercial scale since the end product only serves small specific markets. In particular, it has been found that torrefied pellets (sometimes known as black pellets) are three times more expensive than coal which hurts the demand for large-scale torrefaction technology and production [42]. However, this is beginning to change in the 21st Century, and there are several start-up pilot and demonstration scale torrefaction units owned by a variety of companies including Airex, American Biocarbon, Andritz, AREVA, BioEndev, Biolake, CENER, CMI-NESA, ECN, Pechiney, Rotawave, Topell, Torr-Coal, TSI, and Wyssmont [3]. The pilot-scale technologies used today were modelled after units that dry solids (T = 105°C) but use more power to increase the reactor temperature (225°C < T < 325°C). These reactors include the rotating drum, screw conveyor, multiple hearth furnace, and moving bed units [3].

1.3.4. Densification

Material densification is broadly defined as the compression of material to reduce its volume with the same mass. In general, Tumuluru *et al*. [65] discussed a large variety of densification techniques for the biomass, food, feed, and pharmacy sectors. There are a variety

of commercial technologies available for pelletization and briquetting with a range of target markets including combustion (barbeques), agriculture (crops and animal feed), and pharmaceuticals [66,67]. These industries use extrusion, single compression cylinders, and centrifugal compression to generate a solid densified product [3]. Pelletization (a) and briquetting (b) technologies are compared side by side in simple schematics in Figure 1-6.

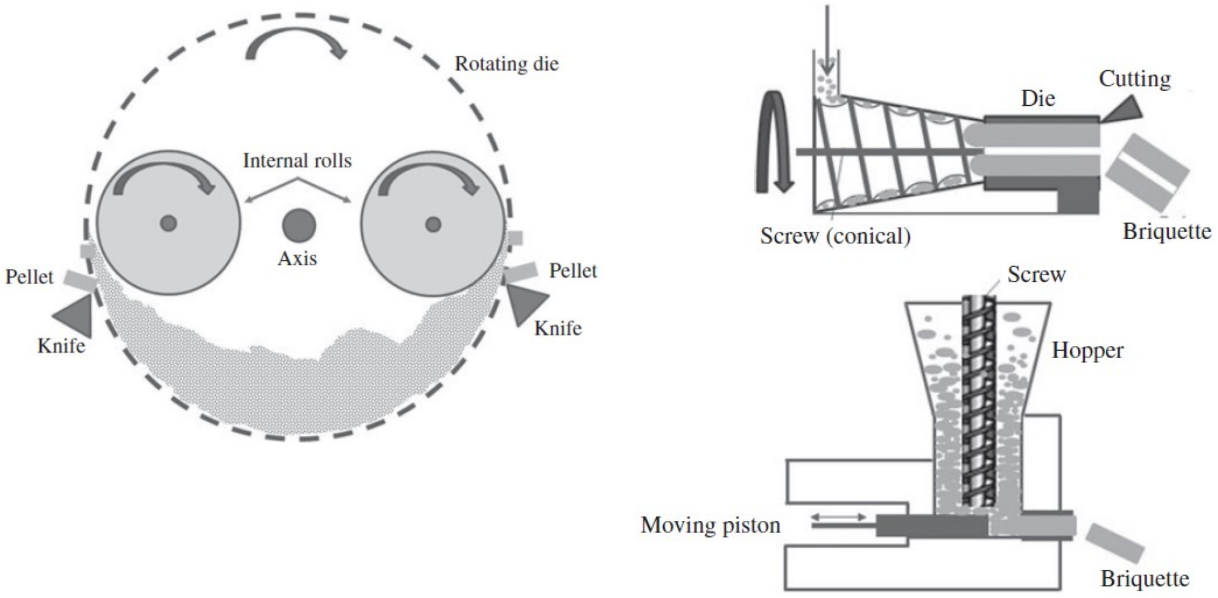

(a) (b)

Figure 1-6: (a) Pelletization by rotating die, and (b) briquetting by extrusion or moving piston.

There are good reasons for spending capital and energy on densification including the increase of energy density (MJ/kg) and geometric uniformity which eases transport, handling, storage, and downstream solid fuel charging (in metallurgical and power industries). In industrial processes, pellets and briquettes are typically the main densified products. Pellets are approximately 6-8 mm in diameter and no greater than 25 mm with a length of 5 to 40 mm. In contrast, briquettes are larger densified products with a diameter greater than 25 mm and a length of 60 to 100 mm [68]. One of the advantages of biomass densification is a reduction of the dust released after the process [3].

When characterizing a good densified product, there are two inter-related key metrics: the durability and the moisture content. The durability of a product depends on the total moisture content (sum of inherent and surface moisture contents); good mechanical strength translates into less material losses before its end use (example: combustion for steam or process

energy generation). Therefore, a good evaluation of coal substitutes should consider the physicochemical properties (energy content) and mechanical properties (durability and hydrophobicity).

1.4. Advanced Solid Biofuel Assessment

Chen *et al*. [69] published a review article in which they note: 1) the lack of a commercial torrefied pellet production facility; 2) the great potential of torrefied pellets to replace coal in thermal processes; and 3) the need to study the "integrated torrefaction and densification (ITD) processes for the production of torrefied pellets". The solid product from torrefaction has a similar volumetric energy density (MJ/m^3) to raw biomass because 1) the energy density (MJ/kg) increases, 2) the envelope density decreases (kg/m^3), and 3) the volume of biomass is not greatly affected; instead the solid becomes more porous resulting from thermochemical reactions at the surface of the pores and the particles [3]. Torrefaction alone leads to an increase in the energy density and hydrophobicity, but the treated biomass has a lower bulk density. Therefore, companies have been investigating means to produce torrefied pellets, but found that torrefied biomass has weaker binding characteristics. Researchers have considered using inexpensive binders or moisture additions to the torrefied material to improve the durability of these advanced solid biofuels [70].

Densification alone can serve to increase the bulk density but does nothing for the hydrophilic surface groups of raw biomass. Industries recognize that there are good reasons for spending capital and energy on biomass drying after the harvest and prior to transportation (entry point to the supply chain). Biomass has a high water absorption capacity, while coal can be shipped with a lower concern for humidity control because its surface is hydrophobic. For example, the biomass moisture content after harvesting is typically 45-55 wt% (wb) and will increase if stored outside [71,72]. Biomass pellets will absorb water and swell leading to disintegration and biodegradation from microorganisms, which is to be avoided at all cost. As a result, some utility companies are forced to spend significant financial resources (tens of millions of dollars) in storage and handling facilities for wood pellets. In turn, this makes the co-firing of biomass pellets with coal an expensive proposition. This makes product characterization of advanced solid biofuels critical when considering alternatives to coal usage.

1.4.1. Product Characterization

The goal of product characterization is to compare results from the laboratory-scale experimental solid biofuel to commercial pellets and briquettes already considered by some industries as a potential fuel source. Qualitative checks can be used to spot any production anomalies.

- The envelope density and compression ratio point to improvements in bulk material transport for industry.
- The solid yield is a quantitative check on the extent of torrefaction in ITD.
- A durability test will compare the strength of the different products which is important to avoid losses during bulk material transport for industry.
- A hydrophobicity test will compare the resistance to moisture uptake which helps evaluate the potential to store fuel outside in temperate climates (which is more cost efficient).

1.4.1.1. Envelope Density

The densification parameters to consider include moisture content, temperature, pressure, density, compression ratio, durability and hygroscopicity. Specifically, densification improves the particle density. Solid fuel density is less straightforward than liquid fuel density because of the nature of solid particles. As a result, a few definitions are used to qualify solid density metrics for different users. Two of these metrics are the envelope density and the bulk density [31]. The envelope density uses the combined volume of the solid, the closed pores, and the open pores as the reference. In contrast, the bulk density uses the sum of the envelope density reference volume and the void space between particles. In this thesis, pellet/briquette density refers to the envelope density. The bulk density will be used for comparisons of fuel transport logistics.

1.4.1.2. Compression Ratio

The compression ratio is defined as the volume of material corresponding to the mass collected ($V_{material}$) divided by the pellet volume. Mathematically, the former volume ($V_{material}$) depends on mass losses (via water vapour and torr-gas) and is expressed in Equation (1-3).

$$V_{material} = \frac{m_{pellet}}{m_{bio}} * V_{bio} \quad (1\text{-}3)$$

In addition, the bulk density is defined as the bulk mass divided by the bulk volume. So, the compression ratio (1-4) can be simplified as follows:

$$Compression\ Ratio = \frac{V_{material}}{V_{pellet}} = \frac{m_{pellet}}{m_{bio}} * \frac{V_{bio}}{V_{pellet}} = \frac{\rho_{pellet}}{\rho_{bio}} \quad (1\text{-}4)$$

A biomass compression ratio after densification can be redefined as the ratio of the envelope density to the starting bulk density (see Section 1.3.4). Theoretically, a woody biomass pellet with a density of 1100 kg/m^3 and a starting bulk density (uncompressed material) of 150-450 kg/m^3 would have an expected compression ratio of 2.4 to 7.3.

1.4.1.3. Solid Mass Yields

The mass loss (1-5) is the opposite parameter to solid mass yield in torrefaction. The mass loss due to the integrated torrefaction and densification is best evaluated on a dry basis to filter the differences in equilibrium moisture contents for various biomass species. Therefore, it represents the complement to the mass of the pellet divided by the starting mass used for pelletization (m_{bio}).

$$m_{loss} = 100 * \left(1 - \frac{m_{pellet}}{m_{bio}}\right) * \left(1 - \frac{m_{water}}{100}\right)^{-1} \quad [wt\%\ db] \quad (1\text{-}5)$$

The moisture content is the mass of water per mass of biomass used before pelletization. By removing the water content from the mass loss quantity, the ITD dry basis mass loss can be used to determine the extent of reaction for each ITD condition.

1.4.1.4. Durability

Product characterization of commercial and in-house laboratory pellets/briquettes was carried out in this work using existing and drafted ISO methods. These standards can evaluate mechanical robustness against shipping and handling routines as well as moisture aversion after production for more flexible storage conditions before fuel usage. In particular, the post-weathered durability describes the strength of an advanced solid biofuel in case of exposure to moisture and ideally should be similar or equal to the as received durability index.

1.4.1.5. Hydrophobicity

The second criterion for good thermally treated pellets/briquettes is the resistance to moisture uptake or hydrophobicity. Industrial operations would incur increased expenses if their

new fuel source (renewable biomass) required additional storage expenses (covered storage) compared to their current fuel source (non-renewable coal). Various laboratories around the world, from Europe to North America, have studied the hydrophobicity problem from various angles [73]. Proposed methods include to: 1) measure the contact angle, 2) use a laboratory rainfall simulation, 3) expose biomass to water using humid air, or 4) use a full water immersion process. To differentiate a good and a poor hydrophobic product, there are some strengths and weaknesses to these four methods as summarized in Table 1-4.

Table 1-4: Proposed methods to determine the degree of hydrophobicity of advanced solid biofuels and how it relates to questions for industrial operations.

Hydrophobicity Test	Method of Water Contact	Relative Severity	Context for Industrial Simulation
Contact Angle	Droplet of surface water	Low	Heterogeneous and porous biomass surface unsuited for measurement
Rain Simulation	Liquid water falling from above	Low	Biomass outdoor piles are exposed to falling rain
Hygroscopicity	Humid air (70% RH)	Medium	Biomass is shipped through warm humid climates (canal shipping lanes)
Immersion	Water surrounding particles	High	Biomass is exposed to a deep, prolonged exposure to water

The common fuel storage strategy in industry is to leave non-renewable coal in a yard which cannot be done with untreated biomass in a wet climate for the same time frame. The hydrophilic biomass fuel will take on more water after drying compared to coal which is hydrophobic and stays dry longer after removing moisture. The successful implementation of biomass as a coal substitute must include ways to economically process renewable fuels along the life cycle of the fuel. Although biomass pellets or briquettes have a lower water re-absorption after drying and densification, the impact of this process varies depending on the presence of hydrophobic or hydrophilic surface groups and the porosity of the material [3,71,72].

1.5. Thesis Objectives

The main goal of this research is to convert low-value Canadian forest and agricultural residues into a consistent and commercially-viable fuel and/or carbon source for heating, generating electricity, or reducing metal oxides. The aims of this thesis are directed at

substituting current fuel sources (especially coal) in full or in part with solid renewable resources – and in particular – advanced solid biofuels in industries including iron/steel, cement and power generation. Current projections suggest that iron production via the blast furnace will continue to dominate the market until 2050 [11]. However, the iron/steel industry is not, in isolation, responsible for the 2016 figure of 43 400 TWh of primary energy derived from coal [7]. The raw material transformations in the cement and mining industries are energy intensive as well. Researchers in the European Union (specifically the Netherlands, France, Belgium, Sweden and Finland), Asia (specifically, China, India, Japan, and Korea), as well as Canada, United States, Brazil, Australia, and Egypt are examining ways to reduce the net carbon dioxide release from industrial processes including using more sustainable carbon from biomass [19,20,74–80]. The organization EUBIONET noted in 2012 that: "One possible solution for those industries could be replacing coal with torrefied wood. The largest potential for increased bioenergy use lies in the cement industry, where the requirements for fuel quality are not so strict." [81].

The conversion process proposed in this thesis should accommodate a variety of biomass feedstocks in order to minimize potential upsets in the fuel supply chain, and generate some potential side products to improve the process economics. For the fuel supply chain, an integrated thermochemical and densification process has the potential to create a homogeneous product from biomass with slightly different chemical compositions in hemicellulose, cellulose, lignin and extractives. One of the key directions in this line of research is the production of quality advanced pellets (or briquettes) that could be stored and handled akin to coal. For the co-product processing route, the bio-oil or tar components could be used as a chemical sealer or binder for biochar pellets or coke briquettes. The specific objectives of this research are:

1) Evaluating three routes to create densified biomass for possible fuel substitution of coal. They include: (a) densification with no thermal treatment; (b) thermal treatment followed by densification; and (c) integrated torrefaction and densification (ITD).
2) Developing micro-scale durability and hydrophobicity protocols that can correlate to the methods of the International Standards Organization (ISO);

3) Evaluating the produced densified biomass for mechanical strength in comparison to commercial densified products;
4) Evaluating the resistance of produced densified biomass for moisture uptake in comparison to commercial densified products; and
5) Determining the drying characteristics of produced densified biomass and commercial densified products.

The International Standards Organization (ISO) is a governing body responsible for "requirements, specifications, guidelines, or characteristics that can be used consistently to ensure that materials, products, processes and services are fit for their purpose" [82]. It consists of technical committees and one such committee publishes standards on solid biofuels, which are of particular importance to this work. The product characterization steps listed above will help identify suitable technologies for renewable solid fuels which energy intensive industries can rely on and still meet demands for their respective markets and consumers.

1.6. Thesis Outline

The second chapter of this thesis presents results related to the production of densified biomass via the three routes (see Section 1.5.1) and further discusses results of the product characterization. The characterization schemes include the qualitative evaluation of the appearance of each product, the pellet/briquette density determination following the compression step compared to uncompressed biomass, the extent of reaction via ITD, and the durability and hydrophobicity of the densified biomass.

The third chapter of this thesis focuses on the hydrophobicity of commercial advanced solid biofuels. In addition, the drying characteristics of advanced solid biofuels at moderate temperatures and fluid velocities was modeled from experimental data. The effects of thermal treatment, initial moisture content, and oven configuration were investigated.

Finally, the fourth chapter of this thesis presents some overall conclusions and recommendations for further study with a continuous laboratory and pilot scale system. Additional research remains to see how the combustion of the proposed fuels compares with conventional coal.

Chapter 2.

Development of Advanced Solid Biofuels for Direct Coal Substitution in Power and Metallurgical Industries

Peter Gaudet[1,2], Guy Tourigny[1], Poupak Mehrani[2] and Jules Thibault[2]

[1]Canmet ENERGY – Natural Resources Canada, 1 Haanel Drive, Ottawa, ON, Canada K1A 1M1

[2]Department of Chemical and Biological Engineering;

University of Ottawa, Ottawa, ON, Canada K1N 6N5

Abstract

Major industries including the metallurgical and power generation are energy intensive, and coal combustion is the current mature technology for many plants. However, the iron/steel, cement and power sectors are searching for a sustainable replacement for coal usage. The industrial-scale combustion of coal is the major contributor to greenhouse gases such as CO_2 which directly contribute to climate change phenomena observed on a global scale. Thus, using biomass to supplement and eventually replace coal as a solid fuel has received a great deal of attention in recent years. Biomass usage is considered more sustainable since the once living organic matter consumed CO_2 during growth. However, biomass solid fuels have a lower energy and material density which make the economics of using them prohibitive at large scale. In this investigation, biomass solid fuels were upgraded by integrating torrefaction and densification (ITD). Loose biomass samples from woody, agricultural, and pulp residues were heated to 300°C with low oxygen concentrations within a single pellet/briquette press and then compressed. Results show that pellets and briquettes produced in this manner have a strong mechanical strength (97-99% durability) similar to accepted commercial materials. In addition, ITD products are less porous and more hydrophobic after a 48 h immersion in water compared to commercial materials (three-fold) and untorrefied materials (ten-fold). The energy content of ITD briquettes improved from 20 MJ/kg to 24 MJ/kg with a compression ratio of 3-6. Future work includes pilot-scale ITD studies to inform industry leaders.

2.1. Introduction

Presently, iron/steel, cement and power production are in high demand for an ever increasing human population looking to build on successes of the 20th century. At the same time, these industries are increasingly aware of the unintended consequences of the Industrial Revolution. Namely, the burning of fossil fuels such as coal, while good for commercial scale efficiency, is contributing to climate change by adding excess CO_2 in the atmosphere. Now, research and development projects around the world are looking to maintain consistent industrial output of desired products while minimizing waste products for optimum sustainability criteria [19,20,26,74–80]. Burning coal is not considered sustainable over a timeline of decades since the rate of formation of reserves is closer to millions of years. A more sustainable direct coal substitution option is biomass which regenerates within decades and consumes CO_2 during its lifetime. To that end, biomass pre-treatment facilities could supply a new solid fuel for industrial energy requirements.

Biomass is sourced from a wide variety of naturally occurring reserves and processed waste residues, but their availability depends on a number of socio-economic factors [3,83]. There are large gaps in biomass transport from source to end-use for any industrial capacity. The bulk density of raw biomass (200 kg/m^3) is lower than coal (800 kg/m^3) [47]. As a consequence, biomass fuel shipments to industry would need larger shipping volumes, leading to higher GHGs during transport, and biomass has a lower energy density (15 MJ/kg versus 25 MJ/kg) which compounds the issue [46]. There are significant knowledge and experience gaps that come from nonhomogeneous feedstocks. However, coal (rank of sub-bituminous and higher) has a high carbon concentration, high energy content, and low fouling ash content [43,44]. These issues with biomass, along with non-homogenous particle sizes, increase the costs of co-firing in a continuous process. There is not a single biomass supply stream that can be thermally treated and used in lieu of coal, which in turn will impact the supply chain for energy intensive industries (power and metallurgical sectors).

There are a variety of processes considered to improve biomass properties of energy and bulk density which, in turn, improve co-firing with solid renewable fuels, and eventually replace coal as a fuel source. Thermochemical conversion of biomass in the absence of oxygen (and

presence or absence of water) can serve to increase the carbon and energy content of biomass. These methods include torrefaction, slow pyrolysis, carbonization, fast pyrolysis, hydrothermal carbonization and steam explosion [3]. While these processes improve the biomass energy content, the product bulk density is low and particle shape distribution is still non-homogenous making transport and continuous combustion challenging. Densification is an energy intensive process but makes up for biomass non-homogeneity by pressing the material into compact defined shapes (small and large cylinders or bricks) also known as pellets or briquettes [65]. Previously, products from thermochemical conversion such as torrefaction and slow pyrolysis have been tested for densification performance to improve biomass as a solid fuel for energy and mass density simultaneously. However, evidence suggests that the binding properties of thermally treated biomass are weaker and therefore need additives such as binders (which can be expensive) or water (which has to be dried off before fuel usage) [70,84]. Product quality shortcomings from torrefaction or densification on their own are partly negated if the final pellet or briquette is also torrefied biomass instead of raw biomass. The purpose of this research is to explore an integrated route for torrefaction and densification (ITD) whereby the resulting biomass solid fuel has an improved energy and material density. The successful biomass solid fuel should be derived from waste biomass residues and the end product should have some homogeneity with coal properties. This would facilitate an industrial transition from fossil fuels in energy intensive industries by minimizing costly infrastructure changes.

2.2. Materials and Methods

Biomass solid fuels made in this study and from commercial sources were evaluated against metrics that are important for the industrial life cycle of solid fuels. The materials used in this research include residues from: 1) CEATI - the Centre for Energy Advancement through Technological Innovation (hardwood sawdust, willow and poplar bark); 2) AAFC - Agriculture and Agri-Food Canada (switchgrass stem and switchgrass leaves); and 3) the Resolute pulp mill (knots, hog, and sludge). These materials were shipped to CanmetENERGY-Ottawa with a particle size range of micrometres to millimetres. The biomass species were received relatively dry (2-15 wt% moisture) compared to the harvested biomass materials found in nature (45-55 wt% wb). Other commercial densified biomass samples (with applied torrefaction and steam explosion pre-

treatments) were sent to CanmetENERGY-Ottawa with the support of industrial partners for an evaluation program of thermally treated materials for energy intensive processes. The ultimate and proximate analysis of each biomass species was performed in advance of sample preparation. Whenever possible, methods of the International Standards Organization (ISO) related to solid fuels were used to test products [81]. Any deviations or modifications of ISO methods are described and justified in this Chapter.

2.2.1. Sample Preparation

The sample preparation included assaying moisture content, particle size distribution, and bulk density which are key metrics for making fair comparisons between potential solid fuels.

2.2.1.1. Moisture Content

The oven dry method was used to assay the moisture content of all biomass samples and commercial materials to isolate any moisture changes that may result from long-term storage (ISO 18134-2). Samples were dried in a Fisher Scientific Class A oven at a heating rate of ~5°C/min to constant mass (within 0.1 wt%) between measurements after 3 and 4 hours drying at 110°C.

2.2.1.2. Biomass Sieving

Biomass sieving was done for two states: commercial pellets needing manual screening before durability assays; and loose biomass used to make ITD pellets (which had a wide particle size distribution). Manual pellet screening (via 5-10 circular movements) was done using a 340-mm diameter round sieve with round screen holes of 3.175 mm (1/8 inch). These specifications are comparable to the ISO standard (ISO/DIS 17831-1) for 3.15 mm round screen holes, and a 400-mm diameter sieve. The loose biomass samples were sieved to a mesh size range (14-28 mesh) in order to narrow the particle size distribution for easy reactor loading, create a more uniform residence time distribution during the experimental work (ISO 18135); and allow for comparisons between different sources.

2.2.1.3. Bulk Density

The bulk density of commercial pellets/briquettes was tested, and the envelope density was measured for micro-batches from the single pellet/briquette press. Pellet densification samples were prepared by adding approximately 1.5 g of material to a 10 mL graduated cylinder of known mass while keeping in mind the fixed chamber volume of the internal die was 10 mL

(target 8.5-9.0 mL of biomass). The mass and volume of each sample was recorded and the sample was added to labelled 1.0 g aluminum tins. Briquette densification samples were prepared in a similar manner using a calibrated 200 mL glass jar and a fixed 40 g of biomass. This protocol differs from the ISO standard on solid biofuel bulk density which requires a minimum of kilograms and is orders of magnitude greater than the sample mass required.

2.2.1.4. Ultimate and Proximate Analysis

Ultimate analysis gives information on the elemental species balance for a given biomass fuel, and like coal, can be used to determine the amount of air needed for combustion [31]. Proximate analysis determines the moisture, volatile matter, ash, and fixed carbon contents which can help to explain the dynamics inside a blast furnace or a steam boiler. Taken together, the ultimate and proximate analysis is required information for energy intensive industries switching to a new fuel source.

The characterization laboratory at CanmetENERGY-Ottawa performed an ultimate and proximate analysis for the three types of biomass (woody, agricultural, and pulp residues). The data for ten raw biomass feedstocks and the pre-torrefied willow are presented in Table 2-1. Pure laboratory grade cellulose was also studied to see the extent of reaction on the single macromolecule. The ultimate and proximate analysis of cellulose fines used for this study were determined from the supplier and literature [56,85]. The macromolecular structure of poplar bark was not measured by the Characterization Laboratory, but a typical yellow poplar bark sample is cited from Jin *et al*. [86].

Two portions of the switchgrass plant (stem and leaves) were used to study ITD and isolated densification effects on agricultural biomass. Hardwood sawdust and low quality woodchips were also considered as a possible feed additive for agricultural biomass densification. Lignin and carbon content are typically greater in woody biomass compared to the agricultural biomass samples, and this is consistent with observations in this study [87]. Woody biomass growth is typically much larger and needs extra strength and rigidity. The total ash and moisture content are presented as measured before densification. All of the biomass sources were loose, pre-densified material, which were densified at different temperatures. The resulting product quality (mainly durability and hydrophobicity) was evaluated (Sections 2.3.6 and 2.3.7).

Table 2-1: Chemical properties and composition of woody, agricultural, pulp waste and cellulose used for ITD/densification [56,85,86].

Chemical Properties	Willow	Torrefied Willow	Poplar Bark	Switchgrass Stem	Switchgrass Leaf	Hardwood Sawdust	Low Quality Woodchips	Hog Fuel	Knot Fuel	Sludge Fuel	Cellulose
Calorific value [MJ/kg][1]	19.3	21.7	20.8	18.7	19.1	18.2	20.4	20.1	19.6	19.9	17.9
Moisture total (wt%)[2]	2.70	1.60	1.80	3.64	3.89	3.41	4.49	5.19	3.23	6.22	2.91
Volatile (wt%)[1]	N/A[1]	N/A[1]	N/A[1]	84.5	81.7	79.0	80.9	77.4	73.4	76.4	93.4
Fixed Carbon (wt%)[1]	N/A[1]	N/A[1]	N/A[1]	14.1	14.5	13.3	17.5	18.0	22.1	18.1	6.10
Ash total (wt%) (575°C)[3]	2.30	2.16	6.37	1.37	3.81	0.36	1.65	4.55	4.54	5.54	0.30
Extractives (wt%)[1]	6.49	7.91	31.8	7.74	N/A[1]	N/A[1]	N/A[1]	N/A[1]	N/A[1]	N/A[1]	N/A[1]
Hemicelluloses (wt%)[1]	18.4	5.59	16.7	26.8	N/A[1]	N/A[1]	N/A[1]	N/A[1]	N/A[1]	N/A[1]	N/A[1]
Cellulose (wt%)[1]	37.9	37.2	31.5	34.7	N/A[1]	N/A[1]	N/A[1]	N/A[1]	N/A[1]	N/A[1]	N/A[1]
Lignin (wt%)[1]	35.6	47.1	18.0	27.4	N/A[1]	N/A[1]	N/A[1]	N/A[1]	N/A[1]	N/A[1]	N/A[1]
Carbon (wt%)	48.2	55.7	51.1	49.0	48.3	45.6	51.1	50.8	49.0	48.8	44.4
Hydrogen (wt%)[1]	5.85	5.82	5.96	6.07	5.84	5.54	6.00	6.07	5.90	6.02	6.22
Nitrogen (wt%)[1]	1.41	0.63	0.62	0.18	0.53	0.11	0.14	0.45	0.13	1.51	0.00
Sulphur (wt%)[1]	N/A[1]	N/A[1]	N/A[1]	0.03	0.04	0.05	0.01	0.00[4]	0.45	0.35	0.00[4]
Oxygen (wt%)[1]	42.4	37.9	35.9	43.4	41.5	41.1	41.1	38.1	40.0	37.8	49.3

[1]The data for the calorific value, structural analysis (extractives, hemicelluloses, cellulose, and lignin), and the elemental analysis were measured on a dry basis, except where the data was not taken, denoted by N/A.

[2]The moisture content was assayed in a single trial the method presented in Section 2.2.1.1.

[3]The ash content was assayed using the TGA and all results are presented on a dry basis.

[4]There was no sulphur content measured for the hog residue.

The total carbon content of raw biomass is in the 45-50 wt% range. However, the important distinction is that the fixed carbon – which is indicative of the energy content – is approximately 15 wt% and improves with thermochemical conversion of biomass. A specific example of biomass upgrading was demonstrated between the ultimate and proximate analysis of untreated and torrefied biomass from the exact same source. The lab received a batch of thermally untreated willow residue and a separate shipment of torrefied willow. The torrefaction conditions (temperature and residence time) were 280°C and 20 minutes. The results show an increased energy and carbon content and a decreased oxygen content as expected. The extent of hemicellulose reactions is relatively large (70 wt%), whereas the cellulose is largely unreacted at 280°C. The lignin content is relatively inert at these temperatures, but increases because of the loss of hemicellulose.

2.2.1.5. Thermogravimetric Analysis

Thermogravimetric analysis permits the study of mass changes resulting from thermochemical conversion. The solid fuels were compared in terms of moisture, volatile matter, fixed carbon, ash content, and the gases evolved during the process in the 100-700°C temperature range. As seen previously in Section 1.3.2 (Thermochemical Conversion), this analysis aligns well with studies ranging from drying to slow pyrolysis and torrefaction to fast pyrolysis and carbonization.

The TGA instrument used in this work was the Discover Model DSCV_TGA. Experiments were conducted under non-isothermal and isothermal conditions to illustrate different effects on the substrate for a given temperature profile. The program used for all non-isothermal experiments included: 1) a step change from ambient temperature to 105°C; 2) isothermal drying for 15 minutes; 3) addition of 50 mL/min of N_2 and a temperature ramp rate of 10°C/min between 105°C and 700°C; and 4) the shutdown. Some isothermal TGA experiments were conducted at 220, 260, and 300°C to simulate torrefaction which is useful for comparison to results in ITD trials. All experiments used 50 mL/min of nitrogen gas to create anoxic conditions expected during the torrefaction or slow pyrolysis.

2.2.2. Torrefaction and Densification

In this work, a single pellet/briquette press (simply a cylindrical batch reactor) was used to create a combination of densified and torrefied products. The purpose of this research was to determine, at bench scale, the mechanical and chemical characteristics of pellets and briquettes created at different conditions of pressure, temperature, and feedstock blend. With insulation and heating tape, the internal reactor temperature could reach 225-300°C for torrefaction. The dry basis solid yield was used to assess the degree or severity of torrefaction which puts results from this work into context with other torrefaction experiments [45,47,88,89].

The assembly consisted of a double acting piston powered from pressurized hydraulic oil (rate = 1.7 cm/s). The piston is inside a barrel rated for 20.8 MPa (3000 psig), but was tested at 0.80-3.5 MPa (100-500 psig). The pressure during the compression stage is related to the cross-sectional area of the reactor and the hydraulic pump gauge pressure set point. In order to make briquettes, and account for the lower solid yield of slow pyrolysis, the internal diameter was scaled up by a factor of 5. The surface area increased and the maximum compression pressure of the single briquette press decreased compared to the pellet press. A bench scale labelled schematic of the apparatus is shown in Figure 2-1.

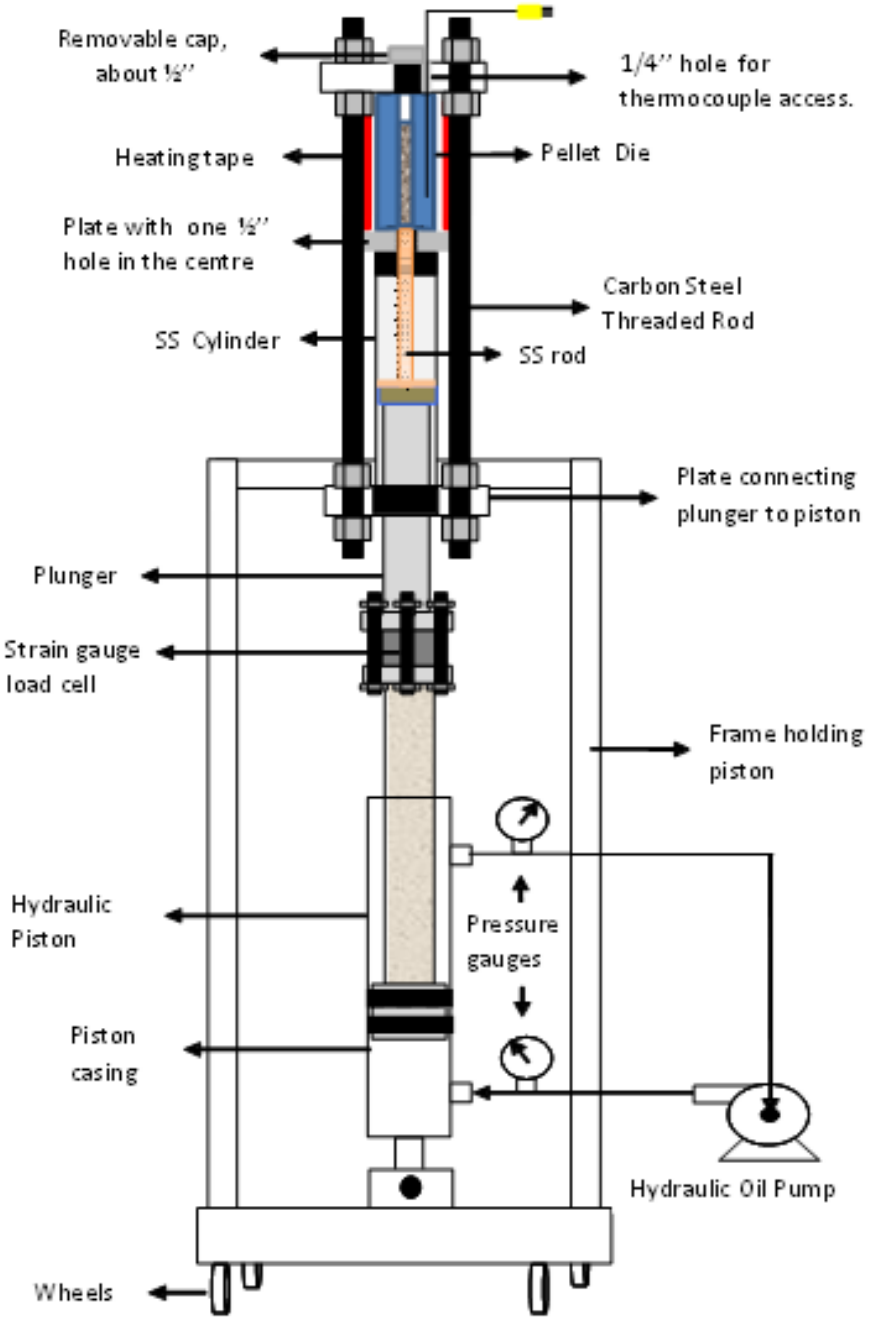

Figure 2-1: Single pellet press schematic with pressure gauge, heating tape and removable cap.

2.2.3. Pellet and Briquette Formation

Table 2-2 outlines the experimental pellet and briquette formation based on 1) biomass sources (woodchips, switchgrass, hardwood sawdust, blends of switchgrass and sawdust, willow, poplar bark, knot, hog and sludge pulp, and cellulose), 2) temperature, and 3) cylinder and applied pressures.

Table 2-2: Scope of experimental biomass, temperature, pressure, and sample sizes tested.

Biomass Source	Temperature (°C)	Cylinder Pressure Applied Pressure[1] (MPa)	Pellet / Briquette	Sample Size (n)
Low Quality Woodchips	250, 300	0.80 40	Pellet	1
Switchgrass Stem				1, 5
Hardwood Sawdust				1, 5
Willow Residue				1, 5
Blends				0, 5
Low Quality Woodchips	50, 150, 250	2.2 125	Pellet	5
Switchgrass Stem				5
Low Quality Woodchips	50, 150, 250	3.5 215	Pellet	5
Switchgrass Fractions[2]	50, 150, 250, 300			4, 5, 8
Hardwood Sawdust	250, 300			5, 6
Willow/Torrefied Willow[3]	90, 145, 200, 250			1, 2, 5
Knot, Hog, Sludge Pulp	120, 220, 260, 300			3, 5
Blends	80, 250, 300			6, 10
Cellulose	80, 250, 300			5
Willow	300, 325	3.5 45	Briquette	4, 6
Poplar Bark	120, 300			5

[1]Applied pressure calculated from the ratio of areas between the piston and the column.

[2]Pellets of switchgrass leaves were produced at 250°C and 300°C; stem tested at all 4 temperatures.

[3]Pellets of pre-torrefied willow were not produced at 250°C in the torrefaction range.

After the reaction, the densified, torrefied biomass was collected from the single pellet/briquette press and its key parameters including envelope density, compression ratio (CR), length over diameter aspect ratio (L/D), and percentage of mass lost (solid yield) were measured. A micrometer was used to measure pellet/briquette diameter and length to estimate its volume. The mass of the pellets and briquettes were measured followed by the envelope density determination based on the assumption of perfect cylindrical samples with known mass (see Figure 2-5, Figure 2-6, and Figure D-2).

2.2.4. Durability

There are ISO specifications that exist to properly evaluate pellet and briquette durability in bulk. However, there is no standard to assess a small batch of pellets (5-10 g range) or briquettes (200 g). Each pellet takes about 15 minutes to process on a single pellet press, and briquette production is 25-50 minutes (depending on the heat transfer). The pellet standard tests

500 g ± 10 g for 500 revolutions ± 20 to match shipping and handling stress encountered by pellets during transport. Briquette durability methodology uses 10 kg at 25 rpm. This fact motivated protocol development studies for in-house products. The methodology included the use of a custom bench top tumbler, a commercial pellet tumbler, and a custom briquette tumbler, and the latter two specifically meet ISO standards (in Table 2-3).

Table 2-3: Comparison of durability methods for in-house batch products and commercial shipments.

Design Characteristic	Units	Bench Top Tumbler	Commercial Pellet Tumbler	Custom Briquette Tumbler
Rotation Speed	rpm	50	50	25
Chamber Volume	L	0.3	12	390
Mass Pellets Charged	g	5-10	500	10000
Production Time/Exp[1]	h	1-3	125	200
Baffles Present	N/A	No	Yes	Yes
Surface Material	N/A	Plastic	Stainless Steel	Stainless Steel
Surface Roughness	N/A	Smooth	Sharp edges	Sharp edges

[1] Production time per experimental condition to produce enough product for a single ISO measurement.

The purpose of the standard durability test is to compare how the structural durability compares between different advanced solid biofuels. This test identifies the weight fraction of fine powder compared to the quantity of starting material after a certain amount of material handling (2-1). Results of this test are used to determine the degree of handling and storage risks associated with each product and, more particularly, the formation of fines which are considered a safety hazard. The pellet/briquette durability index (PDI/BDI) is defined as the ratio of the remaining mass of pellets/briquettes (less the fines from tumbling) and the initial mass of the pellets/briquettes (P/B).

$$Durability = 100 * \frac{m_{P/B-fines}}{m_{P/B}} \quad [wt\%] \tag{2-1}$$

All durability testing was done alongside positive controls (commercial pellets and briquettes). Small scale pellet durability was tested using the bench top tumbler, and similar work was done by Schilling *et al*. [90]. The protocol development work is supported in Appendix B. The commercial pellet tumbler was used for bulk pellet durability and small-scale briquette durability.

2.2.5. Hydrophobicity

The purpose of this test is to compare the hydrophobicity of pellets/briquettes produced from different sources and put that measure in context with common ranks of coal [47,49]. The International Standards Organization is currently developing a hydrophobicity protocol. The goal of the ISO work is a standardized method that can be performed in a relatively short time frame and still identify the degree of hydrophilicity risk associated with candidate advanced solid biofuels (ASB) for energy intensive industries (similar to the final document on pellet/briquette durability). Similarly, SECTOR (the Solid Sustainable Energy Carriers from Biomass by Means of Torrefaction) is interested in quantifying hydrophobicity for members of the European Union.

As with the durability assays, protocol development work was key for assessing experimental samples from the single pellet/briquette press. Commercial pellets/briquettes were available in bulk to assess the repeatability of the assay. In this work, the total water absorption of each material was evaluated by using rainfall simulation or immersion. The methods used in this thesis at different scales are compared in Table 2-4.

Table 2-4: Differences in hydrophobicity methods for different scales of available material [73].

Hydrophobicity Test	Pellet / Briquette	Biomass (g)	Water Volume (L)	Container Area (cm^2)
Rain Simulation	Pellet	6-25	0.06	20-80
Rain Simulation	Both	500	0.25	70
Immersion CANMET	Pellet	6-25	0.125	80
Immersion CANMET	Both	200-600	4.50-5.00	960
Immersion SECTOR	Pellet	600	2.50	960

The measure of hydrophobicity, via the hydrophobicity index HPI, is defined as:

$$HPI = 100 * \frac{m_{wet\ ASB} - m_{dry\ ASB}}{m_{dry\ ASB}} \quad [wt\%\ db.] \tag{2-2}$$

Two semi-batch rain simulation setups were designed in-house (CanmetENERGY-Ottawa) by the Bioenergy Systems Group (see Section 2.2.5.1). Two water immersion experimental setups were adapted from a reference SECTOR method (see Section 2.2.5.2): Water Absorption-Immersion Test for testing commercial materials in bulk [73]. In all cases, a sieve or Buchner

funnel was used to separate surface moisture before evaluating the mass change after water uptake. Using these experimental setups, it is possible to account for the formation of fines after the water exposure test period.

2.2.5.1. Rain Simulation

The rainfall simulation method was employed for two reasons: 1) a low severity simulation of water exposure for pellet samples with unknown moisture resistance; and 2) a method that could better simulate a real-world situation. If a coal or pellet yard pile was left uncovered and a large fraction was submerged in water, the sample integrity would likely be compromised by oxidation and microbial degradation. Two semi-batch versions of the rainfall simulation or shower test are shown in Appendix C, Figure C-2. For the burette testing, the sample mass was recorded (± 0.01 g), and the pellets were placed in a monolayer underneath the water source and Buchner funnel. The average water flow rate was 0.5 g/s from when water first started hitting the pellets (the residence time was 2 minutes). The endpoint was recorded when the water stopped falling. Finally, the pellets were collected and laid out carefully on a Buchner funnel for 30 minutes. After the hydrophobicity test, the mass of water collected in the pan, the mass of the wet pellets, and the laboratory temperature were recorded. The pump version (Figure C-2b) mirrors water flow to match 1 mm/min of rain for a total of 750 mm [91].

2.2.5.2. Immersion

In the immersion test, a number of pellets are completely immersed in a container of stagnant water, where pellets are completed surrounded by water. This method – developed by the researchers of the SECTOR project – requires a sufficiently large pan to contain 600 g of pellets with an approximate bulk density of 750 kg/m^3 plus 2-3 times that volume in water [92]. The immersion assay was scaled down by a factor of 20 based on the number of samples available from the single pellet press (see Figure C-2). During protocol development, a full 25 g of steam exploded pellets were placed in a monolayer. During pellet testing, 6 g of pellets were immersed if that was the total mass after production. The pellet sample (mass ± 0.01 g) was placed in a 200 mL dish, and then 2-3 times the volume of deionized water (120-140 mL) was added. The pellets were gently pushed to the bottom of the dish (2-3 cm below the surface), and then the start time

was recorded. The test portion was allowed to sit for 60 minutes, and the water-soaked pellets were transferred to a Buchner funnel and allowed to rest for another 30 minutes.

2.2.5.3. Post Weathered Durability

A final metric described as post-weathered durability allows for a mechanical strength comparison between the original sample and the sample stressed by a hydrophobicity test. All post-weathered durability tests were done immediately after the incubation at ambient conditions for 30 minutes (on a Buchner funnel). This period allows the surface moisture to fall off the pellets which – if present during tumbling – may cause fines to adhere to the pellet surface and bias the results of the testing.

2.3. Results

In this thesis, biomass upgrading processes were investigated using common methods in literature (example TGA, torrefaction, and densification), and uncommon methods (durability evaluation from 5 g batches). All statistical analysis, where applicable, were tested at a 95% confidence level. The average value (± the standard deviation) will be used to show the range of uncertainty. The ultimate and proximate analysis of woody, agricultural, and pulp residue biomass show the starting point for raw materials that are energy deficient compared to coal (Section 2.3.1). Section 2.3.1 will present data on micro-scale thermogravimetric analysis (TGA). Section 2.3.2 and 2.3.3 will introduce the topic of integrated torrefaction and densification (ITD) as a means of biomass upgrading. Sections 2.3.4 and 2.3.5 will focus on studies of quantitative densification (pelletization and briquetting respectively). Section 2.3.6 will focus on examining the durability metrics of pellets and briquettes. Finally, Section 2.3.7 will focus on hydrophobicity for pellets and briquettes.

2.3.1. Thermogravimetric Analysis

Before testing materials in a lab-scale or pilot-scale thermochemical conversion process, a comparative study of the thermogravimetric profile was performed for different solid fuels. The particle size distribution is kept constant (14-28 mesh) so that comparisons of reaction rates and solid yields were viable between biomass sources.

2.3.1.1. Non Isothermal: Dry Basis

Agricultural and woody biomass (Table 2-1) were studied by thermogravimetric analysis in triplicate to determine the maximum devolatilization rate and corresponding temperature on a dry basis. The data was studied using the evolution of gaseous products over the reaction coordinate and the rate of devolatilization (dm/dt). The analysis shows that the maximum devolatilization rates occur at approximately 360°C for all samples, as shown in Table 2-5.

Table 2-5: Maximum devolatilization rates and optimum pyrolysis temperature by reaction rate.

Biomass	Maximum Reaction Temperature (°C)	Reaction Rate (wt%/min)
Switchgrass Stem	358.1	-12.05
Switchgrass Leaf	356.9	-11.15
Hardwood Sawdust	364.6	-12.77
White Birch	362.4	-12.24
Hog Residue	356.6	-10.34
Knot Residue	356.6	-10.18
Sludge Residue	359.8	-9.71

Non-isothermal TGA of the six samples (excluding white birch) is presented in Figure 2-2. The standard error bars (black curve surrounding the weight percent curve in Figure 2-2c, d) show the degree of uncertainty in the biomass reaction rate. The uncertainty is significant between 250°C and 370°C where the chemical reaction is most rapid. In all data sets, the rate of reaction decreases by a factor of 10 between 370°C and 400°C.

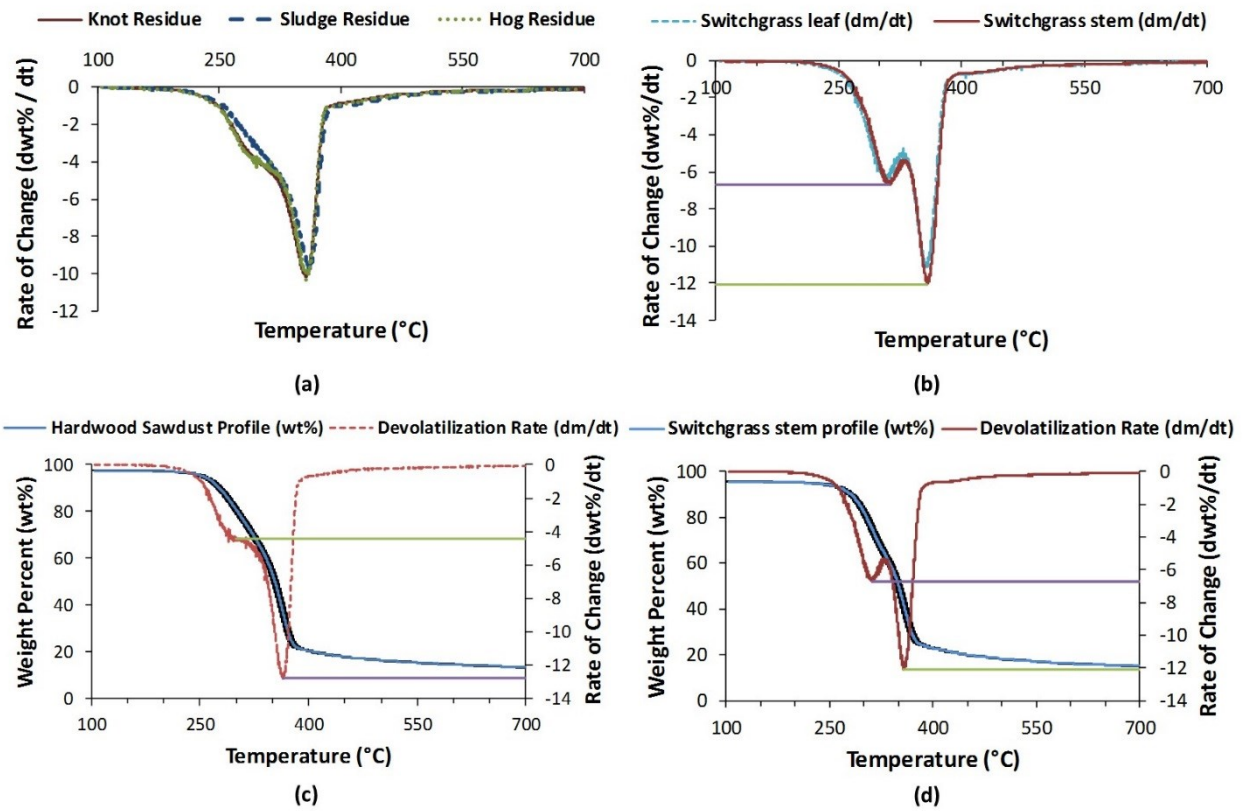

Figure 2-2: Non-isothermal TGA (105-700°C), showing the devolatilization rate (dm/dt) as a function of temperature (°C) (at heating rate of 10°C/min), for 6 biomass residues. In addition, the mass loss (wt%) is shown as a function of temperature for (c) hardwood sawdust and (d) switchgrass stem.

The results from the non-isothermal pulp and paper TGA experiments shed some light on the effect of the pulping process on the macromolecular structure (Figure 2-2a). Specifically, some comparisons can be made between the knot and hog fuel versus some typical hardwood residues (see Figure 2-2c). A typical hardwood upon harvesting would likely maintain its natural structure at the macromolecular level (leaving more material to react at 360°C). Knot and hog residues are by-products from the initial stages of the pulping process (milling and digestion) and experience comparably less processing compared to sludge [93,94]. Secondly, while the hog and knot residues have similar non-isothermal devolatilization profiles, there is a notable distinction with the sludge residue. The reaction rate has two distinct linear regions (260-330°C; 340-360°C) and the average rate of change (between 260°C and 330°C) is greater for the sludge residue compared to the other pulp residues. Effectively, the sludge residue is broken down significantly more compared to knot and hog residues thus exposing lots of functional groups to thermochemical conversion [95–97]. A comparison of two switchgrass fractions (leaves and

stem) show the reaction rates are quite similar as seen in Figure 2-2b. Second, the switchgrass stem devolatilization rate data shows a local minimum at approximately 310°C of -6.7 wt%/min and a global minimum at approximately 360°C of -12.1 wt%/min (Figure 2-2d). In contrast, an inflection point can be seen in the data with hardwood sawdust at 300°C (Figure 2-2c). A second difference to note is the maximum reaction rate in hardwood sawdust was observed to be -12.8 wt%/min Figure 2-2c), which may be related to differences in the shape or structure of the particles.

2.3.1.2. Isothermal: Dry Basis

Switchgrass stem was studied by isothermal thermogravimetric analysis in triplicate at 300°C. At the onset of the TGA experiment, 10 mg of switchgrass stem was dried for 15 minutes at 105°C (data not shown). Secondly, the temperature was ramped at a rate of approximately 130°C/min to its final constant test temperature where it was held constant for 30 minutes (see Figure 2-3). This test provides experimental conditions that prevail in a batch reactor such as the single pellet press.

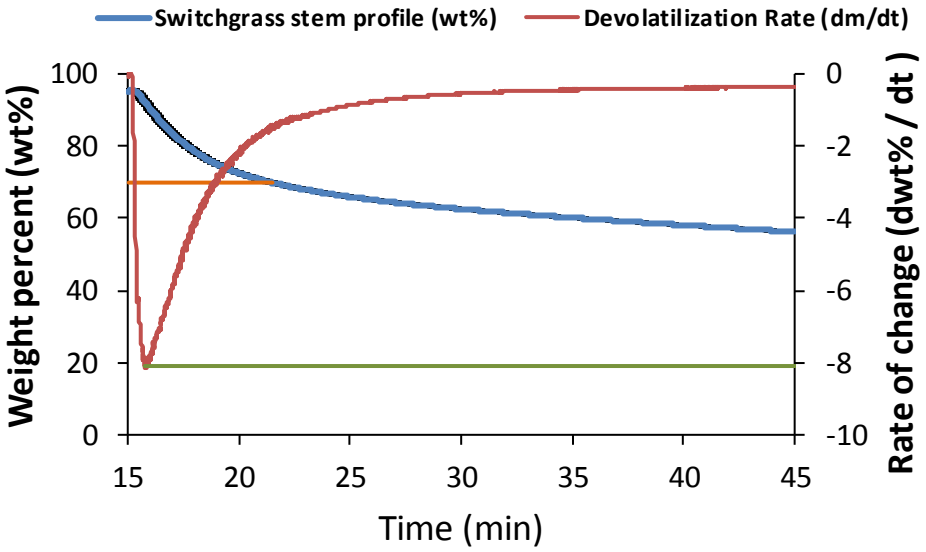

Figure 2-3: Isothermal switchgrass stem TGA (300°C) for 30 minutes performed in triplicate. A span of five minutes gives a 30 wt% loss by torrefaction (orange). The maximum devolitization rate is in green. The same test was repeated at 260°C in Figure D-5.

The rate of reaction increases quickly when the biomass is subjected to the anoxic conditions in the furnace at 300°C. The maximum slope of the devolatilization rate in (-7.2 wt% / min^2) is within the first minute from the step change (comparable to Figure 2-2b). After five

minutes in the TGA at 300°C, the switchgrass stem lost about 31.6 wt%. In comparison, the same species lost 8.8 wt% at 260°C (see Figure D-5). The rate of torrefaction significantly decreases after five minutes in the TGA and the reaction is very limited from 10-30 minutes of isothermal conditions.

2.3.2. Torrefaction and Extrusion

The investigation of switchgrass stem torrefaction using the single pellet press as a microreactor provided the foundation for further studies in this field known as integrated torrefaction and densification (ITD). The results of torrefied switchgrass stem in duplicate at two temperatures are given in Table 2-6.

Table 2-6: Micro reactor torrefaction results at 250°C and 300°C for switchgrass stem.

Torrefaction Temperature (°C)	Particle size distribution % (Above the 3.15 mm sieve)	Average of Mass Loss (wt% db)	Standard Deviation (Mass Loss)
250	49.0	8.0	1.0
300	55.6	30.9	0.5

A partially formed pellet was observed at the bottom of the die after loose torrefied biomass was extruded out with the piston. At both temperatures, about half the remaining mass formed a pellet and the balance remained as uncompressed fines. The solid yield was compared with the initial biomass loaded into the microreactor. The torrefaction severity was observed as a function of temperature as expected. Photographs of the resulting products for both temperatures are shown in Figure 2-4.

(a) **(b)**

Figure 2-4: Torrefied switchgrass stem at 250°C (a) & 300°C (b) extruded from the single pellet press with an applied pressure of approximately 10 MPa.

At a temperature of 250°C, the switchgrass stem retains its original light brown colour and a higher percentage of biomass remained as fines (see Figure D-1d). At 300°C, the discolouration is significant leading to a dark brown colour and a higher proportion of material forms a densified pellet. The colour changes and the formation of a partial pellet is significant. The evidence suggests that combining densification following torrefaction could make strong pellets with: 1) an energy density (MJ/kg) higher than simple densification; and 2) enhanced durability compared to torrefaction alone. High temperatures (250-300°C) experienced in densification processes cause the partial softening of feedstock constituents. The melting of these constituents facilitates molecular diffusion between particles at heightened temperatures. As the densified product cools, the melted constituents solidify and form solid bridges similar to sintering in the metallurgical field. In addition, the activation of the inherent binders in the feedstock (lignin, proteins, and starches) promotes the formation of solid bridges and thus particle agglomeration [84]. These solid bridges largely determine the strength of the final products [98]. These results help distinguish the effect of treating biomass at elevated temperatures and the subsequent pressurization to make pellets. The evidence suggests that the chemical reactions during torrefaction and the frictional force exerted during extrusion (45 kN or 10 MPa of applied pressure [99,100]) are enough to begin forming solid bridges between particles. This observation and its effect on durability, hydrophobicity, and energy content was studied for a variety of different biomass sources.

2.3.3. Qualitative Densification

Integrated torrefaction and densification (ITD) was studied for the formation of pellets and briquettes. The first four elements of product characterization (qualitative results, density, compression ratio, and solid yield determinations) were noted immediately after production of a single sample (Section 2.3.4 and 2.3.5). The last four product metrics include proximate analysis, durability, hydrophobicity, and drying curve profiles (Section 2.3.5-2.3.7 and Chapter 3). Durability and hydrophobicity were studied for both pellets and briquettes. The drying curve profiles and proximate analysis were done only for briquettes because each individual briquette was 20 times larger: appropriate for the analytical methods used (mass balance and ASTM methods). Pellets and briquettes were produced in five replicates for a given experimental

condition unless otherwise noted. Two reasons for producing less than five replicates include limited resources and unformed pellets at a given condition. This will be discussed more in Section 2.3.3.

2.3.3.1. Pelletization

Qualitative results can demonstrate product mechanical strength moments after formation as seen with the results from Section 2.3.2. Pellets were first produced using the highest pressure set point (215 MPa) which should give the best-case scenario for this metric. This analysis was done for eight materials from Section 2.2.1.4 and the results are presented in Figure 2-5. The average aspect ratio for all samples was 2.3 (± 0.5).

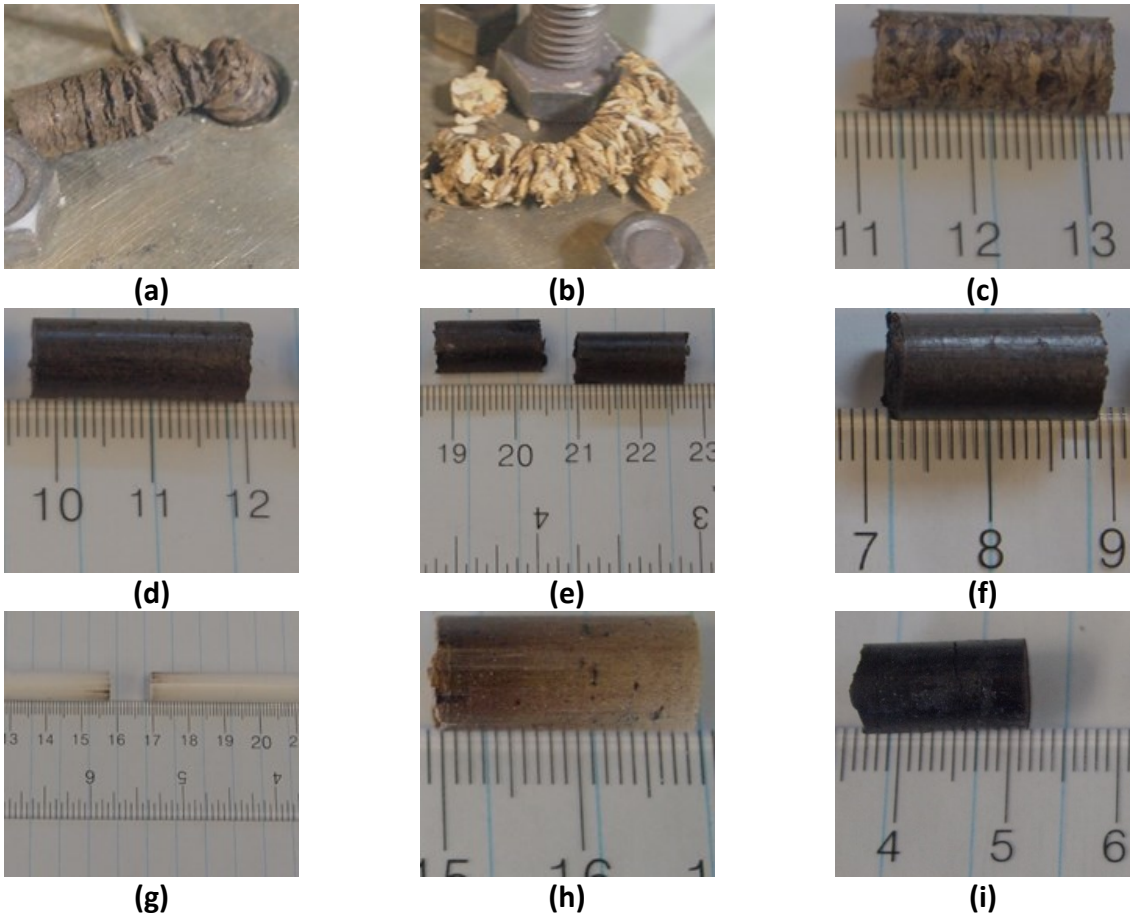

Figure 2-5: Qualitative pellet results for 5 biomass materials (woody, agricultural, pulp, and cellulose). (a) Pelletization for wet torrefied willow at 90°C; (b) untreated willow pelletization tested the same as in (a); (c) untreated willow with 2 wt% moisture at 200°C; (d) torrefied willow pellets produced the same as (c); (e) two switchgrass stem pellets at 300°C; (f) sludge pulp residue at 300°C; and pure cellulose produced (g)-(i) at 80, 250, and 300°C respectively. All pellets presented produced at 215 MPa. Additional qualitative results available in Figure D-2.

Qualitatively, willow and torrefied willow pellets produced at 90°C and 2 wt% moisture shattered after a simple drop test. When moisture was added to torrefied (Figure 2-5a) and untreated willow (Figure 2-5b), the pellet would not form at 90°C. The unsuccessful binding and densification in Figure 2-5 (a) and (b) was not observed as the remaining experimental conditions were made at mid to high range densification temperatures. Representative images of the biomass pellets produced at 200°C are given in Figure 2-5 (c) and (d). Qualitatively, the pellets produced from willow and torrefied willow topped up to 20 wt% moisture were identical (data not shown). Willow residue pellets produced from pre-torrefied willow (280°C) that was cooled and densified have the same qualitative result as ITD willow residue pellets (300°C) in Figure D-2i. Similar results were demonstrated with 1) the AAFC blends of switchgrass stem with hardwood sawdust (produced at 250°C and 300°C); 2) pulp residues (produced at 220, 260, and 300°C); and 3) pure laboratory grade cellulose (produced at 80°C, 250°C, and 300°C). The cellulose pellets changed colour from white to brown to black with increasing temperature beyond 80°C (Figure 2-5 g-i), which matches previous work in literature [45].

2.3.3.2. Briquetting

The production of briquettes by ITD demonstrated similar results with a few differences in methodology (Figure 2-6). The scaled up press diameter correspondingly had an impact on the maximum applied pressure (45 MPa), and the residence time (25-45 minutes). The aspect ratio was 0.6 ± 0.2 compared to pellets (2.3 ± 0.5).

Figure 2-6: Qualitative briquette results for 4 biomass materials (primary and tertiary sources) produced at 45 MPa. Integrated torrefaction and briquetting shown in (a)-(d) and low temperature briquetting (e). (a) Strong and (b) weak willow briquettes, (c) construction and demolition waste, and (d) poplar bark tests ranged from 300-325°C. (e) Poplar briquettes with (bottom) and without (top) tar binder shown at 120°C.

The briquettes' ITD residence time was increased to 25 minutes for willow (Figure 2-6a) and 40 minutes for poplar (Figure 2-6d) and show the same qualitative colour changes. Some

willow bio-briquettes formed, albeit with poor quality, during the ITD process (Figure 2-6b). When this happened, excess oxygen was drawn into the system, and the reactor temperature increased substantially above the 300°C set point. Finally, the non-ITD tests on poplar bark were done with (Figure 2-6e, bottom), and without (Figure 2-6e, top) a slow pyrolysis tar binder additive (at 10 wt%). A single briquette was produced from construction and demolition waste (Figure 2-6c), but no further quantitative analyses were done. The results, taken together, suggest that pellets or briquettes produced via ITD look similar to the pre-torrefied willow pellets that were densified after cooling (Figure 2-5c). Furthermore, it is clear from the pellet and briquette ITD qualitative results that compressing biomass after a hot, dry torrefaction produces a glossy surface that appears more homogeneous and less porous. This is an important observation that will be discussed again when comparing ITD and non-ITD samples for hydrophobicity.

2.3.4. Pelletization and Integrated Torrefaction

The temperature effect on densification includes three zones: 80-90°C (low temperature drying), 145-220°C (high temperature drying), and 250-325°C (ITD). One sample of torrefied willow produced for the Bioenergy Systems Group (CanmetENERGY-Ottawa) was already cooled prior to densification. The densification of the cold torrefied willow is different than ITD, and the effects of this process difference were studied for all product characterization metrics. Second, blending feedstocks was considered to improve the strength of a single pellet/briquette. For example, the densification of materials like switchgrass is more difficult than woody biomass in part because of the differences in biomass fibre composition (hemicellulose, cellulose, and lignin). Two potential remedies were investigated to overcome this challenge including: 1) a blended pellet feed containing agriculture residue and woody biomass; or 2) integrating torrefaction and densification. For the first proposition, a hardwood sawdust was chosen as the blended feed for switchgrass stem pellets. This research is of interest to AAFC looking to find use for switchgrass as a fuel crop. For the second proposition, pellets were produced at 215 MPa using different harvests from a switchgrass cultivar: switchgrass stems and leaves. The different fractions on the switchgrass plant have different chemical compositions, which may influence the binding characteristics between particles. In the torrefaction regime, a mid-point (250°C) and

high-point (300°C) temperature were chosen with consistent residence times (5 minutes) to Sections 2.3.1.2 and 2.3.2. Third, a pressure scheme was devised using a low point (40 MPa), a mid-point (125 MPa), and a high point (215 MPa) to confirm the extent of differences in applied pressure to the biomass. Finally, the moisture content was deliberately tested by adding deionized water before densification to improve pellet properties. This is a common practice especially for torrefied materials which tend to need specialized densification conditions [70]. Unfortunately, adding moisture during this stage requires extra drying before pellet/briquette fuel usage, so sometimes binders are considered for this effect. In this study, torrefied and untreated willow were tested at a uniform 2 wt% and 20 wt% moisture content. The pulp and paper residues (hog, knots, and sludge) were tested as received and at a 15 wt% moisture content. All other samples were tested at the sampled moisture content (2-6 wt%).

2.3.4.1. Quantitative Density

Pellet and briquette envelope density (see Section 1.3.4) is a function of the bulk density. Shipping coal for fuel is more economical compared to biomass in part because the logistics of transporting low bulk density biomass are prohibitive. The bulk density was not measured because the single pellet/briquette press has a low throughput. The samples were assumed to be uniform cylinders, and simple mass and length measurements were used for Figure 2-7.

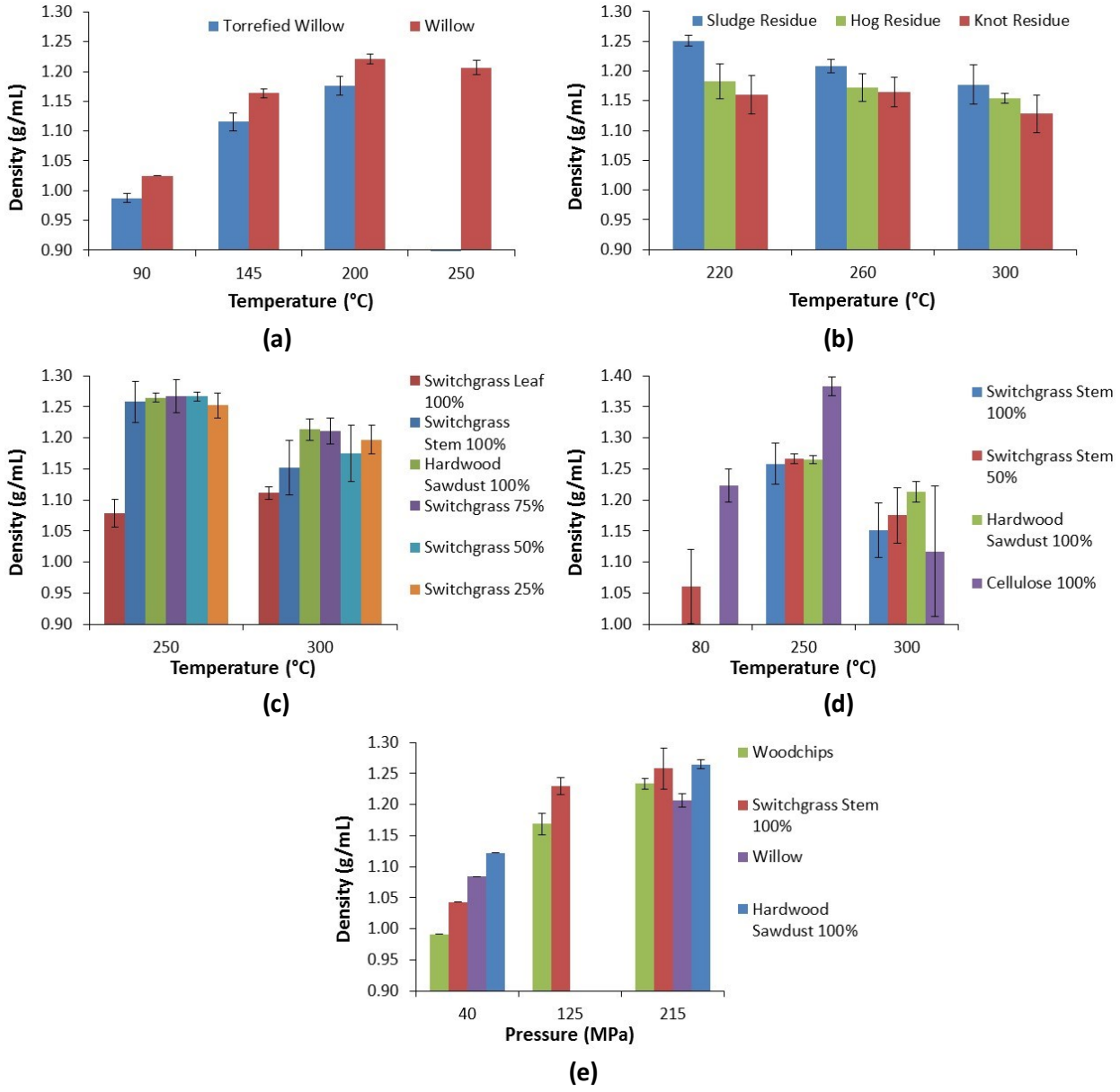

Figure 2-7: Pellet densities for 8 biomass residues. Relationships in (a)-(d) for temperature at constant pressure (215 MPa), and (e) for pressure at constant temperature (250°C).

These measurements are representative of commercial materials used for protocol development and positive controls [1.08 to 1.22 g/mL]. For example, a commercial steam exploded pellet has a density of 1.14 g/mL (Appendix D: Table D-1). First, the temperature effect is more noticeable on willow pellet density (Figure 2-7a) and compression ratio (data not shown) in non-ITD conditions. The pellet density comparison between willow and torrefied willow (at 145°C and 200°C) has a p-value less than 0.002. Second, the ITD sludge residue pellet density is

significantly different than the other two pulp and paper residues ($p < 0.05$) regardless of temperature (Figure 2-7b). Third, experiments testing agricultural biomass pellet blends in the ITD range (Figure 2-7c) show an optimal density at 250°C (average = 1.26 g/mL ± 0.02) rather than 300°C (average = 1.19 g/mL ± 0.04). Next, the densification of pure laboratory grade cellulose seems to indicate that lignin is not the only factor in quality pelletization or briquetting as has been suggested in literature [101]. The cellulose particle size is finer compared to the woody, agricultural, and pulp residues, but lacks lignin to aid in binding. The density of cellulose pellets (Figure 2-7d) produced at 80°C is greater than steam exploded pellets, and the density observed at 250°C is greater than any other pellets produced during this thesis. Finally, some quality ITD pellets were produced at the low to mid-range pressures (40, 125 MPa) at 250°C from woodchips, sawdust, switchgrass, and willow (Figure 2-7e). When the pellet density data for an individual biomass source was compared between 250°C and 300°C, the scope of the difference was 0.01-0.05 g/mL or 10-50 kg/m^3. As expected, the density increased with increasing pressure. The density was similar to typical woody biomass pellets (1.1 g/mL) but varied as a function of the applied pressure, and the type of biomass (which shows variance in lignin, cellulose, and hemicellulose depending on the source). The results show that the density is a stronger function of pressure [40-215 MPa] compared to temperature [250-300°C] at ITD conditions.

2.3.4.2. Quantitative Solid Yields

Torrefaction is a process with a solid yield significantly less than 100% and the literature discussed in Chapter 1 shows how thermochemical conversion process yields are a strong function of temperature. The analysis of dry basis mass losses for all samples is presented in Figure 2-8.

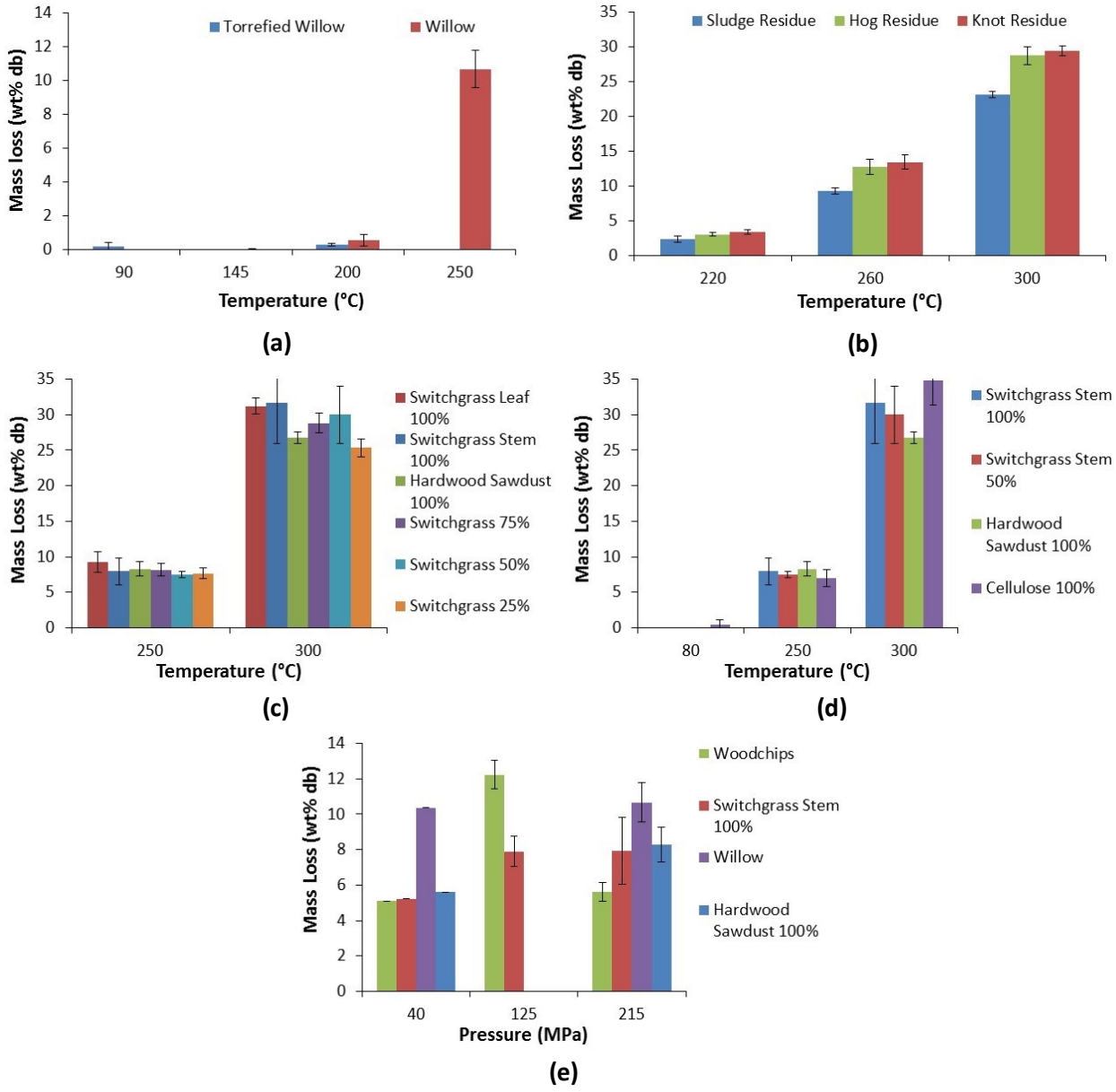

Figure 2-8: Dry basis mass loss for 8 biomass residues. Relationships in (a)-(d) for temperature at constant pressure (215 MPa), and (e) for pressure at constant temperature (250°C).

The impact of integrating torrefaction with the densification process for willow, switchgrass stem/hardwood sawdust blends, and pulp residues is important for creating a new homogenous fuel. The observed torrefaction yield shows minimal statistical differences between the three fractions (willow, switchgrass/hardwood blends, and pulp residues). For each pellet that was produced from 250-300°C, gases were expelled to a ventilation system during pellet formation and extraction. The average dry basis mass loss observed upon forming each pellet

blend was 8.0-12.0 wt% at 250-260°C and 28.9 wt% at 300°C; typically, the mass loss observed in torrefaction is close to 30% [89]. Finally, a mild torrefaction of cellulose occurred at 250°C compared to a typical torrefaction at 300°C (Figure 2-8d). The cellulose reaction was less pronounced at 250°C because rapid reaction rates begin at higher temperatures (280°C), and the pure laboratory grade cellulose lacks the reactive hemicellulose. In general, cellulose reacted similarly during a five minute torrefaction than switchgrass plants (34.8 wt% mass loss compared to 31.4 wt% respectively).

The expectation is that the applied pressure does not impact the solid mass yield, but it is a strong function of temperature. First, willow pellets lost about 10 wt% upon treatment at 250°C (Figure 2-8a, e) and 28.3 wt% at 300°C (data not shown), regardless of the production pressure. The mass loss observed at 40 MPa is appreciably similar to pellets produced at 215 MPa (Figure 2-8e). Second, pulp residues were assessed at three temperatures to see the gradient of torrefaction severity and solid yield. A typical differential thermogravimetric (DTG) curve suggests that the relationship between solid yield and temperature is exponential, and (Figure 2-8b) shows this ($R^2 > 0.97$). The limit of integrated torrefaction and densification was observed at the 200-220°C boundary. It is clear that there is very low conversion at less than 220°C (residence time 5 minutes) for pelletization (Figure 2-8a, b). Third, mass loss observed between the switchgrass leaves and stem at two production temperatures (Figure 2-8c) was very similar (p value > 0.22). In comparison, a single switchgrass pellet produced from a mesh size greater than 28 had a mass loss of 16 wt% at 250°C. This observation follows from the decrease in particle size and the corresponding larger surface area and faster reaction rate. Finally, the starting moisture content of the biomass blends was 2-6 wt% most of which would be lost to evaporation at these temperatures. Macroscopically, the untreated and torrefied willow each showed a mass loss of about 2 wt%, and similar results were seen with cellulose at 80°C (Figure 2-8d).

There is some consistency in the data between the thermogravimetric (TGA) results and the integrated torrefaction and densification results (ITD). Isothermal TGA studies were done at the same ITD temperatures for switchgrass stem and pulp residues. For switchgrass stem data, the mass loss was 7.9 wt% db. at 250°C (ITD), and 8.8 wt% db. at 260°C (TGA). When switchgrass stem particles were tested via ITD and TGA at 300°C, the mass loss was statistically similar (p =

0.50). Among the three pulp residues, sludge has the highest mass yield in both TGA torrefaction (see Section 2.3.1) and from ITD testing (see Figure 2-8b) regardless of temperature. Although, TGA data suggests hog residue was more reactive, ITD experiments show statistically similar reactivity ($p > 0.07$). As seen in Section 2.3.1, the hog residue and knot residue TGA curves were almost identical, and both experienced a greater mass loss than sludge. Therefore, it seems most likely that knot and hog residues react similar to each other during torrefaction. Finally, the average ratio of pulp residue yield in the TGA versus ITD for all three temperatures and residues was 0.97 ± 0.20. This suggests that the results from the TGA and ITD are appreciably similar in terms of predicting the thermochemical conversion yields.

2.3.5. Briquetting and Integrated Torrefaction

From an industrial point of view, briquettes are less expensive to produce than pellets which is of interest since biomass sources are already more expensive than non-renewable resources like coal. From an experimental point of view, these briquettes were large enough to get proximate and ultimate analysis. A single pellet weighed one gram or less while the briquettes weighed around 20 or 30 g. This is important for assessing the severity of the torrefaction with respect to the higher heating value (HHV). The HHV on a dry basis (db) can be estimated using the IGT formula (2-3) [31]. The severity factor (SF) assumes a first order reaction rate, and the integral form is in (2-4) (see Figure D-4).

$$HHV_{db} = 0.341X_C + 1.323X_H + 0.0685 - 0.0153X_{ash} - 0.1194 * (X_N + X_O) \quad (2\text{-}3)$$

$$SF = \log_{10} R_0 = \log_{10}\left[\int_0^t \exp\left(\frac{T(t) - 100}{14.75}\right) dt\right] \quad (2\text{-}4)$$

The IGT formula is based on the biomass ultimate analysis (carbon, hydrogen, nitrogen, oxygen and ash content). The severity factor (SF) depends on the function *T(t)* is defined as the temperature as a function of time. The temperature was measured at five locations along the centre axis of the ITD briquette. The average and standard deviation calculated from all five thermocouple data sets was reported for each briquette experiment. Willow residue and poplar bark were chosen for this study because of 1) the availability of material for the Bioenergy Systems group (CanmetENERGY-Ottawa); 2) the connection to previous ITD studies making

willow pellets; and 3) the stated interest from the Canadian steel industry for poplar bark bio-briquettes.

Willow briquettes were produced at two different temperatures (300 and 325°C). Poplar bark briquettes were produced on three different conditions: 1) ITD poplar at 300°C, 2) raw poplar at 120°C, and 3) raw poplar at 120°C with 10 wt% slow pyrolysis tar. The ITD study would compare to willow ITD briquettes produced in the same conditions. The raw poplar at 120°C would be a control treatment using densification only. The addition of slow pyrolysis tar was tested to generate research data on a value-added opportunity. Approximately 40 wt% of the mass yield represents non-condensable materials (syngas mixture) plus condensable materials (sometimes known as tar). While the non-condensable gases could be used for process heat, the condensable gases could provide value added opportunities. The tar has adhesive properties that could potentially make a good binder.

2.3.5.1. Quantitative Densification

Briquettes were collected and analyzed in a similar fashion to the pellets. The briquette was removed from the top of the reactor via the modified threaded screw cap and allowed to cool down to room temperature before the briquette mass and dimensions were recorded. The briquettes were stored in glass jars until further testing (ultimate and proximate analysis, durability, and hydrophobicity). The willow and poplar densification data (density, compression ratio, mass loss, and severity factor) are presented in Table 2-7.

Table 2-7: Quantitative densification results for willow and poplar bark in two studies.

Biomass Source	Temperature (°C)	Tar Additive (wt%)	Density (g/mL)		Compression Ratio (N/A)		Mass Loss (wt% db)		Severity Factor	
			Mean	Std. Dev.	Mean	Std. Dev.	Mean	Std. Dev.	Mean	Std. Dev.
Willow	325	0	0.94	0.08	5.6	1.1	39.6	1.3	6.8	0.2
Willow	300	0	1.01	0.07	5.8	1.2	33.8	6.9	6.7	0.6
Poplar	300	0	1.10	0.02	3.0	0.2	29.8	1.7	6.8	0.5
Poplar	120	0	1.15	0.01	3.3	0.2	0.0	0.0	1.9	0.2
Poplar	120	10	1.11	0.03	2.9	0.2	0.3	0.4	1.9	0.2

The impact of ITD on the willow and poplar briquettes compared to raw biomass is seen with a number of different parameters. The bulk density and compression ratio increased to a

similar range for pellets produced at 40 MPa (0.90-1.15 g/mL and 3.0-6.0 respectively). Possible improvements to these figures could be realized with a new system at a higher pressure set-point (~125 MPa). The briquette density for poplar with tar was different from the control with no tar ($p = 0.048$). The compression ratio was found to be less for poplar bark compared to willow in all cases. The mass loss is significantly lower for the two 120°C tests (as reflected by the severity factor). On a dry basis, the mass loss is approximately 0 wt%. It is likely that some light tar volatiles were driven off at 120°C. The mass loss at 300°C to make ITD poplar briquettes was comparable to willow ITD ($p = 0.23$).

2.3.5.2. Ultimate/Proximate Analysis

The analysis was performed on the fines from the willow and poplar bark briquettes because these assays require feed samples that are less than a millimetre compared to the 40 mm briquette diameter. The temperature treatment, characterization results, residence time, and torrefaction severity factor are presented in Table 2-8.

Table 2-8: Influence of torrefaction on physicochemical properties of fines from ITD briquettes.

Parameter	Willow ITD (300°C)	Willow ITD (325°C)	Poplar ITD (300°C)
Carbon Content (wt%)	57.30	61.10	58.10
Hydrogen Content (wt%)	5.81	5.57	5.43
Nitrogen Content (wt%)	0.58	0.65	0.51
Oxygen Content (wt%)	34.15	30.07	28.51
Ash Content (wt%)	2.17	2.59	7.46
Actual HHV (MJ/kg)	22.56	23.96	22.91[1]
Predicted HHV (MJ/kg)	23.11	24.57	23.49
Energy Content (% difference)	2.46	2.53	3.99
Residence Time (min)	20	25	40
Severity Factor (± Std. Dev.)	6.7 (±0.6)	6.8 (±0.2)	6.8 (± 0.5)

[1]The poplar briquette elemental analysis was measured, but not the higher heating value. The actual higher heating value of poplar briquettes was calculated with an adjustment factor (average percent difference). The empirical correlation was first used to find the predicted HHV values of the two willow briquette samples. The average fractional difference was 0.0249 (standard deviation = 0.0005).

The major factors for solid fuel combustion (carbon content, oxygen content, and energy content) all improved from the ultimate analysis values for raw willow and poplar (see Section

2.2.1.4). The range of improvements varied from 10-25% in all categories. As expected for biomass samples, the sulphur content was negligible for all species which is an improvement from coal fuel. The carbon content and energy content increase with increasing severity factor, but the oxygen content does not strictly decrease with increasing severity factor. Using elemental analysis from Table 2-8, the O/C and H/C ratios could be calculated and the coordinates for four samples were placed on a typical van Krevelen diagram (Figure 2-9).

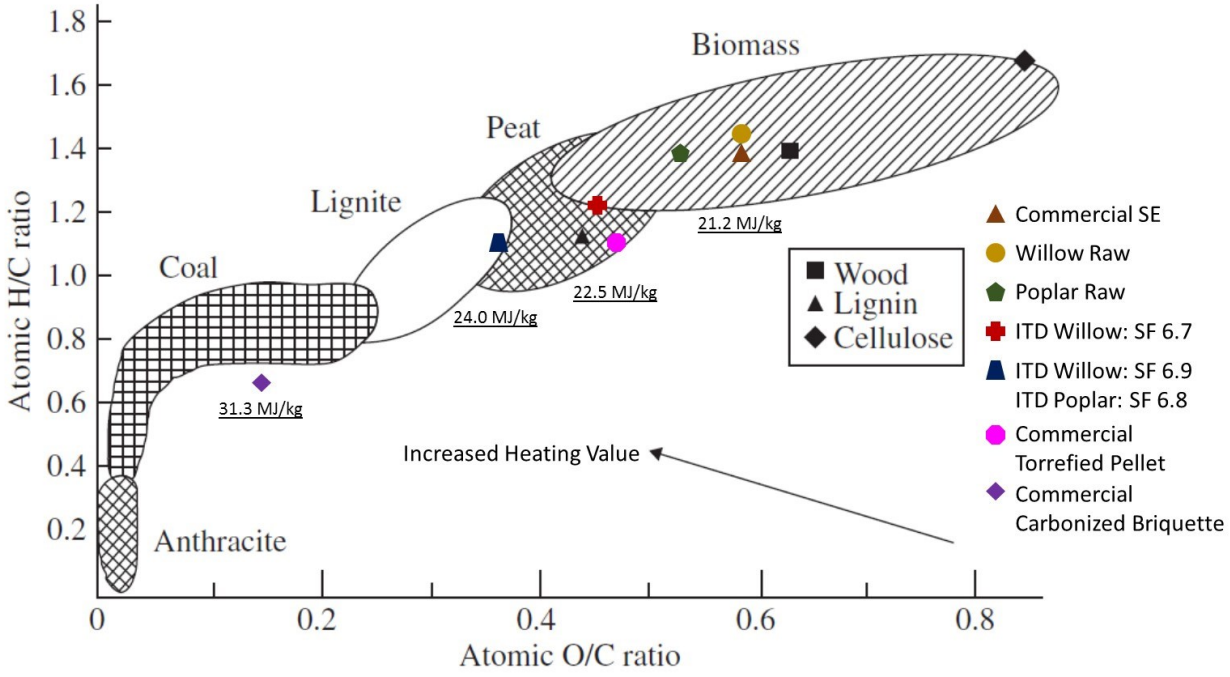

Figure 2-9: Results for untreated willow (yellow circle), poplar (green pentagon), and ITD willow and poplar briquettes (red cross and blue trapezoid) plotted on a van Krevelen diagram (adapted from [3]). Additional commercial materials for the industrial evaluation program include: steam explosion pellets (brown triangle), torrefied pellets (pink octagon), and carbonized briquettes (purple diamond).

The increase in heating value (on a dry basis) and similarities with low rank coals (lignite) can be seen for ITD briquettes with a severity factor of ~7.0. An increase in severity factor (carbonization) leads to a much lower solid yield (30 wt%). The two woody biomass sources before treatment can be seen to fall well within the biomass space in a van Krevelen diagram.

2.3.6. Durability Quantification

The previous quantitative densification results do not give all the information necessary for a techno-economic analysis. The pellets and briquettes from Sections 2.3.3 to 2.3.5 were assessed for durability in Sections 2.3.6.1 and 2.3.6.2.

2.3.6.1. Pellet Durability

Limited durability quantification was chosen to study the impact of 1) material (including blended feeds and moisture content), 2) pellet density, 3) densification pressure and temperature (including ITD), and 4) differences in commercial and ITD pellets. Quantitative durability analysis was done for eight materials from Section 2.2.1.4 (see Figure 2-10). The durability of pellets was measured for batch sizes of sufficient mass (approximately 5 pellets like in Table 2-2), and this measure was informed by protocol development in Appendix B.

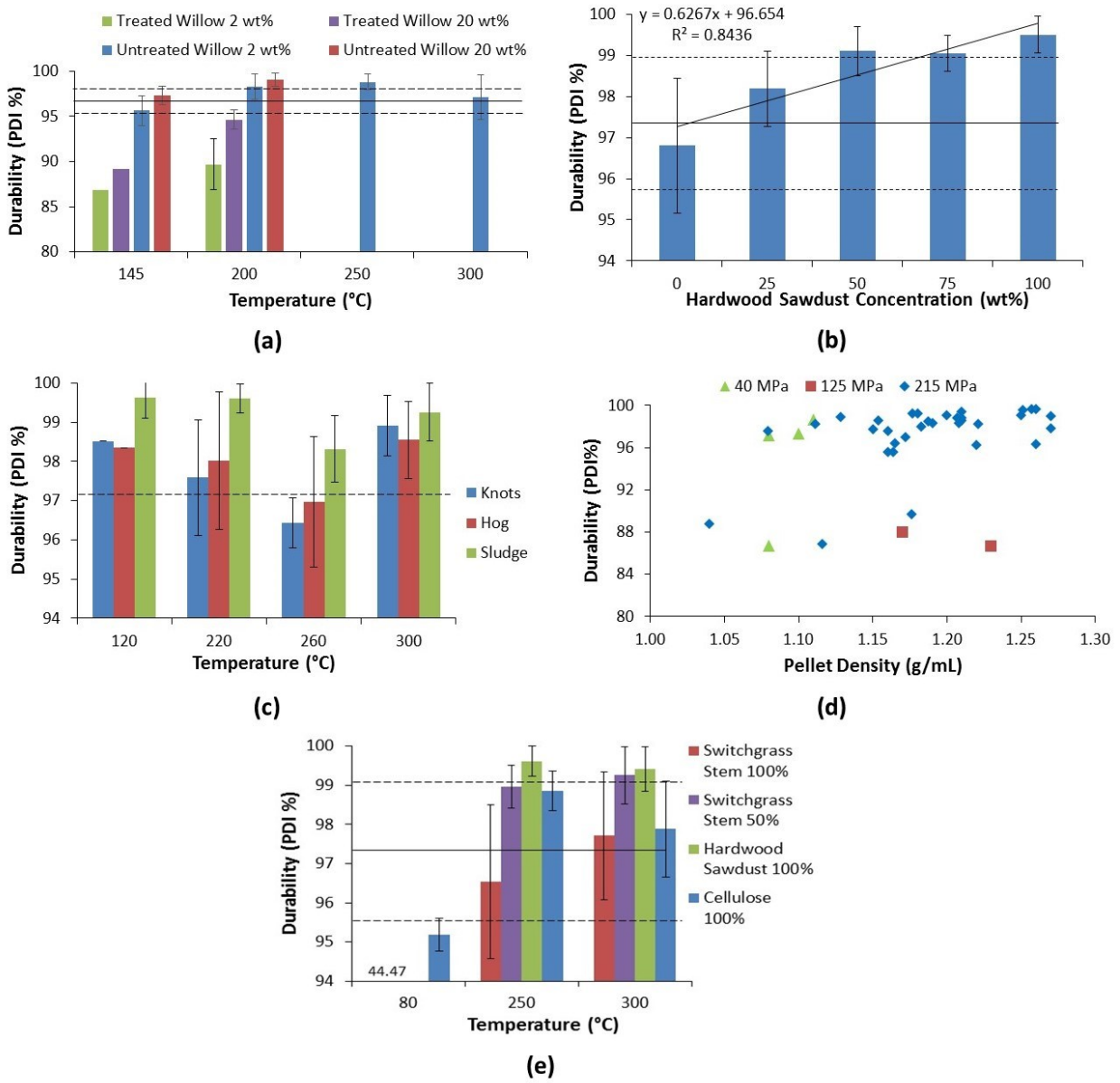

Figure 2-10: Pellet durability for 8 biomass residues as a function of temperature, material, & density compared to the average positive control (solid line) and the standard deviation (dashed line). The

measurements in (b) include data at 250°C and 300°C since the means were statistically similar. Pellet durability was generally assayed in triplicate. Durability values less than 90% were tested in replicates.

First, all willow and torrefied willow pellets tested for durability were produced using a compression pressure of 215 MPa except for the ITD willow pellets produced at 300°C where the pressure was 40 MPa. The torrefied (treated) willow consistently had lower durability than the untreated willow, and the durability of pellets produced at 200°C was greater than those produced at 145°C (Figure 2-10a). The addition of moisture prior to densification had a minimal impact on the untreated or torrefied (treated) willow pellet durability ($p > 0.25$).

The switchgrass stem and leaf pellet durability at two temperatures are statistically similar with $p > 0.4$ (data not shown). Second, the switchgrass stem/hardwood sawdust pellet blends produced at 300°C and 250°C was combined into a complete model for switchgrass stem concentration and pellet durability (Figure 2-10b). An analysis of variance (ANOVA) was performed to compare PDI versus blend ratio and the model passes the criteria for model significance using the 'F' distribution. It appears that increasing the concentration of hardwood sawdust helps improve the durability of switchgrass stem (which agrees with a report from the Vermont Grass Energy Partnership) [41]. The single pellet press temperature did not influence the durability between 250°C and 300°C for all five switchgrass stem and hardwood sawdust blends; this may suggest the durability of solid bridges formed at the two temperatures are similar. However, the temperature difference during pelletization was expected to affect the hydrophobicity and subsequent pellet durability (post-weathered).

Third, the durability for knots, hog and sludge fuel (Figure 2-10c) showed no statistical difference for the same residue at ITD conditions ($p > 0.25$), or between the three residues at any given temperature ($p > 0.40$). The knot fuel was close to 97% at 220°C and 260°C, but increased to 99% at 300°C. The hog fuel showed no difference in durability versus temperature with an average of approximately 98%. Finally, the sludge residue had the greatest durability (regardless of temperature) hovering around 99%. The durability of pellets produced at high moisture content and low temperature (15 wt% and 120°C nominal) were not all tested in duplicate because of time constraints (Figure 2-10c). All three pulp residues had very good durability (greater than commercial Phoenix pellets at 97%) produced at 120°C with moisture added

beforehand. Phoenix hardwood pellets are produced with downstream steam sterilization, cooling and hardening processes [102].

Next, Figure 2-10d provides answers to the next hypothesis on pellet quality: namely, the relation between pellet densities from the quantitative densification analysis to pellet durability as a second quality metric. Pellets that had superior densities were considered to have stronger solid bridges between particles and therefore have an improved durability. The results show that no statistically significant correlation exists between pellet density and durability. The envelope density relates more to the pellet pore volume which does not impact abrasion stress (otherwise known as durability) at the pellet surface.

Finally, the data suggests that cellulose pellets produced at the higher temperatures (250°C and 300°C) are statistically better than the pellets produced at 80°C (Figure 2-10e). The durability values of the biomass pellets (switchgrass stem and hardwood sawdust) are comparable to cellulose pellets produced at the same temperatures, but structurally include lignin, hemicellulose and extractives. Both of the positive controls (woody and steam exploded SE pellets) match the historical durability data (97.0% and 99.5%, respectively). In order to draw some useful conclusions from ITD and non-ITD experiments, pellet durability was tested for a set at three pressures, three temperatures, and four biomass sources in Figure 2-11.

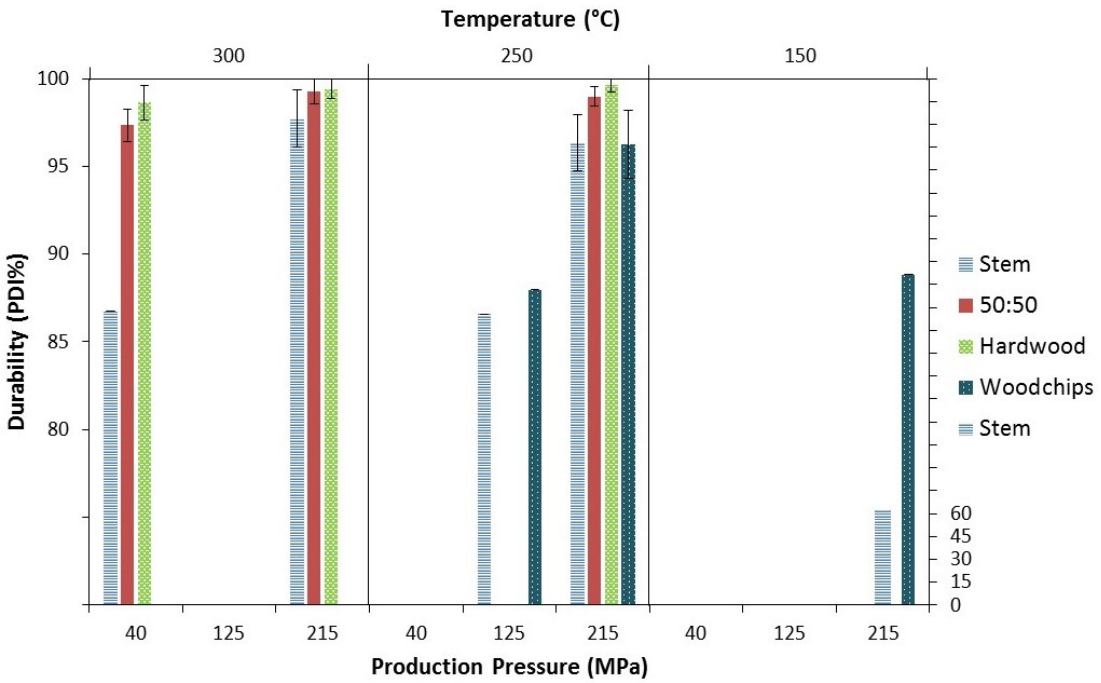

Figure 2-11: Durability results for a three level experimental design including: 1) three blends of switchgrass stem and hardwood sawdust for 40 & 215 MPa at 250 & 300°C; 2) switchgrass stem at 125 MPa & 250°C and at 215 MPa & 150°C; and 3) low quality woodchips at 125 & 215 MPa at 250°C and at 215 MPa & 150°C.

The pellets produced from lower quality feedstocks such as AAFC switchgrass stem and woodchips at different system pressures are greatly influenced in terms of their durability. At 250°C, a change in pressure from 215 MPa to 125 MPa caused a net change in durability from 96% to 86%, and the durability at 40 MPa and 300°C is still 86%. Woodchip pellets produced at 150°C and 215 MPa had a similar durability to those produced at 250°C and 125 MPa (88.8%). Therefore, the application of 40-125 MPa of pressure during pellet formation may not have been sufficient to compress the disks formed during the five minute residence time for some low value agricultural feedstocks. By increasing the pressure to 215 MPa, the solid bridges formed are more robust across a range of biomass sources and the effect on pellet durability is evident. An analysis of the three AAFC feedstock blends suggests that the switchgrass stem pellets are the weakest and that blending the feed with hardwood sawdust improves the durability regardless of the temperature or pressure of production. The results from this scope of testing suggest that pellets produced at low pressure or low temperature require an initial feedstock superior in quality to meet the standards necessary for commercial pellets (PDI > 98.5%) [101]. Quality pellets can be

produced at two extreme production pressures (40 and 215 MPa) as long as the temperature is in the torrefaction range.

The products from the single pellet press would break into smaller disks after tumbling. The original product was constructed within the confines of the single pellet press where the material forms a packed bed. Several researchers have observed that optimal pellet quality is achieved with a mixture of particle sizes due to increased inter-particle bonding (mechanical interlocking) and the elimination of inter-particle spaces (attractive forces, adhesive and cohesive forces) [103–105]. During the five minute residence time, layers of disks are formed as the material reaches the characteristic glass transition temperature of the sample feedstock; the application of the maximum system pressure compresses these disks together creating new solid bridges [84]. One way to influence this process is the system pressure and other influential factors include the moisture content and mesh size of the initial feedstock (see Section 2.4.1).

Agricultural residue ITD pellets and commercially available pellets were then compared on the basis of durability. The sample means for the durability of agricultural residue pellet blends were compared between both production temperatures (250°C and 300°C) and compared to both positive control data sets (Phoenix and SE pellets). Phoenix pellets are made from woody biomass with no thermal treatment and SE pellets are made from woody biomass using steam explosion (a thermochemical conversion method). The positive control sample statistics and the hypothesis test results are presented in Table 2-9.

Table 2-9: Statistical assessment for 5 switchgrass stem concentrations of 14-28 mesh (215 MPa).

Sample Size	Positive Control PDI (%)	Standard Deviation	AAFC Blend (Stem: Hardwood)	p-value (Phoenix)	p-value (SE)
30	97.3	1.6	100:0	0.41	2E-03
			75:25	0.10	0.02
15	99.5	0.3	50:50	1E-04	0.15
			25:75	3E-05	0.05
			0:100	7E-07	0.87

When the pellets produced from the single pellet press were compared to Phoenix pellets in terms of durability, it was found that the 100 wt% and 75 wt% switchgrass stem pellets were statistically indistinguishable from the Phoenix control (97.3%). The lower switchgrass stem

concentrations (50 wt%, 25 wt%, and 0 wt%) were all observed to have statistically different means from Phoenix pellets and, in general, aligned with durability results from SE pellets (99.5%). Both positive controls used during the testing agree with historical data on the 300 mL tumbler. The Phoenix pellet control mean ± one standard deviation was compared using the Student's t-test for comparison of means and the null hypothesis (equal means) was not rejected (Appendix B). Similarly, the SE pellets showed no statistically significant difference in means between those used as controls and those used during protocol development.

Finally, there appears to be no difference in durability between the pellet batches produced by two different operators. Pellets produced from low quality woodchips at 215 MPa and 250°C had durability values of 96.3% and 96.2% from the principle researcher and the other operator respectively ($p = 0.98$). Pellets produced at the same conditions from switchgrass stem had durability values of 96.6% and 96.2%, respectively ($p = 0.81$). Finally, there is no statistical difference between the woodchip feedstock and the switchgrass stem ($p = 0.95$). The pellets produced from AAFC woodchips and switchgrass stem at both pressures were rather uniform in their durability.

2.3.6.2. Briquette Durability

The quantitative densification results for poplar briquettes (see Table 2-7) were selected for a follow-up study on briquette durability. Protocol development results using commercial briquettes found that briquette durability at ISO scale (10 kg) was equal to briquette durability found using 200 g within the commercial sized ISO tumbler (meant for 500 g of pellets) as seen in Appendix B. The results for commercial torrefied briquettes and in-house products from the single pellet/briquette press are shown in Table 2-10.

Table 2-10: Small scale durability of briquettes in commercial scale pellet tumbler.

Advanced Solid Biofuel	Sample Size (n)	Durability (%)	Moisture content (wt%)
Commercial Torrefied	4	91.9	2.7
Poplar Bark	1	96.6	2.6
Poplar Bark (10 wt% tar)	1	97.4	2.9
Poplar Bark ITD	1	96.2	0.4

As expected, the moisture content of ITD poplar briquettes is exceptionally low (about six-fold less than other briquettes). The moisture was driven off during ITD preparation and there was limited moisture uptake while samples were stored in jars. The initial durability assay on briquettes shows that the in-house briquettes were slightly stronger than the commercial torrefied briquettes, and that ITD briquettes were slightly weaker to tumbling compared to the other poplar briquettes. The sample size and resources were limited, and no statistical comparisons were done. However, based on the standard deviation for commercial torrefied briquettes, it is possible that the p value is greater than 0.05 for poplar briquette durability.

2.3.7. Hydrophobicity Quantification

The last metric to evaluate the pellets and briquettes is hydrophobicity. The structure of this section is built in the same manner as the durability quantification section.

2.3.7.1. Pellet Hydrophobicity

Hydrophobicity was evaluated using two different experimental set-ups: 1) water falling on the pellets from a suspended burette, and 2) water surrounding the pellets within a glass dish. Some photographs were taken to qualitatively assess the results and to illustrate the differences between hydrophobic and hydrophilic pellets as seen in Figure 2-12.

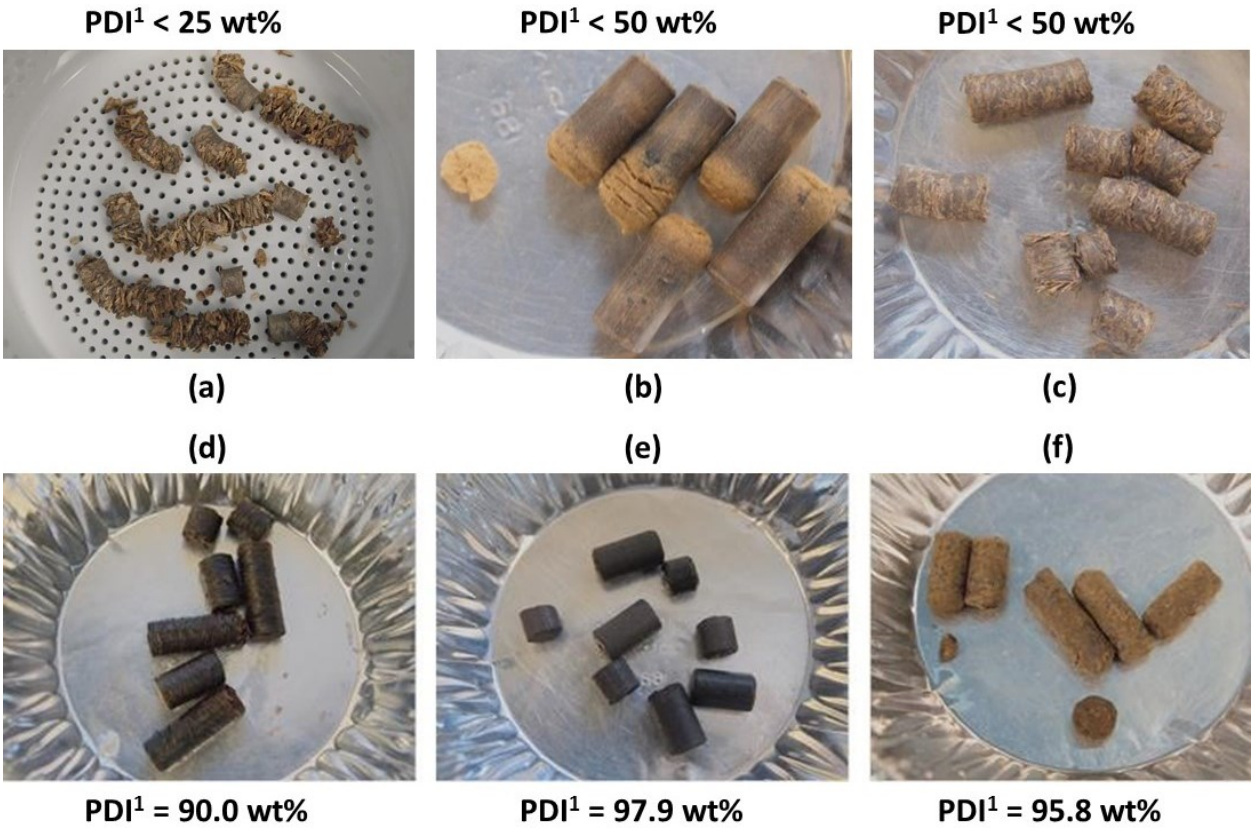

Figure 2-12: Qualitative hyrophobicity of pellets produced at 215 MPa. (a)-(c) shower test and (d)-(f) immersion test with the post-weathered Pellet Durability Index (PDI)[1]. Results for (a) willow, (b) cellulose, and (c) knot residue pellets produced at 200-250°C. Results for ITD switchgrass blended pellets (75:25) at two temperatures: (d) 250°C and (e) 300°C and a positive control (f) SE pellets.

No post weathered durability assays were conducted for results in Figure 2-12a-c because the value was expected to be less than 50%. The qualitative results show that non-ITD conditioning will cause some pellets to fall apart after the shower test. During the drying period, the non-ITD willow pellets (a) (200°C), hydrophilic cellulose pellets (b) (250°C), and non-ITD pulp knot residue pellets (c) (220°C) started to fall apart. Although the durability values of these pellets were all between 98.3% and 98.8% initially, these pellets break apart easily after absorbing water. The knot pellets were swollen and fragile which was expected, and the picture of this sample (after drying in air for 30 minutes) is shown above (Figure 2-12c). One long pellet broke in half with some mild handling of this sample, and some fines were observed. These observations are unique to the experiment with knot pellets at 220°C. When pellets were tested for hydrophobicity after production at 260°C, the pellets did not swell (no picture taken).

The ideal pellets (resistant to abrasion and moisture absorption) require production at torrefaction conditions. As expected, the immersion test demonstrates the most severe moisture conditions that pellets can experience, but pellets typically are not submerged in water during storage. An organic odor was noticeable after the water immersion of 75 wt% switchgrass stem pellets produced at 250°C, but not observed for the same pellet blend produced at 300°C. In comparison, the same organic odor was not consistently observed for pellets subjected to the shower test. The leachate from the 300°C product appears clear whereas the SE pellet leachate has a yellow tinge. The SE pellets (Figure 2-12f) look qualitatively better than the pellets produced at 250°C but are not as smooth as the pellets produced at 300°C. Next, quantitative shower test results from Figure 2-12 and other materials are presented in Figure 2-13.

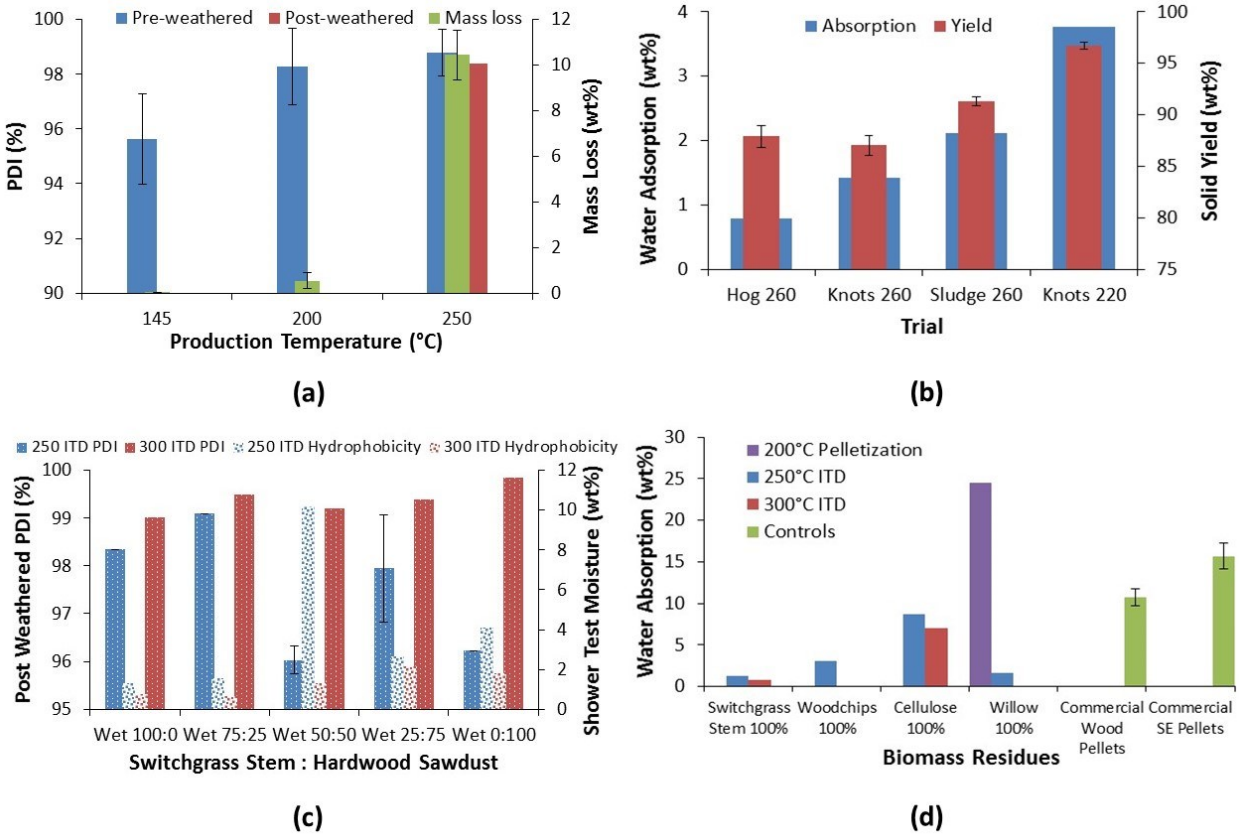

Figure 2-13: Low severity shower test on pellets produced from 7 biomass sources and controls. (a) Willow produced by densification (145°C, 200°C) and ITD (250°C) shown with mass loss (dry basis). (b) Blends of switchgrass stem (100:0) and hardwood sawdust (0:100) shows better durability at 300°C versus 250°C. (c) Water absorption and mass yield for three pulp residues at 260°C and one trial at 220°C. (d) Select residues compared to positive control samples.

First, the distinguishing feature observed during the production of willow pellets was a difference in mass loss (Figure 2-13a). At 145°C and 200°C, the solid yield likely represents moisture evaporation (p value 0.01), while the pellets produced at 250°C had a mass loss of 12 wt% (p value 10^{-5}). Previously, the durability of pellets produced from the two highest temperatures (200°C and 250°C) was greater than 98% (Figure 2-10a). However, the post-weathered durability of the ITD willow pellets (250°C) is actually comparable to the pre-weathered durability (n = 1). The test was repeated to assay untreated willow pellets produced at 200°C (Figure 2-13a, d), and the durability was estimated as less than 50%. The qualitative results support this from Figure 2-12a. The pellets produced at 145°C were left untested for hydrophobicity, but it is expected the results would be more extreme compared to pellets produced at 200°C. The chemical changes in the biomass after torrefaction make the pellets more resistant to moisture and only occur in willow above 225°C.

Second, the pulp and paper mill residue results support the hydrophobicity results for other ITD pellets. The pellets with the highest mass yield (sludge) had the lowest degree of torrefaction and resistance to moisture uptake at 260°C (Figure 2-13b). Furthermore, the hog residue had the lowest mass yield and a higher degree of torrefaction and resistance to moisture. Finally, pellets produced at 220°C (maximum mass yield in this study) absorbed the most water among the four experiments (see also Figure 2-12c).

Third, each switchgrass stem/hardwood sawdust blend was tested with exposure to deionized water by means of the shower test and then re-evaluated for the post weathered durability (Figure 2-13c). Two switchgrass stem concentrations (25 and 50 wt%) were selected for a repeat trial (n = 2) while the other three blends were assayed once (n = 1). The degree of torrefaction was greater for pellets produced at 300°C and one consequence is an apparent increase in hydrophobicity and durability. The average moisture content after the shower test is 1.3 wt% for pellets made at 300°C compared to 4.0 wt% for pellets made at 250°C. The greatest switchgrass stem concentrations (100 wt% and 75 wt%) show the largest increase in durability after weathering effects regardless of temperature. The data also appears to suggest that higher concentrations of hardwood sawdust decrease the durability after exposure to deionized water.

The PDI was greater than 99% after weathering for pellets produced at 300°C, and the data suggests a possible increase in PDI compared to the pre-weathered trials.

Finally, Figure 2-13d summarizes results for ITD conditions of cellulose (250°C and 300°C) relative to results from Figure 2-13a, c. The production temperature of 300°C once again proved to yield hydrophobic pellets and the subsequent durability was 99.1% (n = 1) compared to 97.9% (n = 3) from the pre-weathered assay. The pellets produced at 250°C were expected to perform poorly in the 300 mL tumbler on the basis of qualitative results (Figure 2-12b). For similar reasons, the pellets densified at 80°C were not tested for hydrophobicity. This production was outside the torrefaction temperature range and these pellets were expected to be very hydrophilic. The positive controls (commercial wood and steam exploded pellets) were used during the protocol development for the shower test. Since the woody biomass pelletization and steam explosion treatments are not strong thermochemical conversion techniques, the pellets are hydrophilic and have really high responses to the rain emulation testing.

The tested hypothesis is that the shower test is less severe compared to the immersion test. Therefore, the shower test could be used as an initial evaluation and the more severe immersion test was appropriate for tried and tested materials. Results for the immersion testing are in Figure 2-14. These results were limited to hog, knot, and sludge fuel at three temperatures, one switchgrass stem/hardwood sawdust blend (75:25) at two temperatures, plus some torrefied and steam exploded material controls.

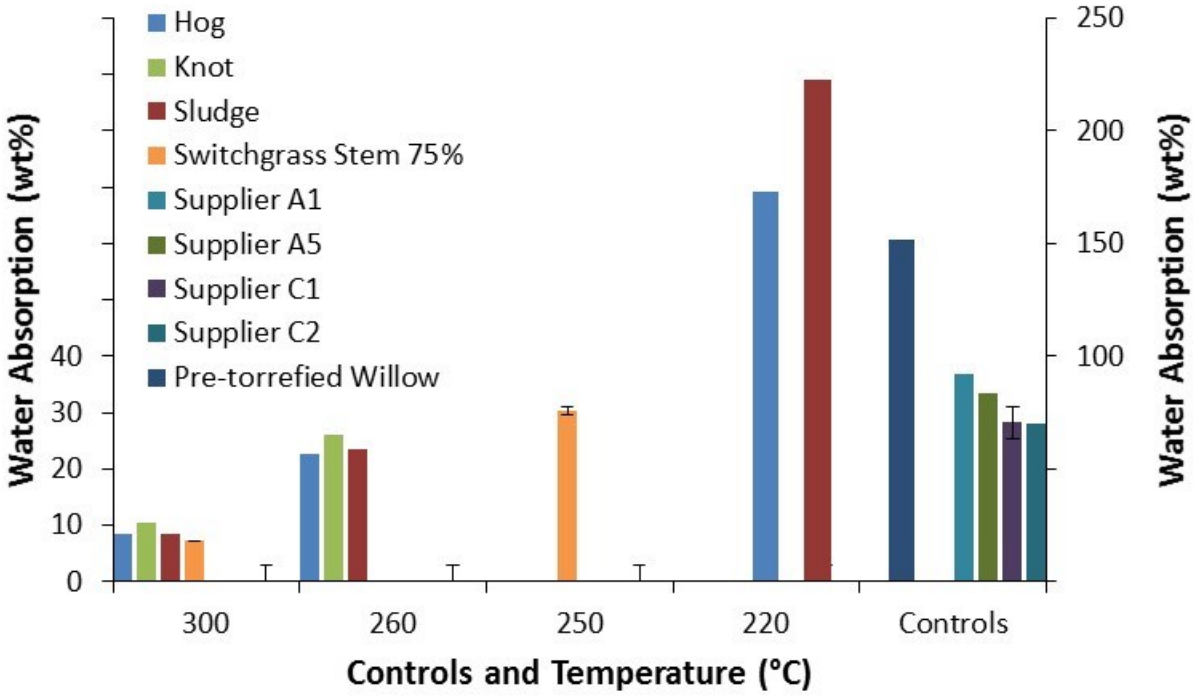

Figure 2-14: Immersion of ITD pulp and switchgrass residues compared to torrefied pellets/controls. Hog, knot and sludge fuel tested at 220, 260, and 300°C with the exception of knots (see Figure 2-12). Single switchgrass stem blend (75 wt%) tested at 250 and 300°C. Commercial pellet samples (A1, A5, torrefied; C1, C2 steam explosion) had high water absorption after 1 hour (30-40 wt%). Pre-torrefied willow allowed to cool before densification was hydrophilic.

The first part of these results was for torrefied willow pellets immersed in water. The previous hydrophobicity results using a falling water test suggest that untreated and densified willow pellets can be durable but not hydrophobic. At the same time, ITD willow pellets have proven to be both durable and hydrophobic. By densifying the pre-torrefied willow (280°C and 20 minutes), the product can be compared to ITD willow pellets. Despite 215 MPa of applied pressure, the torrefied willow showed a sorptivity of 150 wt% and fell apart. In fact, current technologies used to densify pre-torrefied material employ a variety of strategies to create a durable product including the use of binding agents [106]. The torrefied pellets produced in-house do not compare favourably to commercial pellets for the hydrophobicity metric. However, the water falling tests showed that integrating torrefaction and densification may have a synergistic positive effect on durability and hydrophobicity. Second, immersing switchgrass/hardwood blend pellets produced at 250°C in water for 60 minutes shows a 30.3 wt% change in moisture content (Figure 2-12d). However, by increasing the production

temperature to 300°C, the data suggests pellets are more resistant to water uptake (more hydrophobic) than steam exploded pellets and the resulting durability is greater (Figure 2-12e). By increasing the temperature in the batch reactor from 220 to 300°C (as with the ITD and non-ITD pulp waste residues), the torrefaction severity increases and the solid yield drops (97 to 73 wt%). However, the ITD pellets absorb less water than those produced at lower temperatures. The pellets produced at 300°C were expected to be strongly hydrophobic and absorb very little moisture (7.5-10 wt%). For comparison, the commercial thermally treated pellets had a sorptivity between 30-40 wt%. In contrast, the pellets produced at 220°C disintegrated into constituent biomass particles in still water. This was a consequence of moisture absorption in the range of 200 wt% moisture (db.) which causes swelling and mechanical integrity failure. These data sets, taken together, strongly suggest that ITD pellets are durable and resistant to moisture uptake which sets them apart from previous woody biomass densification techniques.

Preliminary tests suggest that ITD could improve the overall pellet durability and hydrophobicity. Ideally, the durability difference after a hydrophobicity test should be minimal. The five switchgrass stem/hardwood sawdust pellet blends showed an apparent average net change in durability of +0.6 when produced at 300°C. However, the effect is less pronounced for the five different blends all produced at 250°C: the average PDI net change observed was -0.8. These results prove equal to or better than results for SE pellets which show a net change in durability of about -0.7 (n = 6). Furthermore, the Phoenix pellets saw a PDI net change of -7.2 (n = 4) from the shower test. A more severe water immersion test shows the same trends observed in the water shower test. The pre- and post-weathered durability for ten samples is shown in Table 2-11.

Table 2-11: Evaluation of pre- and post-weathered durability for commercial/in-house materials.

Biomass Pellet	Immersion Test (L, t)	Pre-weathered PDI (wt%)	Post-weathered PDI (wt%)	Net Durability (wt%)
Supplier A1	4.5, 48	97.5	87.4	-10.1
	0.125, 1	97.3	91.2	-6.1
Supplier A5	4.5, 48	97.6	94.9	-2.7
	0.125, 1	97.6	94.3	-3.3
Supplier C1, C2	4.5, 48	98.2, 97.9	96.5, 97.6	-1.7, -0.3
	0.125, 1	99.5, 98.7	95.8, 99.5	-3.7, +0.8
Hog (300°C)	0.125, 1	98.6	99.5	+0.9
Knot (300°C)	0.125, 1	98.9	99.5	+0.6
Sludge (300°C)	0.125, 1	99.3	99.4	+0.1
75% Stem (300°C)	0.125, 1	98.6	97.9	-0.7
Pulp Hog (260°C)	0.125, 1	97.0	90.2	-6.8
75% Stem (250°C)	0.125, 1	97.8	90.0	-7.8

The 75 wt% switchgrass stem pellets produced at 250°C and immersed once in water shared a similar decrease in PDI (-7.8) with commercial Phoenix pellets only showered with water (-7.2). Beyond that, the same blend was produced at 300°C, immersed in water, and shared a similar decrease in PDI with steam exploded pellet showered with water (-0.7). The quality of pellet resistance to abrasion stress after treatment with moisture can be ranked (greatest to least durable) as follows: 1) integrated torrefaction and pelletization at 300°C; 2) steam exploded pellets (C1, C2) and torrefied pellets with a binder (A5); 3) torrefied pellets without a binder (A1); and 4) woody biomass pellets (such as commercial Phoenix pellets). The combination of torrefaction and densification produces pellets that are equal or possibly superior to other advanced solid biofuels.

2.3.7.2. Briquette Hydrophobicity

In-house and commercial briquettes tested for durability (2.3.6.2) were immersed in water to analyze hydrophobicity. Of the four samples, two included a thermal treatment (torrefied commercial briquettes and ITD in-house briquettes), and two were produced at 120°C with and without a binding agent (slow pyrolysis tar). A sample of commercial torrefied briquettes after immersion is in Figure 2-15. Poplar briquettes (a), poplar briquettes with 10 wt% tar (b), and ITD poplar briquettes (c) are shown in a three point (i-iii) time lapse (Figure 2-16).

Figure 2-15: Commercial torrefied briquettes and the resulting fines after a 48-hour immersion.

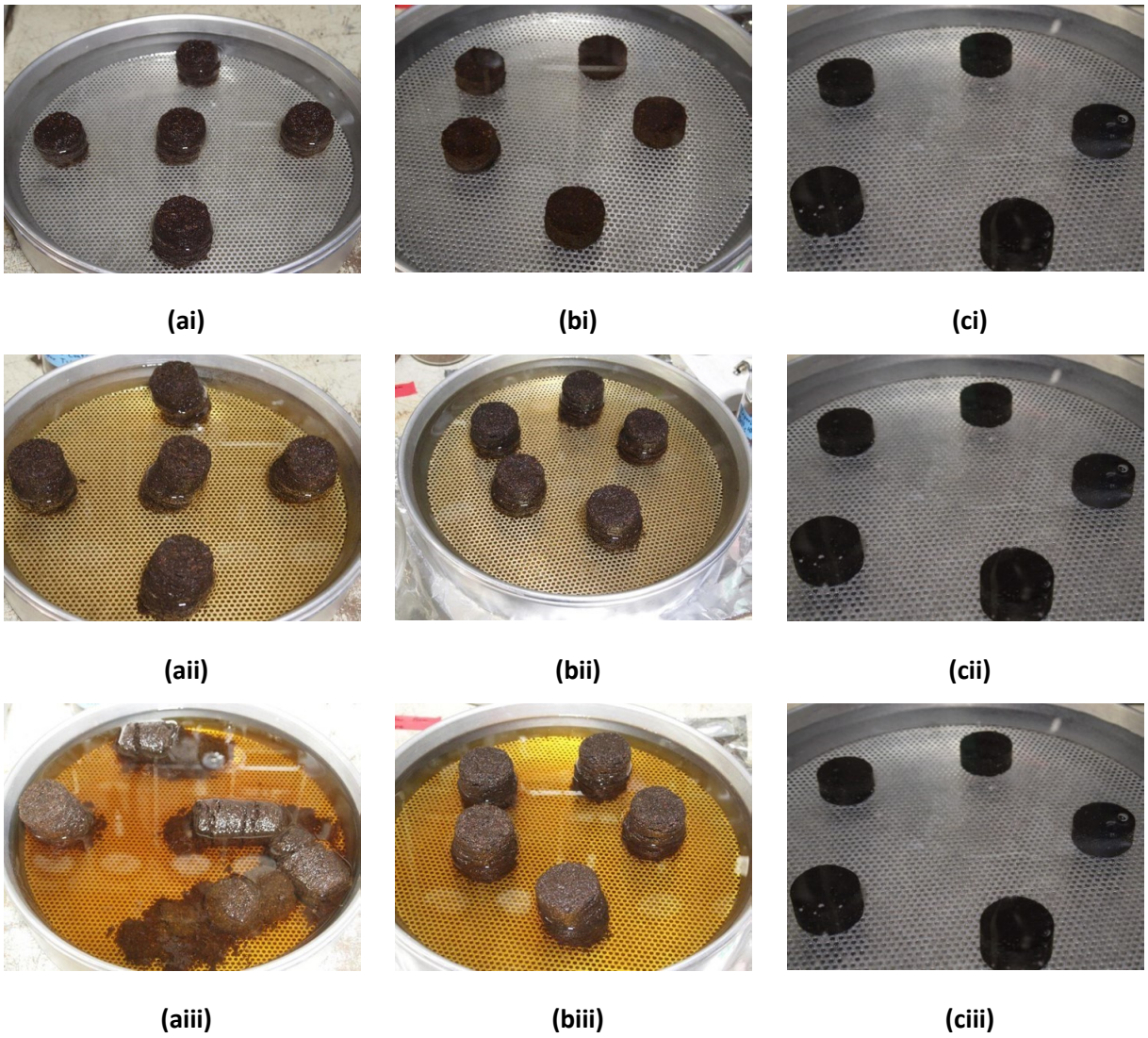

Figure 2-16: Time lapse of (a) raw poplar, (b) poplar with 10 wt% tar additive and (c) ITD poplar briquettes immersed in deionized water. Three time points during the immersion were selected: (i) 1 hour, (ii) 8 hours, and (iii) 48 hours.

The ITD briquette appearance was unchanged over 48 h (Figure 2-16ci-ciii). The addition of tar has a qualitative effect on poplar briquetting. The swelling observed after 8 h in pure poplar bark briquettes (Figure 2-16aii) lead to a collapse after 48 h (Figure 2-16aiii). The swelling of poplar plus tar briquettes was limited and could be dried for further testing (Figure 2-16biii). The quantitative analysis of briquette hydrophobicity includes analyzing the mass of material used, the moisture after immersion, the sorptivity, and the durability after immersion. The initial biomass used depended on material availability, where commercial torrefied briquettes were used in bulk (600 g) or in-house materials (poplar study) were used (200 g). The details concerning these tests are shown in Table 2-12.

Table 2-12: Immersion of torrefied and ITD briquettes compared to thermally untreated poplar.

Advanced Solid Biofuel	Initial Biomass (db.) (g)	Moisture after Immersion (g)	Sorptivity (db. wt%)	Durability after Immersion (%)
Commercial Torrefied	579.0	363.2	57.1	53.0
Poplar Bark	202.8	432.4	207	0.0[1]
Poplar Bark (10 wt% tar)	205.9	359.9	175	0.0[1]
Poplar Bark ITD	220.4	57.2	27.6	94.9

[1]The post weathered durability was not assayed, but the dried briquette had lost so much mechanical integrity that 5-10 circular motions on the sieve caused ~100% of particles to pass the 3.15 mm round holes.

The ITD briquettes were the only solid products that maintained any mechanical integrity during the immersion process. Commercial torrefied briquettes and thermally untreated biomass all had water uptakes after immersion in the 350-450 g range compared to just 60 g of water by the ITD briquettes. The sorptivity of each briquette sample reflects this significant difference by accounting for the total mass at the start of the process. ITD briquettes were 2.5-fold better than commercial torrefied briquettes and almost 10-fold better than thermally untreated biomass briquettes. Finally, the post-weathered mechanical durability was still in the mid 90% range whereas the other briquettes began falling apart into individual fines.

2.4. Discussion

The discussion that follows analyzes some overall themes from this work: densification and the corresponding moisture content, a block flow process analysis of ITD, some chemical reactions associated with devolatilization (torrefaction), and product characterization of in-house samples and positive controls (commercial samples).

2.4.1. Densification and Moisture Content

There are chemical and physical factors contributing to the pellet quality that were a minor focus within the scope of this thesis. Moisture content plays a critical role in pellet formation; however, the reason for this effect is not well understood. Traditional thinking is that some moisture content is necessary to develop intermolecular (van der Waals forces and hydrogen bonds) and interfacial forces that serve to bring particles in closer contact with one another during the binding process [84]. Previous data suggests that the optimal moisture content for the densification of woody biomass is between 6 and 12% and 8 and 12% respectively [107,108].

The addition of moisture is a common practice in the manufacturing of pellets from biomass. For pellets produced at 50°C or 80°C in a closed system, there will not be a significant proportion of mass loss observed during the five minute residence time (system pressure 100 kPa). When pulp residues were spiked with moisture, the nominal moisture content was 15 wt%. However, the mass loss observed during densification at 120°C was close to 12.5 wt% (data not shown). Furthermore, there will not be any water evaporation during the five seconds of maximum pressure during pelletization (40-215 MPa). The major difference between pelletization at 50°C and 150°C (studied by a previous operator) is the evaporation of water which did have an observable impact on mass loss but not for the pellet density (regardless of feedstock). The only other source of biomass loss is during pellet press loading, which should be negligible compared to the phenomena of evaporation and torrefaction. The addition of 10-15 wt% moisture to switchgrass stem improved the durability from 50% to 60% after production at 215 MPa and 150°C.

Qualitatively, the 50 wt% switchgrass stem pellets containing 13.6 wt% moisture content appeared quite delicate with individual switchgrass stem pieces evident on the outside of the

pellet. This result differs from switchgrass stem pellets produced at elevated temperatures with 5 wt% moisture content. The resulting durability of the 50 wt% switchgrass stem pellets produced at 80°C was lower than any other measurement taken during the campaign (see Figure 2-10). The biomass blend lost moisture content (8.7 wt%) and perhaps lost moisture during the time between sample preparation and the start of the densification tests. In turn, this could affect the ability to make a good pellet at 80°C. Alternatively, the temperature could be too low for producing quality pellets from this blend without the use of binders.

Previous studies by Greinöcker *et al*. looked at pellet abrasion, moisture content, and post weathered durability. Their results for woody biomass pellets show that the abrasion stress increases (thus leading to durability decreases) as the moisture content increases and the abrasion losses increase exponentially after exceeding a threshold value of 10 wt% [109]. These results are reflected in the post weathered durability assay for commercial Phoenix hardwood pellets. However, single data sets from Figure 2-13c suggest that pellet blends of switchgrass stem and hardwood sawdust produced at elevated temperatures (250-300°C) show marginal increases in mechanical durability when the pellets are showered with deionized water. The addition of water may help stabilize solid bridges within these pellets produced at elevated temperatures, and thus explain why the blended pellets are more durable after treatment with the shower test. However, these data sets have a limited scope (sample size). Larger scale densification tests will have to be done to obtain a clearer picture of the mechanical characteristics of – and moisture effects on – blended pellets.

2.4.2. ITD Process Requirements

In 1978, Reed *et al*. [110] conducted laboratory scale densification tests on pine sawdust "to determine the work required for densification under various laboratory conditions and to compare this to the energy consumed by practical operating equipment". These authors (at the Solar Energy Research Institute) observed that pre-heating the feedstock to 200-225°C before densification can reduce the pressure of compression or extrusion by a factor of about 2 [110]. The authors further go on to explain that the extra thermal energy required to heat biomass to 200°C is offset by lower electrical power costs, pressure requirements, equipment costs, and possibly reduced die wear for densification all the while increasing the fuel value [110]. The work

from 1978 suggests that pellets made at 225°C and 250°C had considerably high energy content compared to pellets produced at lower temperatures which the authors attribute to a "pre-pyrolysis" reaction for biomass [110]. Combining the processes could eliminate the feedstock selectivity issue of pelletization, as well as improve the hydrophobicity. The volumetric energy density may improve by the integration of – and synergy between – both processes. A proposed block flow diagram is in Figure 2-17.

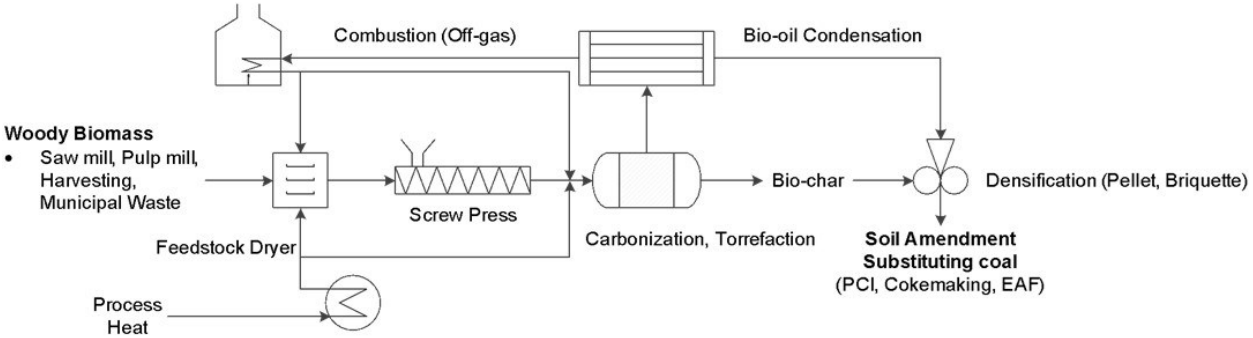

Figure 2-17: Block flow / process flow diagram with heat integration (for drying) and ITD.

At the reactor outlet, the fittings must be purged with nitrogen to prevent combustion risks, and kept hot upon entering the densification unit to preserve product quality. Some torrefied softwood sawdust pellets need a mold temperature greater than 170°C or a moisture content of 10 wt% to make strong pellets; these results may favour an integrated approach to save energy usage during pellet production [88]. These conditions have to be verified at pilot scale before drawing conclusions on the benefits described above.

It should be noted that researchers observed devolatilization reactions occurring between 250°C and 300°C [111]. The authors at the Swedish University of Agricultural Sciences observed the auto-oxidation of wood extractives in pellets at high pelletizing temperatures and the emission of volatile organic compounds in pellet storage [112]. The TOP process (Torrefaction and Pelletization) developed by the ECN (Energy Research Centre of the Netherlands) does not combine torrefaction and densification in a single step for the same reason as well as the idea that "charging the necessary thermal heat for torrefaction to a reactor in which torrefaction and densification are integrated" is too complex [111]. A detailed design analysis will need to be undertaken to create a pilot scale system to integrate torrefaction and densification. The

motivation for this engineering research will be based on the laboratory scale research conducted in this report and others like it.

2.4.3. Macromolecular Cellulose

The study of cellulose thermal degradation has highlighted three chemical reaction sequences: the dehydration of cellulose found to occur between 200°C and 280°C, the depolymerization reaction following the creation of levoglucosan at 280°C, and the exothermic degradation of cellulose into gaseous products (e.g.: carbon monoxide, carbon dioxide, water, and methane) and solid residual tar [113]. The dehydration of cellulose occurs as early as 210°C, which can help explain the solid and gaseous products observed during cellulose pelletization between 250°C and 300°C. The chemical structures of levoglucosan and two cellulose monomers (with the β 1→4 linkage) are shown in Figure 2-18 [114].

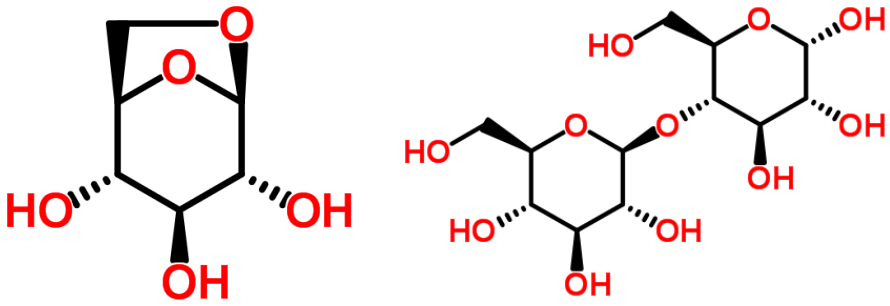

Figure 2-18: 3D structural formulae of levoglucosan (left) and cellulose (two monomers) (right)

Furthermore, the depolymerization of the unreacted cellulose becomes significant at 270°C which may be a key factor in the chemical transformations of pellets produced at 300°C [113]. It may also have affected results for pellets produced at 250°C (nominal value) because one thermocouple exceeded the set point during the first 35 tests on AAFC feedstocks (data not shown). The volatilization and exothermal decomposition of levoglucosan to form gases and char occurs simultaneously to varying degrees depending on the heating rate, sample thickness (8 mm), pressure (100 kPa for 5 minutes and 40-215 MPa for 5 seconds), and other factors [113]. Since the dehydration of alcohol groups typically proceeds by a carbonium ion mechanism, there are a variety of chemical intermediates and eventual large array of chemical products during the degradation of cellulose at elevated temperatures (200-300°C). These products will have an

important role in the durability of the resulting pellets (from either pure cellulose or agricultural biomass samples).

2.5. Conclusions

The purpose of this research was to adapt biomass into a useable solid fuel for energy intensive industries in order to reduce coal consumption. To that end, biomass was transformed via torrefaction, densification, and integrated torrefaction and densification (ITD) to improve the properties of raw biomass (namely carbon content, energy content, bulk density, hydrophobicity) while maintaining the durability of the product. These factors are important for industrial operations in terms of the capacity for a desired MW rating, a low shipping and handling cost (in terms of GHG emissions and total volume used), and the ability to store and handle like coal (limited moisture uptake from the ambient conditions and good grindability).

The results suggested that the integration of torrefaction and densification has a synergistic positive effect on the overall pellet/briquette quality for coal substitution in energy intensive industries. At torrefaction temperatures, the applied friction force for densification decreases for ITD because the biomass is made somewhat fluid with the applied heat. The ITD conditions changed the biomass properties on a van Krevelen diagram from the biomass sphere to the lignite (low rank coal) sphere based on the ultimate and proximate analysis from ITD briquettes. ITD results showed pellets and briquettes with densities of 1000-1250 kg/m^3, compression ratios of 2.5-10, and the expected solid yield of 90 wt% (250°C) and 70 wt% (300°C). The torrefaction and ITD experiments agreed with continuous thermogravimetric data (within 1% difference). The durability values ranged from 97-99% for in-house pellets and briquettes: comparable to commercially available advanced solid biofuels (average sample durability was 97.7% over 25 tests). Most importantly, ITD products showed an improvement to water uptake resistance (7.5-10 wt%) compared to commercial woody and torrefied pellets (30-40 wt%). Future work includes testing a pilot scale ITD system to begin optimizing process parameters and analyzing a continuous process for production.

Chapter 3.

Evaluating water sorption and mechanical strength of densified solid biofuels after prolonged water immersion

Peter Gaudet[1,2], Guy Tourigny[1], Poupak Mehrani[2] and Jules Thibault[2]

[1]Canmet ENERGY – Natural Resources Canada, 1 Haanel Drive, Ottawa, ON, Canada K1A 1M1

[2]Department of Chemical and Biological Engineering;

University of Ottawa, Ottawa, ON, Canada K1N 6N5

Abstract

Phasing out coal from major industries is seen as one of the means to meet the 2015 Paris Climate Accord targets aimed at reducing greenhouse gas emissions. Energy intensive sectors (ex: metallurgical and power generation) are supported by technology from the industrial revolution (ex: blast furnace and steam boiler) which relies on coal. Researchers are trying to repurpose these technologies without making costly infrastructure changes thus minimizing the disturbance to iron/steel, cement and electricity production economics. The goal of this paper is aimed at evaluating low-value biomass transformed into advanced pellets and briquettes that could be stored and handled like coal. Commercial producers of alternative fuels (ex: biomass) need to comply with several standards for their sale on the open market. The most common properties covered by these standards are the size, moisture content, bulk density, heating value, and durability. These properties influence not only the performance during combustion but also the upstream segment of the life cycle (collection, transport and storage). Owing to the significant differences in surface functional groups, biomass is significantly more hydrophilic than coal and cannot be left outside as is common practice (ex: coal yards). Advanced pellets and briquettes were tested for water absorption capacity by immersion in water for 48 h, and the subsequent drying profiles (at 20 and 40°C with 0.3 m/s air flow) were also obtained and modeled. Results show that commercial steam exploded pellets and custom torrefied briquettes (produced from integrating torrefaction and densification, or ITD) absorbed the least amount of water (28 wt%) and the ITD briquettes dried quicker. The unaccomplished change after 60 minutes was 13.6% for ITD briquettes and 56.1% for steam exploded pellets.

3.1. Introduction

In 2012, approximately 30% of the world's primary energy supply came from infrastructure designed to handle and combust coal to create steam and power turbines [5]. However, conventional coal combustion is a major contributor of environmentally damaging CO_2, SO_x, and NO_x emissions. Industries and policies continue to focus on sustainable solid fuel alternatives, and biomass is one such source of energy being studied. This knowledge transition from coal to biomass will have associated costs, so one important goal is to minimize costly infrastructure changes [51]. With respect to compressed solid biofuels (example: pellets or briquettes), industry is interested in storing the fuel outdoors similar to coal because the strategy is cost effective. Industrial experience has suggested that leaving coal in a coal yard for about a week before being used in the combustion chamber is an acceptable practice in terms of moisture contact [29]. Karr reported that a decrease in polar surface groups will cause a corresponding decrease in moisture holding capacity of coal [115]. Kadioğlu and Varamaz found that lignite coal with a starting moisture content of 1.0-1.5 wt% only gained an additional 1.6-4.2 wt% moisture after immersion in water for 24-48 hours [116]. Fry *et al*. found that the immersion of coal in water completely filled the pore volume with water for all but low rank coals which had moisture contents slightly greater than the pore volume [49]. In addition, the authors did not find that immersion in water changed the coal swelling beyond observations in humid air (97% relative humidity) [49]. As a result, one important consideration for converting feedstocks to be used in power generation technology is the hydrophobicity of the fuel.

For industrial fuel usage, the solid fuel is typically dried to a low moisture content before combustion in order to get the full use of the expected heating value of the solid material [31]. When the feedstock is stored outside, it is in direct contact with, for example, inclement rain, snow, and humidity. Raw biomass has a high water sorption capacity; for example, the moisture content after harvesting is typically 45-55 wt% and will increase if stored outside [71,72]. Compressed biomass tends to swell during the sorption process which causes the compressed material to lose its mechanical integrity. Pellets and briquettes also are at risk of biological degradation in the presence of water, and both consequences are to be avoided at all cost. Unlike raw biomass, advanced solid biofuels have some appreciable resistance to moisture uptake.

Advanced solid biofuels refer to biomass products that were upgraded with thermal treatments (e.g. torrefaction or steam explosion), and material densification (forming pellets or briquettes) to match certain coal characteristics. Any study comparing coal and advanced solid biofuels for co-firing applications must appreciate this water sorptivity difference. The loss of mechanical integrity increases the tendency of the material to generate explosive dust upon drying. As a result, utility companies spend a lot of money (tens of millions of dollars) in storage and handling facilities for solid biofuels. In turn, this makes the co-firing of pellets with coal an expensive proposition.

The purpose of this paper is to analyze commercial and in-house produced advanced solid biofuels for 1) their durability (resistance to abrasion stress); 2) their proclivity to water uptake or sorptivity; 3) the drying performance by forced convection; and 4) any observed differences in durability after immersion and drying. The results from this work can provide information on a specific point along the life cycle analysis of solid fuels between storage and combustion. First, the biomass harvest, drying, and processing stages create an advanced solid biofuel for the end user. Next, the solid fuel must be shipped which incurs some transport and handling stress. The durability was used to quantify pellet and briquette losses. Although raw biomass was dried after harvest, the resulting advanced solid biofuel is exposed to water during transport and storage to varying degrees (depending on the local climate and infrastructure). Therefore, this work shows the risk associated with water uptake as well as data describing the resulting drying. Industry must be aware of the variation between thermally treated biofuels based on their drying characteristics [117]. Experimentally, generating a precise drying curve requires recording the weight of the sample as a function of time. Therefore, it would be beneficial to generate a numerical solution that describes these drying curves given the experimental operating conditions. A representative drying curve for a given sample can be obtained experimentally and the theoretical mass and heat transfer coefficients can be estimated by developing a numerical solution via finite differences. After completing the sorptivity test, the thermally treated biofuel is dried to a moisture content equivalent to the one of the original sample. Since the durability of the compressed biomass is a function of its moisture content, a reasonable interpretation of the durability after the sorptivity test can only be achieved by comparing the durability to the

sample at the original moisture content (i.e. the moisture content of the sample as received or as produced).

3.2. Materials and Methods

A series of tests were performed to assess the quality and characteristics of the pellets and briquettes used in this investigation. Specifically, these include commercial steam exploded pellets, torrefied pellets and briquettes, and in-house briquettes produced by ITD (see Chapter 2). The evaluation methods are mostly derived from the Solid Biofuels Working Group of the International Standards Organization (ISO). In fact, ISO currently has a working group tasked with developing a sorptivity procedure for these fuels. Therefore, the method presented here is meant to be along the same spirit as the ISO working group's current recommendations. The other ISO methods include sample preparation, pre-weathered (as received) durability, biofuel immersion, and post-weathered durability (after immersion and drying).

3.2.1. Sample Preparation

Pellet and briquette samples were prepared in accordance with ISO 14780, which is dedicated to the preparation of solid biofuels. The methods include the selection of bulk samples of an appropriate size, the determination of moisture content, and the use of a sieve for the separation of fines.

3.2.2. Biofuel Durability

The mechanical durability of solid biofuels was determined using ISO 17831-1 standard for both pre-weathered and post-weathered samples of pellets and briquettes. The mechanical durability of a solid biofuel is a function of its total moisture content, where larger moisture contents tend to make the material lose its mechanical integrity. The purpose of this test is to compare how the structural durability compares between pellets or briquettes produced from different sources after immersion. This test will identify the weight fraction of pellets or briquettes (starting material: 500 g ± 10 g) that forms fine powder (less than 3.15 mm) after a controlled material handling intensity. Each sample will be tested in a 12-L chamber at 50 rpm for 10 minutes using a Seedburo tumbler (Model # SKU PDT). This tumbler meets the ISO standard specifications for pellet durability. Protocol development work supports small scale briquette durability testing using this same tumbler (see Appendix B).

3.2.3. Hydrophobicity by Immersion

The immersion method is partially adapted from the following protocol: Water Absorption-Immersion Test [73]. This method – developed by the researchers of the SECTOR project (Solid Sustainable Energy Carriers from Biomass by Means of Torrefaction) – requires a sufficiently large pan to contain 600 g of pellets with an approximate bulk density of 0.75 g/mL plus 2-3 times that volume of water [92]. Out of the 600 g of pellets, approximately 500 g were used for post-weathered durability testing, and the remaining 100 g was used to determine the moisture content after immersion via a simplified oven drying method. The latter allowed as well to assess the losses resulting from dissolved material and fines during soaking. Tests were performed in triplicate, except if otherwise noted, for 48 hours in a climate controlled laboratory. The soaking was done with 4500 g ± 10 g of deionized water which allows full submersion with approximately 2-3 cm of water above the pellets in each pan. The pan defined here is an ISO standard sieve plus a bottom pan having a diameter of 0.35 m and round holes with a diameter of 3.15 mm. The pans were covered to minimize evaporation losses. The pan containing the test portion was removed and inspected after 48 hours of soaking. The samples were removed from the water by lifting the screen with the pellets and allowing a drip dry. The perforated screen was allowed to rest above a dry surface or stand where the residual surface moisture can be collected. The mass of pellets was recorded immediately after the water stops dripping (approximately 5 minutes at room temperature) in a laboratory environment. The tray was gently agitated to screen out any remaining water bridges between the pellets and the screen. The mass was checked again after 5 minutes and sent to a dryer oven. Wettability, characterized with the contact angle between a surface and a droplet of water, is sometimes used instead of sorptivity to infer the affinity of water for solid biofuels. However, compressed biomass does not typically have well-defined surfaces and therefore this methodology is not recommended.

3.2.4. Unsteady State Drying

Following the complete immersion of the pellets in water for a sufficient period of time to achieve maximum water sorption and allowing the excess water to drip off [116], the wetted material, initially at room temperature, was air dried in an oven. The average operating conditions of the drying air in the oven were 40°C with a relative humidity (RH) varying from 10-

70% and a velocity of 0.3 m/s to provide a gentle forced convection. A schematic diagram of the pellet drying setup is shown in Figure 3-1.

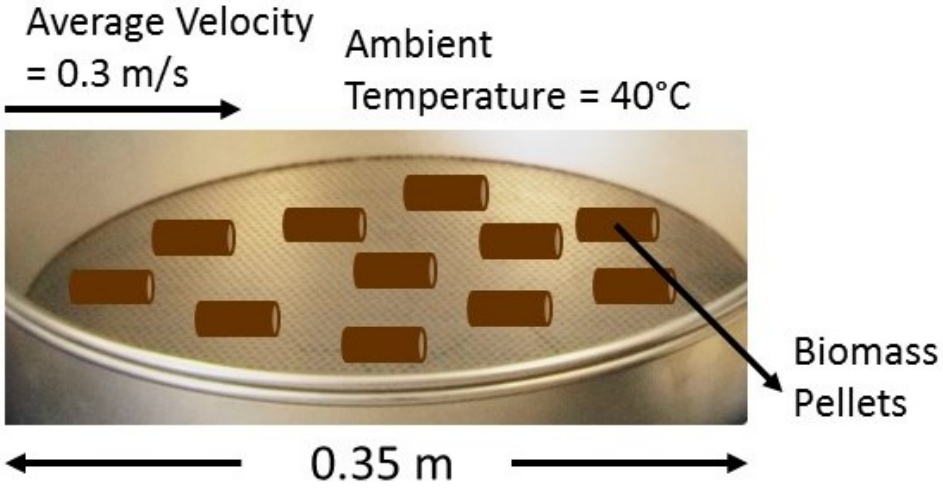

Figure 3-1: Process schematic diagram for biomass pellet (represented by brown cylinders) drying by gentle forced convection with air speed of 0.3 m/s and a temperature of 40°C.

The pellets were disposed relatively uniformly in a single layer on the 0.35-m cylindrical pan described earlier.

3.2.4.1. Mathematical Models

Drying is a dynamic process where fuel pellets, exposed to a 40°C stream of air, undergo a simultaneous temperature increase and evaporation. The final target mass at the end of the drying process was to reach the mass prevailing before immersion (within 5%) for the purposes of a weathered durability evaluation. A sub-sample of this material was evaluated for the inherent moisture content using forced convection in an oven at 105°C for a duration of 3-4 h. The drying performance after immersion was evaluated with two different models: an empirical model from the literature, and a model based on first principles. The empirical model for the variation of the moisture content on a dry basis (ω') is based on the exponential decrease of the moisture content that was proposed by da Silva *et al*. (2013) and given by Equation (3-1) [118].

$$\omega'(t) = \left(\omega'_i - \omega'_{eq}\right) * \exp(-at^b) + \omega'_{eq} \quad (3\text{-}1)$$

The limitations of this model are in the applicability to future simulations since the parameters 'a' and 'b' are very specific to the material, moisture content, and temperature. On the other hand, the first-principle model considers the specifics of the drying process including

1) the heat transfer to bring the species from room temperature to 40°C; 2) the energy balance to account for evaporation at the surface; 3) the migration of water within the pellet/briquette to the surface; and 4) the mass transfer of water vapour from the surface of the solid pellet/briquette to the gaseous environment of the flowing gas in the oven. The governing differential equations to account for the heat and mass diffusion in a cylindrical pellet are presented in Equations (3-2) and (3-3), respectively.

$$\frac{\partial T}{\partial t} = \alpha \left[\frac{\partial^2 T}{dz^2} + \frac{1}{r} \frac{\partial}{\partial r} \left(r \frac{\partial T}{dr} \right) \right] \tag{3-2}$$

$$\frac{\partial \omega'}{\partial t} = D_e \left[\frac{\partial^2 \omega'}{dz^2} + \frac{1}{r} \frac{\partial}{\partial r} \left(r \frac{\partial \omega'}{dr} \right) \right] \tag{3-3}$$

The two-dimensional temperature and moisture content profiles were obtained by solving simultaneously this coupled set of second order differential equations using the finite difference method [100]. The two second order partial differential equations were discretized using an explicit finite difference scheme. It is assumed that the entire external surface of the cylindrical pellet is exposed to the same external conditions. The problem is thereby reduced to a two-dimensional problem, i.e. the angular variation is assumed negligible. In addition, radial and longitudinal symmetry prevails such that a quarter of the r-z middle plane of the cylinder is considered. Equations (3-4) and (3-5) represent the finite difference equations for an interior mesh point to solve the heat and mass transfer equations, respectively.

$$T_{ij}^{n+1} = \lambda_h \left(1 - \frac{1}{2(i-1)} \right) T_{i-1j}^{n} + \lambda_h T_{ij-1}^{n} + (1 - 4\lambda_h) T_{ij}^{n} + \lambda_h \left(1 + \frac{1}{2(i-1)} \right) T_{i+1j}^{n} + \lambda_h T_{ij+1}^{n} \tag{3-4}$$

$$\omega'^{n+1}_{ij} = \lambda_m \left(1 - \frac{1}{2(i-1)} \right) \omega'^{n}_{i-1j} + \lambda_m \omega'^{n}_{ij-1} + (1 - 4\lambda_m) \omega'^{n}_{ij} + \lambda_m \left(1 + \frac{1}{2(i-1)} \right) \omega'^{n}_{i+1j} + \lambda_m \omega'^{n}_{ij+1} \tag{3-5}$$

Variable λ, which can interpreted as a stability factor, is defined in Equations (3-6) and (3-7). In this work, the geometrical mesh size in the radial (Δr) and in the longitudinal directions (Δz) were identical and equal to Δs. This applies specifically to Equations (3-4) and (3-5).

$$\lambda_h = \frac{\alpha \Delta t}{\Delta s} \tag{3-6}$$

$$\lambda_m = \frac{D_e \Delta t}{\Delta s} \tag{3-7}$$

For mesh points located on the surface of the solids, Equations (3-4) and (3-5) are also used except that the boundary conditions for the heat and mass transfer are considered in the discretization scheme (see Appendix E). The initial and boundary conditions pertaining to this problem are summarized in Table 3-1. The initial temperature condition, assumed uniform throughout the cylinder, varied between 15-20°C depending on the season the tests were conducted (winter/summer). The initial moisture content depended on the sorptivity of the different advanced solid biofuels. There are eight equations to account for the boundary equations: four for the heat transfer equation and four for the mass transfer equation.

Table 3-1: Boundary conditions for the mass and heat transfer system analysis.

Transport Phenomena	Coordinate	Variable	Value	Units
Heat	Boundary r_1	$-k\frac{\partial T}{\partial r}\|_{r=R}$	$h(T_R - T_\infty) + Q_{evap}$	W/m^2
	Boundary r_2	$\frac{\partial T}{\partial r}\|_{r=0}$	0	°C/m
	Boundary z_1	$-k\frac{\partial T}{\partial z}\|_{z=L}$	$h(T_L - T_\infty) + Q_{evap}$	W/m^2
	Boundary z_2	$\frac{\partial T}{\partial z}\|_{z=0}$	0	°C/m
Mass	Boundary r_1	$-D_e\frac{\partial \omega'_{H2O}}{\partial r}\|_{r=R}$	$k_c(H^R_{H2O} - H^\infty_{H2O})$	(m/s) (kg/kg)
	Boundary r_2	$\frac{\partial \omega'_{H2O}}{\partial r}\|_{r=0}$	0	kg/(kg m)
	Boundary z_1	$-D_e\frac{\partial \omega'_{H2O}}{\partial z}\|_{z=L}$	$k_c(H^L_{H2O} - H^\infty_{H2O})$	(m/s) (kg/kg)
	Boundary z_2	$\frac{\partial \omega'_{H2O}}{\partial z}\|_{z=0}$	0	kg/(kg m)

3.3. Results

The results for the evaluation of the hydrophobicity were divided into four subsections: (3.3.1) the mechanical durability before and after immersion (including fines generation), (3.3.2)

the moisture content as received, after immersion, and after drying, (3.3.3) the physical process changes on advanced solid biofuels, and (3.3.4) the drying of the solid biofuels following a 48-h water immersion.

3.3.1. Mechanical Integrity

Results show that the immersion process led to the swelling of the advanced solid biofuels, and the degree of compression is not fully recovered upon drying. This immersion impact is reflected by examining the durability before immersion (as received), the change in durability defined as the difference between the durability after and before solid biofuel immersion, and the fines generated from the immersion process. The results are presented in Table 3-2.

Table 3-2: Mechanical integrity of samples for the Industry Evaluation Program of advanced solid biofuels for direct coal substitution.

Advanced Solid Biofuel	Durability As Received (%)	Net Durability Change (%)	Lost Fines (wt%)
G1: Poplar ITD[2]	96.2	-1.4	0.00
G2: Poplar + 10wt% tar[2]	97.4	No Data	96.26
Supplier A1[2]	97.5	-10.1	1.13
Supplier A2[1]	91.4	-30.6	5.46
Supplier A3[2]	97.6	-4.8	0.73
Supplier A4[2]	96.6	-4.6	0.41
Supplier A5[1]	97.6	-3.2	0.43
Supplier B1[1]	92.3	-39.7	1.70
Supplier C1[1]	98.2	-1.7	0.04
Supplier C2[1]	97.9	-0.3	0.06

[1]Sample size n = 3 [2]Sample size n = 1

The durability of the feedstocks as received were all greater than 90%. Typically, woody biomass has a durability in the vicinity of 97% while non-woody biomass has a durability of 92% [119]. One torrefied pellet and one torrefied briquette sample (A2 and B1) had a durability less than 92%, and neither of these samples used a chemical binder during their production. Samples that had a durability greater than 97.5%, as received, include the steam exploded pellets (C1 and C2) and torrefied pellets using water (A1) or an organic binder (A3-A5). The 98.5% durability

metric is considered for judging the quality of advanced solid biofuels by some organizations [101]. The net durability change will be further discussed in conjunction with the water sorptivity. The post-weathered durability is correlated to the severity of the hydrophobicity method employed as seen in Table 3-3.

Table 3-3: Severity factor of hydrophobicity test (shower/immersion) on post-weathered durability for the Industry Evaluation Program of advanced solid biofuels.

Private Sector Producer	Moisture Content as received (wt%)	Durability as received (wt%)	Durability after shower (wt%)	Durability after immersion (wt%)
Supplier A1	3.3	92.3	81.5	60.8
Supplier B1	2.4	91.4	72.7	53.0
Supplier C1	14.2	98.0	97.9	97.6

The results of Table 3-3 indicate that the post-weathered durability is a function of the hydrophobicity test severity (shower or immersion). Durability of pellets and briquettes after the semi-batch shower test (see Figure C-2b) was significantly lower than the as-received values for torrefied materials (A1, B1), while the steam exploded pellet durability differences (C1) were minute in comparison. The same effect was seen – to a greater extent – for the batch 48 h immersion. The water used in the shower test was based on the total rainfall expected in Sudbury over the course of a year (750 mm rain), which is less water compared to the water immersion test (4 L) (see also Section 2.2.5.1).

3.3.2. Water Sorptivity

The water sorptivity of the ten feedstocks was determined after drying the immersed biomass, and the durability was evaluated on the 'as received' and after immersion samples. The water sorptivity after immersion was calculated on a dry basis. The feedstock performance parameters are presented in Table 3-4.

Table 3-4: Analysis of key feedstock parameters for the Industry Evaluation Program of advanced solid biofuels for direct coal substitution.

Advanced Solid Biofuel	Moisture Content As Received (wb wt%)	Sorptivity (db wt%)[1]	MC_{ai} (db wt%)[2]	MC_{eq} (db wt%)[3]
G1: Poplar ITD	2.6	27.2	27.6	3.6
G2: Poplar + 10wt% tar	2.9	172.0	175.0	5.0
Supplier A1	3.3	53.1	56.5	3.8
Supplier A2	2.4	51.8	54.2	0.7
Supplier A3	4.2	33.1	37.5	4.7
Supplier A4	5.6	38.2	44.1	3.7
Supplier A5	6.1	35.7	42.2	4.5
Supplier B1	3.4	53.6	57.1	12.6
Supplier C1	11.1	21.9	34.4	2.0
Supplier C2	14.2	20.0	36.6	19.0

[1]The sorptivity is a measure of the hydrophobicity excluding the starting moisture content.

[2]Moisture content following the 48-hour immersion.

[3]Equilibrium moisture content after the 48-hour immersion and convective drying.

The differences in the original moisture content for the two thermal treatments (torrefaction from Suppliers A and B, samples G of this investigation, and steam explosion from Supplier C) were significant. Torrefied materials have an as-received moisture content of approximately 3-6 wt% while steam exploded materials can be received at the upper limit of the acceptable moisture content (10-14 wt%). Torrefied samples that used moisture or a chemical binder during densification have a slightly greater moisture content compared to the baseline for torrefied materials (~2 wt%). In contrast, steam exploded materials likely have a higher surface density of polar functional groups which would favour an increase of the moisture content, as received.

Poplar briquettes (Sample G2) produced by the integrated torrefaction and densification were limited to 27.6 wt% db after immersion, and steam exploded pellets were similar to A3 (34-37 wt% db). In general, torrefied materials were more hydrophilic than expected, since the initial moisture content after immersion was between 40-60 wt% db (with one exception). The performance of torrefied materials may be due to excess pore structures to increase the

saturated water absorption threshold. Torrefied pellets using water as a binder during production (A1) does not improve the hydrophobicity as expected (56.5% sorptivity). A comparison of means between A1 and A2 for sorptivity gives a p-value of 0.7. After the immersion and the drying tests, samples were evaluated for post-weathered durability. As expected, torrefied materials become more brittle and are more susceptible to stresses from immersion. The swelling that occurred during immersion was not completely eliminated upon drying such the residual swelling led to looser bonds resulting in lower durability.

The torrefied pellets and briquettes without a chemical binder (A2 and B1) performed poorly after immersion in terms of the sorptivity and net durability. With respect to sorptivity, both materials exceeded 50%, and were found to have statistically similar means ($p = 0.34$). Both samples looked very fragile after immersion. The A2 sample had a durability after immersion close to 60% ($n = 1$), and the B1 sample was similarly affected with a durability after immersion was 53% ($n = 2$); see also Figure 2-15. The torrefied briquettes (B1) were evaluated prior to reaching the target mass (the target mass was overshot by 7.5%, and the moisture content was 10.1 wt%). Applying a binder during production certainly improves the post-weathered durability: A1 was only 10% points less than the durability (AR) compared to A2 (30% points). Applying an organic chemical binder improves both the sorptivity and post-weathered durability: a comparison of A2 and A5 has a p-value for sorptivity of 0.002, and showed a 5% durability difference (compared to 30%). Two independent samples with the same binder (A4 and A5) had a p-value for sorptivity of 0.48. In contrast, the commercial steam exploded pellets withstand the immersion process well. The post-weathered durability of steam exploded pellets (C2) was greater compared to a strong torrefied pellet sample (A5) with a binder (p-value = 0.12). In fact, steam exploded pellets only change in post-weathered durability by about 1% compared to the as received material. Two independent samples from the same company (C1 and C2) had statistically different sorptivity values ($p = 0.04$) because of changes to the industrial process between those two samples (removing surface extractives after steam explosion).

3.3.3. Physical Process Changes

A complete mass balance was performed on all of the immersion tests for hydrophobicity. The mass balance typically closed between 99.2% and 99.8%, which allowed for specific

quantification of losses in the aqueous phase after immersion (extractives from molecular diffusion). The extractives were expected to be dilute on the order of parts per million because the final liquid phase mass was ~4.3 kg. The total moisture uptake was determined by the difference between the immersed material and the subsequent drying of the material.

The leachate is defined as the water from the immersion bath that remained in the liquid phase after 48 hours. For every immersion experiment at 48 hours, the leachate was discoloured in the presence of the advanced solid biofuel. This leachate may contain some extractives. The leachate from the poplar bark briquette tests (ITD condition and the Pyrolysis Tar additive) was tested further to discern the nature of the contaminants. A two-stage liquid-liquid separation was performed using 20 v/v% methanol in dichloromethane as per Kourtchev *et al*. for biomass organics [120]. The mass balance closed on average at 97.6%, which is likely due to the low vapour pressure of dichloromethane (57.3 kPa at 25°C). In general, the gas chromatography-mass spectrometry (GC-MS) results suggest that the contaminant concentration is on the order of 50-100 ppm in a leachate sample that was, on average, 5.0 kg for the poplar briquette experiments. The results show 1 ppm of halides (fluorine, chlorine, and bromine) and sulphates. One interesting difference is 1 ppm of phosphate from ITD briquettes compared to 30 ppm phosphate in the Poplar + Pyrolysis Tar test suggesting either 1) the phosphate washes more easily from porous briquettes; or 2) the removal of some phosphate via the ITD process.

3.3.4. Feedstock Drying

Experimental data and theoretical predictions from literature and first principles models are all analyzed for the resulting changes in temperature by performing an energy balance and changes in mass by diffusion and evaporation.

3.3.4.1. Transient Heat Transfer

The transient temperature profile has not yet been determined experimentally for pellet samples because of their small size (4 mm radius) and the size of available thermocouples. The briquettes are of the order of tens of millimetres and it was possible to insert a thermocouple to register the transient temperature profile. Only one sample, namely the commercial torrefied briquettes (B1), was tested while a thermocouple was inserted within the particle to monitor the

change in temperature with time (dT/dt). For all other samples, the energy balance can be simulated assuming some properties for the wet biomass after immersion (see Figure D-6).

The drying experiment was performed after the 16-hour immersion of a single briquette (for the energy balance), and a 48-hour study in triplicate for the mass balance. Both the temperature of the briquette and the moisture content were recorded as a function of time. These tests were done separately so that the thermocouple was undisturbed by taking mass data. The moisture content was determined with the weight of the sample as a function time. The da Silva (2013) model parameters were used to predict the mass transfer. The change in temperature of the briquette depends on both the convective heat transfer and the rate of evaporation of water. Due to the coupled nature of heat and mass transfer during drying, the da Silva (2013) model was also used to model the energy balance. The model parameter values for 'a' and 'b' were $5\times10^{-3}/\text{min}^{b}$ and 0.979, respectively ($R^2 = 0.9942$ after a time period of 100 min). The experimental and numerical simulation results are given in Figure 3-2.

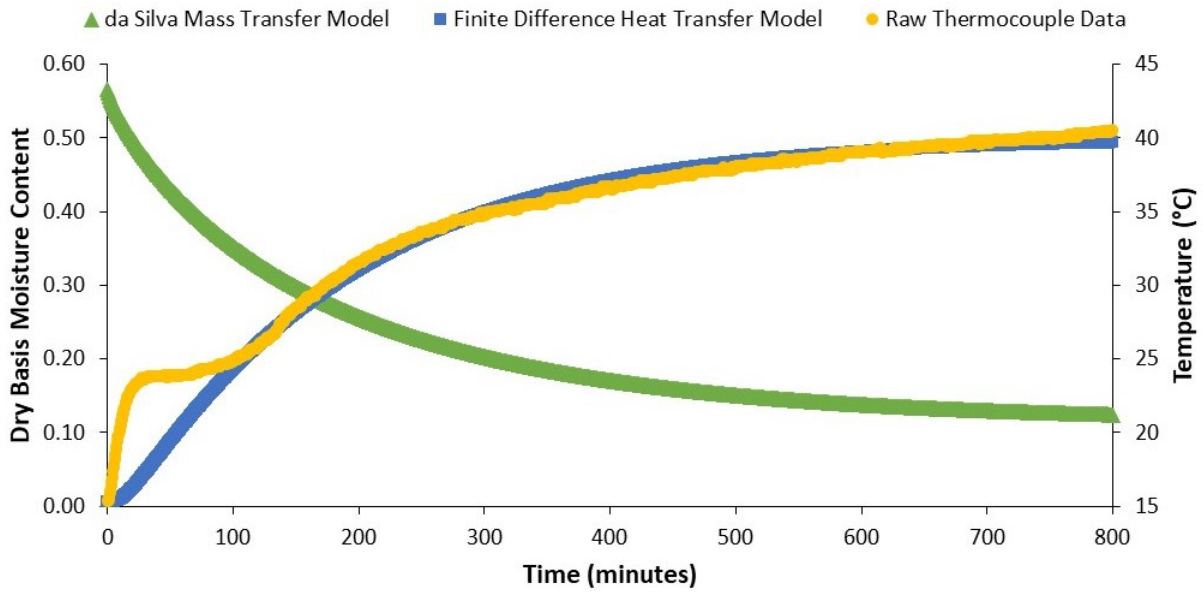

Figure 3-2: Coupled effect of mass transfer and heat transfer during drying. Experimental results with a stainless steel thermocouple (yellow) and the energy balance model solution (blue) are shown. The unsteady state temperature profile was modeled using the da Silva *et al*. (2013) and finite difference models on the secondary vertical axis (right). Accompanying the heat transfer is the fitted response from three trials of unsteady state mass transfer using the da Silva *et al*. (2013) model.

The precise location of the thermocouple was 6 mm from the radial centre (r = 0) and 12 mm from the longitudinal centre (z = 0). The results show a significant delay (a few hours) before

the briquettes reach the ambient temperature (40°C). The temperature of the pellet/briquette did not increase more rapidly because of the evaporation at the surface, which requires the latent heat of vaporization. Within the first 25 minutes, the temperature did rise at a rate of 0.4°C/min, but the observed derivative transitioned for the period [25, 100] minutes. The thermocouple was not adequately insulated and so the first 100 minutes of data is compounded by direct heat transfer from the air to the stainless steel casing protecting the thermocouple. The finite difference model was applied to solve the energy balance as seen in Table 3-5.

Table 3-5: Results from finite difference solutions to the energy balance resulting from experimental data.

Thermal Properties	Time t > 100 min
Conductivity (W/m K)	0.36
Diffusivity (m^2/s)	3.3×10^{-8}
Convection (W/m^2 K)	7.5

The numerical agreement between the data and the finite difference models was good for both time periods: 0.9910 (R^2) for t > 100 min, and 0.9441 (R^2) for t < 25 min [121]. It is possible that the discrepancies in the fit are related to the resolution of the thermocouple (± 0.1°C).

3.3.4.2. Transient Mass Transfer

The drying profiles after immersion were determined for the seven commercial pellet and briquette samples as well as two in-house briquette samples. The methods of drying included room temperature bench top drying in a laboratory controlled atmosphere as well as a drying in an oven at 40°C with some air exchange. Two models (empirical and first principles) were used to simulate each dynamic data set. The results for commercial pellets and briquettes are presented in Figure 3-3, with the exception of the results of sample A2 which are presented in Figure 3-4 where experiments were performed at two drying conditions.

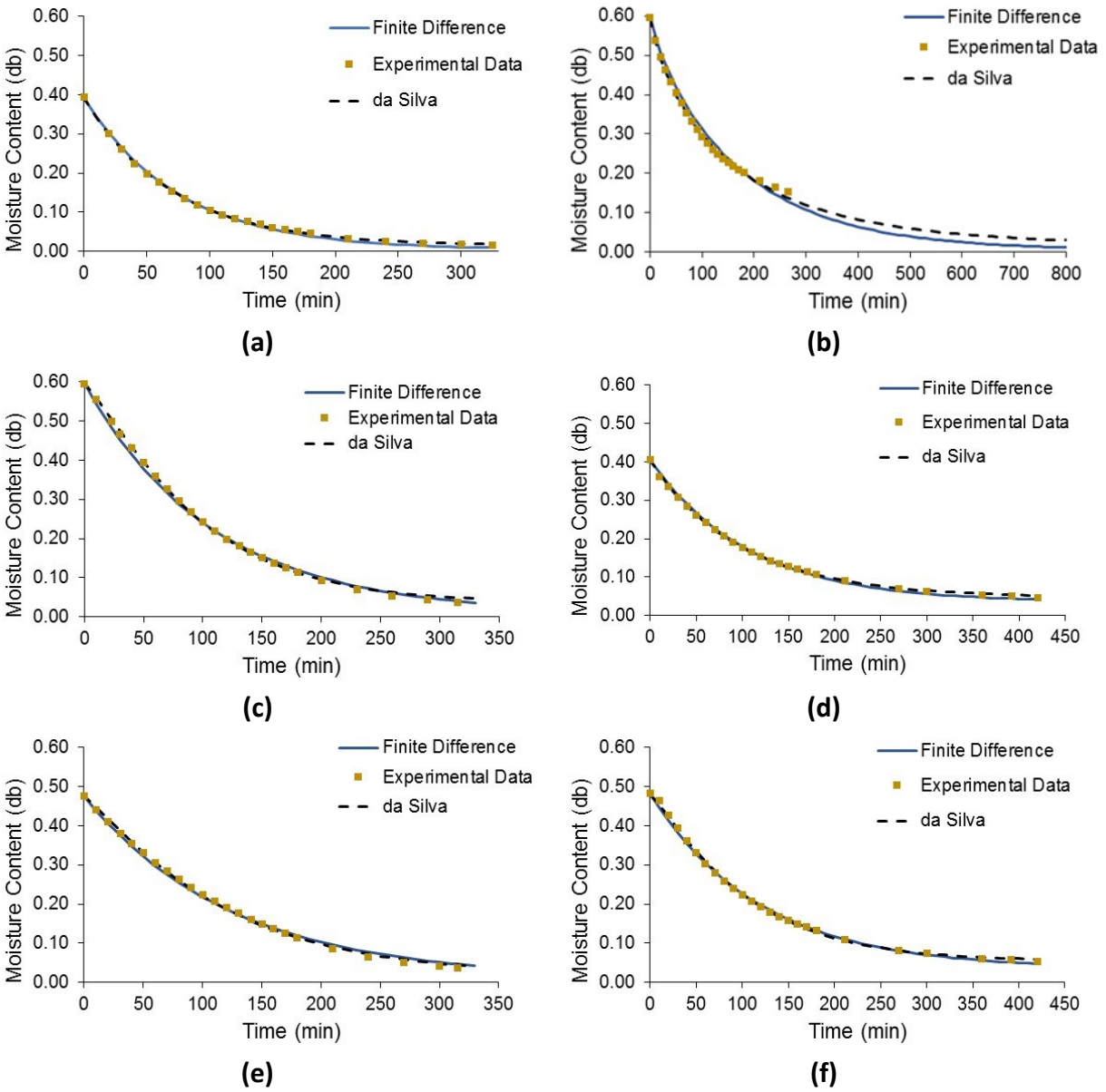

Figure 3-3: Experimental data and finite difference simulated data using the two drying simulation models for the 6 advanced solid biofuels. (a) Commercial steam exploded pellets C1, (b) torrefied briquettes B1, and (c)-(f) torrefied pellets. The plots of the torrefied pellets correspond to samples A1, A3, A4, and A5.

The results in Figure 3-3 show that 1) the initial moisture contents start at 0.4-0.6 (wt% db) depending of the water sorptivity of the samples; 2) the drying times vary between 300-650 minutes (5-10 h); 3) the final moisture contents are less than 10 wt% db; and 4) the variations in the drying rate are due to different pore tortuosity and tightness, which affect the effective water diffusivity. Steam exploded pellets dry rapidly (Figure 3-3a), and return to their initial moisture content of 12.5 wt% db (before immersion) after 100 minutes. In contrast, the torrefied pellets

in Figure 3-3 (c)-(f) had an original moisture content in the range of 3-6 wt% db, and the drying times after immersion needed to reach the initial values were longer. From Figure 3-3a, it takes about 4.5 hours to reach 3 wt% db. Some torrefied pellets, such as sample A3, took as long as 7 hours to reach the desired moisture content (Figure 3-3d). These results support the idea that torrefied pellets may have a greater tortuosity. As a result, the effective diffusivity coefficient is smaller and the drying time increases. When a binder is used to manufacture torrefied pellets (A4 and A5 in Figure 3-3e, f), the moisture content after immersion is lower than simple torrefied pellets (A1). It is possible that the binder filled some of the pores in sample A3 creating a less tortuous path for diffusion leading to an increase in the diffusion coefficient. The drying curve for the commercial torrefied briquettes (Figure 3-3b) shows that a further 60 g of moisture had to be dried off to reach the target mass, and 250 g had been removed in the first 4.5 hours. Effectively, the torrefied briquettes have a 6-fold larger characteristic length compared to the torrefied pellets, and influences the drying time. Unlike the commercial torrefied pellets, which were dried to the target mass after 4 hours, the torrefied briquettes require a minimum of 10-16 hours for drying depending on the initial moisture content after immersion.

Some differences in the drying curve can be attributed to the experimental set up within the oven. All four torrefied pellet samples were done such that both oven trays were used at the same time. As a consequence, the sample on the upper tray was close to the air exchange and higher forced convection. The samples placed on the upper tray are in Figure 3-3d and Figure 3-3e (A3 and A4). The samples placed on the lower tray are in Figure 3-3c and Figure 3-3f (A1 and A5). Results show that the effective diffusion coefficient is repeatable for A5 with two different oven configurations. However, the mass transfer coefficient is 1.54-fold greater for the sample drying in isolation. In contrast, the results in Figure 3-3a and Figure 3-3b (steam exploded pellets and torrefied briquettes) were tested on their own using the bottom tray.

Two different models were generated for commercial steam exploded and torrefied pellet drying. The results from these drying curves are given in Figure 3-4. Forced convection at 40°C was used for two experiments (Figure 3-4a and Figure 3-4c) as in Figure 3-3. Other experiments were performed with forced convection at 20°C on the open laboratory bench

(Figure 3-4b and Figure 3-4d). The drying time to reach the target mass for A2 samples is 4 hours (or 240 minutes) at 40°C and 5 days (7200 minutes) at 20°C, respectively.

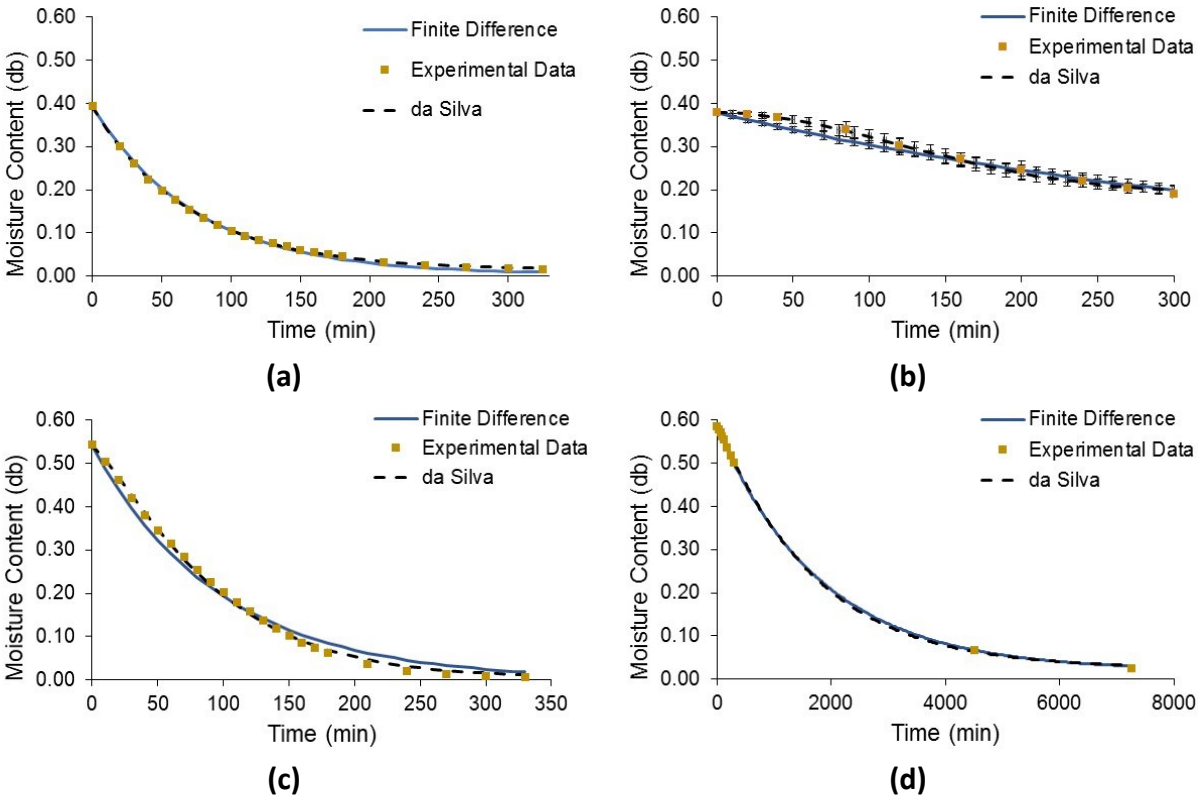

Figure 3-4: Drying profiles of (a)-(b) commercial steam exploded and (c)-(d) torrefied pellets using two drying methods. On the left, drying was done in an oven with air flow and bulk fluid temperature of 40°C. On the right, the corresponding sample was dried on an open laboratory bench at 20°C in stagnant air.

The unsteady state drying profiles for poplar tar briquettes (a) and ITD poplar briquettes (b) are presented in Figure 3-5.

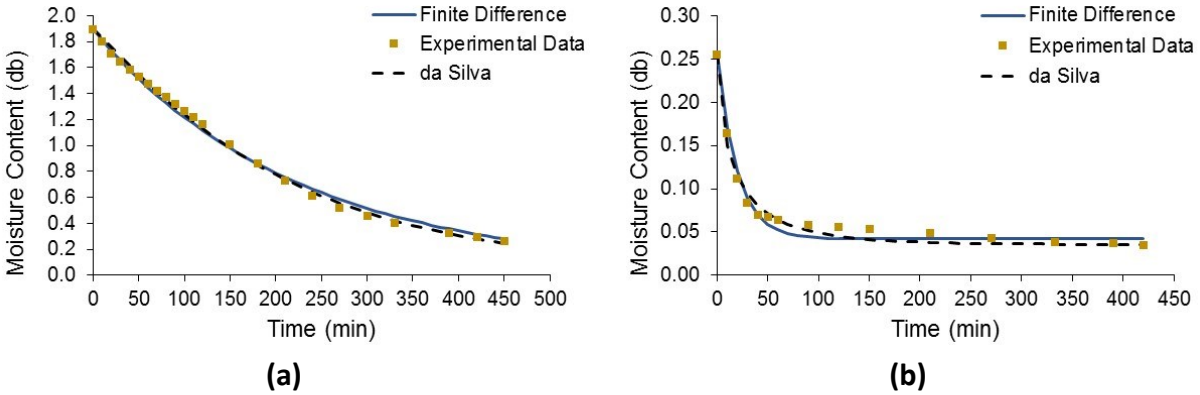

Figure 3-5: Experimental and simulated drying profiles for (a) poplar tar and (b) ITD briquettes following a 48-h water immersion. Drying was performed in an oven at 40°C with mild air flow rate.

The physical appearance of ITD poplar briquettes after water immersion and drying was nearly identical to the original briquettes before immersion, whereas the poplar briquettes without the addition of tar crumbled after lifting the sieve from the water bath. The briquettes produced from poplar with 10 wt% tar maintained their physical shape although there was substantial swelling due to water uptake (see Figure 2-16b i-iii). The most significant difference observed in the two drying curves of Figure 3-5 is the initial rate of change at the onset of drying. The unaccomplished change at 60 minutes was 13.6% and 76.7% for ITD poplar (Figure 3-5b) and poplar tar (Figure 3-5a) briquettes, respectively. This suggests that the ITD poplar briquettes had much of their moisture content closer to the briquette surface and it was more easily driven off by convection. In contrast, the poplar tar briquette had a water sorptivity that was much larger due to the larger porosity. The water was able to penetrate much deeper inside the particle and water had to diffuse from within the particle to the surface for evaporation. Overall, the unaccomplished change for ITD poplar and poplar tar briquettes was 2.3% and 17.2%, respectively after 400 minutes. The parameters of the two drying models to fit Equation (3-1) ('a' and 'b') and (3-5) (D_e and k_c) are summarized in Table 3-6.

Table 3-6: Mathematical modeling results for the drying curves of the seven commercial samples and the two in-house briquettes.

Commercial and In-house advanced solid biofuels	Finite Differences		Empirical Model (da Silva *et al.*)		Correlation Coefficient (R^2 min)[1]
	$D_e \times 10^8$ (m^2/s)	$k_c \times 10^7$ (m/s)	a ($10^3/min^b$)	b	
G1: ITD Poplar	150	55.0	156	0.627	0.9800
G2: Poplar + 10wt% tar	2.90	4.95	3.00	1.083	0.9912
Supplier A1	0.30	2.30	4.64	1.169	0.9974
Supplier A2	0.80	1.65	3.73	1.223	0.9890
Supplier A3	10.5	2.10	11.2	0.979	0.9981
Supplier A4	1.15	1.60	4.92	1.111	0.9971
Supplier A5	0.40	1.73	6.50	1.108	0.9975
Supplier B1	0.73	8.75	18.2	0.797	0.9850
Supplier C1	4.53	3.75	15.2	0.986	0.9978

[1]The minimum correlation coefficient between the finite differences model and the simple empirical model was retained. The minimum correlation was always found with the finite differences model.

ITD poplar briquettes exceed the other samples tested for drying performance with a diffusion coefficient one to two orders of magnitude greater and a mass transfer coefficient one order of magnitude greater. The empirical model also shows a ten-fold improvement in the coefficient 'a.' During ITD, it is postulated that some pores normally free in commercial pellets are sealed due to the hot compression at 300°C. This would also explain the qualitative results (glossy surface), the lower water absorption, and the fast drying performance relative to other pellets and briquettes. Because of the heavy compaction of the ITD briquettes and the resulting lower water sorption, it is possible that the moisture content was much higher at the surface of the particles and drying occurred much faster. If this is the case, then the diffusion coefficient that was found should in fact be reduced as the simulation assumes that water diffuses throughout the whole particle.

3.4. Discussion

The discussion of the results obtained by finite difference solutions and the transport phenomena parameter is extended to include 1) the numerical method error compared to an analytical solution, and 2) the validity of the Chilton-Colburn analogy for heat and mass transfer when evaporation simultaneously influences the result.

3.4.1. Transient Mass Transfer

Some of the potential limitations of the finite differences solution are the assumptions made to solve the drying problem, such as the initial uniform moisture content, constant diffusion and mass transfer coefficients, and the ideal water activity at the surface of the particles. The advantage of the finite differences solution in comparison with the simple empirical model is that, upon determining the model parameters, it can be used with more confidence to simulate other conditions. On the other hand, the empirical model is specific to one given experiment. In using a numerical solution, it is important to ascertain that the integration time step and the geometrical mesh size be chosen large enough to reduce the computation time but small enough to ensure stability and precision. In other words, the solution must be mesh-independent. The error between a benchmark analytical solution and a numerical solution can provide the magnitude of the expected accuracy. In this investigation, a step size of 1 mm, both in the radial and longitudinal directions, and an integration time step of 1 s were used for

simulating the drying of advanced solid biofuels. In general, the accuracy of the numerical solution compared to the analytical solution was within 1.5%. A further investigation of the numerical and analytical solutions is needed to reduce the error using more sophisticated techniques.

The diffusion coefficient for the steam exploded pellets was similar to expectations, while the k_c value was two orders of magnitude lower than expectations (see Table 3-6). The majority of the sum of the squares of the errors can be found at the first two data points after initiating drying. The diffusivity of water molecules in a solid can vary considerably, but is typically on the order of 10^{-7} to 10^{-8} m^2/s; the effective diffusivity in this system is lower because the pores in the biomass are tortuous, and the flow around the pellets is also complex [100]. The diffusion coefficient for torrefied pellets was one sixth of the value for steam exploded pellets, possibly because the torrefied pellets have smaller pores and are more compacted. The convective mass transfer coefficient was typically 10^{-7} m/s in this system because the overall geometry was very similar.

3.4.2. Transient State Heat Transfer

In the drying system with a heat transfer fluid at 40°C and an initial sample temperature at ~20°C, heat and mass transfer occur simultaneously. In practice, the mass transfer and heat transfer coefficient can be determined from the other using the Chilton-Colburn analogy. However, the heat transfer coefficient estimation becomes inaccurate in cases of large mass flux because of the impact of the heat of vaporization on the energy balance [122]. When the mass flux is of the order of 0.001-0.01 kg/m^2s, the Chilton-Colburn analogy holds well [122]. However, experimentally, the mass flux from a single pellet was on the order of 0.06-0.25 kg/m^2s. Therefore, the heat transfer coefficient can be estimated only from the single temperature profile data set from torrefied briquettes. The Chilton-Colburn analogy predicts a mass transfer coefficient k_c of 1.0×10^{-4} m/s for a heat transfer coefficient of 7.5 W/m^2K. Conversely, the same analogy predicts a heat transfer coefficient of 0.03 W/m^2K for a convective mass transfer coefficient of 3.75×10^{-7} m/s. However, if the heat transfer coefficient was that low, then the unsteady state heat transfer would take much longer than 30 minutes. If k_c was that high, the drying would be complete much faster than observed experimentally.

3.5. Conclusions

The purpose of this study was to examine commercial and in-house advanced solid biofuels for water sorption and indirectly hydrophobicity by measuring the moisture uptake after immersion, the impact of biomass pre-treatment methods on water sorption and drying rates, and the changes in mechanical integrity before and after immersion.

The results show that torrefied pellets require an organic binder in order to prevent serious damage to the advanced solid biofuel in case of prolonged exposure to moisture. Torrefied pellets and briquettes have a moisture content after immersion (dry basis) of 40-60 wt% which suggests the materials are not as hydrophobic as previously thought. Rather, torrefied materials are porous and have a high capacity for water uptake. In contrast, steam exploded pellets have a lower hydrophilicity (35 wt%) possibly because the pore volume is smaller which limits the water uptake capacity. Poplar briquettes produced by integrated torrefaction and densification show the lowest hydrophilicity among the tested biomass pre-treatment methods (28 wt%). Coal water immersion for 48 hours from the literature has a sorptivity of about 6 wt%, so future work (larger scale studies of ITD materials substituting coal) must plan for this hydrophobicity gap.

The experimental drying profiles for mass and heat transfer were evaluated and compared to models from first principles and from literature for ten different advanced solid biofuel samples. Integrated torrefaction and briquetting yields a product that dries faster than all other pre-treatment methods studied suggesting the presence of a higher surface moisture content with very small pore volume for water uptake. After 1 hour of drying steam exploded pellets and ITD briquettes, the steam exploded pellets had over half (56.1%) of the unaccomplished change remaining compared to just 13.6% for ITD briquettes. In conclusion, ITD processes lead to an advanced solid biofuel that most resembles coal in terms of the ability to be stored outdoors with a decreased risk to mechanical or biological degradation when exposed to the exterior elements.

Chapter 4. Conclusions and Recommendations

The following conclusions and recommendations follow from the problem statement and the results presented in Chapter 2 and Chapter 3.

4.1. Conclusions

Two important aspects of chemical engineering research are to deliver technical solutions to benefit society and find a cost-effective means of implementation. In the case of limiting CO_2 emissions and curbing the effects of global climate change, chemical engineering research is, and will be, a major player to achieve these ends. A sensitivity analysis would highlight the need to focus on processes that emit large quantities of CO_2 on the nature of their scale and the demand for products. These industries include, but are not limited to, iron/steel, cement, and electric power production. All three of these industries rely on fossil fuels (in particular solid coal) to meet the process energy demands. To that end, one way to limit CO_2 emissions would be to transform these industries away from coal towards a more sustainable fuel source.

In this thesis, renewable biomass waste resources were transformed in order to improve the fuel quality on a few fronts. These include woody biomass such as willow residue and poplar bark which have short life cycles, switchgrass plants which are considered a fuel crop, and waste from the pulp and paper industry (hog, knot, and sludge fuel) which the industry typically pays money to dispose of. The results suggest that treated each material to an integrated torrefaction and densification process (ITD) improves the fuel quality in ways that neither single process can achieve in isolation. Pellets and briquettes were produced by 1) ITD, 2) simple densification, and 3) torrefaction followed by a cool down and subsequent densification. The torrefaction treatment at 300-325°C with limited oxygen improves the energy content of the fuel from 18 MJ/kg to 22-24 MJ/kg. The carbon and fixed carbon content both increase for willow and poplar briquettes as the volatile matter is driven away as condensable and non-condensable gases. The densification step helps improve the bulk density of the fuel which economically is important for industries who pay for shipping costs for fuel (sometimes over 100 km if necessary). When the densification step happens at elevated temperatures (in the torrefaction temperature range), there is less energy needed to compress biomass made somewhat fluid because of the applied heat. Further, the ITD product is less porous, strong against abrasion stress, and resistant to

moisture uptake. This is significant to industry because the ITD fuel product would generate less dust/fines during routine solids handling (decreasing the risk of a dust explosion), absorb less water when stored outside (which is more economical compared to building fuel shelters), and far less biodegradable (which permits fuel storage with less concern for climate controlled fuel storage).

The second important component of this research was to draw comparisons to existing biomass solid fuels (advanced solid biofuels) so named for the thermochemical conversion and densification treatments applied to raw materials. This research would help inform industry by de-risking elements of the supply chain of biomass and its compatibility with existing infrastructure. The best commercial advanced solid biofuels were steam exploded pellets because their durability was high (98%), the water sorptivity was low (20 wt%), and the durability after immersion and drying was greater than 97%. The best torrefied commercial pellet requires the extra step of adding a binder during densification, and results showed performance slightly less than those of steam exploded pellets. However, ITD products (pellets and briquettes) showed a high durability (97-99%), low water sorptivity (27%) and faster drying compared to all other materials on the account of a low porosity (four-fold after 1 hour at 40°C with air flow).

4.2. Recommendations

The major recommendation from this thesis is the examination of commercial and under-development advanced solid biofuels that can be reliably used by industry with minimal additional expenses so that the shift from non-renewable to renewable resources is heavily emphasized. To that end, pilot-scale demonstrations of integrated torrefaction and densification will be one aspect of this evaluation program. The technology needs to be designed such that raw solid biomass is fed, torrefied (sealed off from most oxygen), and sent hot to a densification equipment piece in a continuous process. Other technologies patented and under development will need to be assessed by standards informed by industrial experience with coal. Techno-economic and life cycle analysis will need to be considered for these advanced solid biofuels. The data for these papers will have to originate from scientists and engineers around the world. Only a collective effort will be enough to enact change on the scale necessary to change the path of climate disruptions that have been studied decades ago.

Bibliography

[1] A. Steiner, M. Jarraud, Climate Change 2007: The Physical Science Basis, Intergovernmental Panel on Climate Change, Cambridge, 2007. https://doi.org/10.1017/CBO9781107415324.004.

[2] T.M. Thompson, Modeling the climate and carbon systems to estimate the social cost of carbon, Wiley Interdiscip. Rev. Clim. Chang. 9 (2018) 1–12. https://doi.org/10.1002/wcc.532.

[3] W. de Jong, J.R. van Ommen, eds., Biomass as a sustainable energy source for the future: fundamentals of conversion processes, John Wiley and Sons, Hoboken, 2014.

[4] R.W.. Zwart, H. Boerrigter, E.. Deurwaarder, C.. van der Meijden, S.V.. van Paasen, Production of Synthetic Natural Gas (SNG) from Biomass Development and operation of an integrated, SenterNovem. (2006) 1–61. file:///C:/Users/HP/OneDrive/Favoritos/doutorado/Doutorado/escrevendo artigos/Introdução/zwart 2006.pdf.

[5] B. Dudley, BP Statistical Review of World Energy, in: British Petroleum BP, London, 2017: p. 48. https://doi.org/10.1016/j.egypro.2013.06.172.

[6] R. Symonds, CCUS (Carbon Capture Utilization and Storage): Overview, in: CanmetENERGY-Ottawa (Ed.), University of Ottawa - Graduate Course Lecture CHG 8191, Ottawa, ON, 2018: pp. 1–36.

[7] H. Ritchie, M. Roser, Primary Energy Consumption, Our World Data. (n.d.). https://ourworldindata.org/fossil-fuels#coal (accessed November 28, 2018).

[8] S. Baldwin, Carbon Footprint of electricity generation (POSTnote 268), Parliam. Off. Sci. Technol. (2006) 1–4. http://www.parliament.uk/documents/upload/postpn268.pdf.

[9] Metallurgy - The Extraction of Iron, Chem. Libr. (n.d.). https://chem.libretexts.org/Textbook_Maps/Inorganic_Chemistry/Supplemental_Modules_(Inorganic_Chemistry)/Descriptive_Chemistry/Elements_Organized_by_Block/3_d-Block_Elements/1b_Properties_of_Transition_Metals/Metallurgy/The_Extraction_of_Iron/Iron_Product (accessed November 28, 2018).

[10] M.A. Quader, S. Ahmed, R.A.R. Ghazilla, S. Ahmed, M. Dahari, A comprehensive review on energy efficient CO 2 breakthrough technologies for sustainable green iron and steel manufacturing, Renew. Sustain. Energy Rev. 50 (2015) 594–614. https://doi.org/10.1016/j.rser.2015.05.026.

[11] C. Wang, P. Mellin, J. Lövgren, L. Nilsson, W. Yang, H. Salman, A. Hultgren, M. Larsson, Biomass as blast furnace injectant - Considering availability, pretreatment and deployment in the Swedish steel industry, Energy Convers. Manag. 102 (2015) 217–226. https://doi.org/10.1016/j.enconman.2015.04.013.

[12] M. Anheden, L. Uhlir, Roadmap 2015 to 2025 Biofuels for low-carbon steel industry, Res. Institutes Sweden. (2015) 1–10.

[13] Uses of Coal, World Coal Assoc. (n.d.). https://www.worldcoal.org/coal/uses-coal (accessed November 19, 2018).

[14] Commodities - Metals: Learn about Metallurgical Coal, Balanc. (n.d.). https://www.thebalance.com/what-is-metallurgical-coal-2340012 (accessed November 19, 2018).

[15] H. Suopajärvi, E. Pongrácz, T. Fabritius, The potential of using biomass-based reducing agents in the blast furnace: A review of thermochemical conversion technologies and assessments related to sustainability, Renew. Sustain. Energy Rev. 25 (2013) 511–528. https://doi.org/10.1016/j.rser.2013.05.005.

[16] A. Spanlang, W. Wukovits, B. Weiss, Development of a blast furnace model with thermodynamic process depiction by means of the rist operating diagram, Chem. Eng. Trans. 52 (2016) 973–978. https://doi.org/10.3303/CET1652163.

[17] M. Duchesne, Other Thermal Conversion Systems, in: CanmetENERGY-Ottawa (Ed.), University of Ottawa - Graduate Course Lecture CHG 8191, Ottawa, ON, 2018: pp. 1–30.

[18] Coal & Cement, World Coal Assoc. (n.d.). https://www.worldcoal.org/coal/uses-coal/coal-cement (accessed November 19, 2018).

[19] N. Chatziaras, C.S. Psomopoulos, N.J. Themelis, Use of waste derived fuels in cement industry: a review, Manag. Environ. Qual. An Int. J. 27 (2016) 178–193. https://doi.org/10.1108/MEQ-01-2015-0012.

[20] P. Vesterinen, E. Alakangas, K. Veijonen, M. Junginger, Solutions for biomass fuel market barriers and raw material availability, Jyväskylä, 2010.

[21] R. Saidur, E.A. Abdelaziz, A. Demirbas, M.S. Hossain, S. Mekhilef, A review on biomass as a fuel for boilers, Renew. Sustain. Energy Rev. 15 (2011) 2262–2289. https://doi.org/10.1016/j.rser.2011.02.015.

[22] D. Lu, Fluidization: Fluidization Bed Technologies, in: CanmetENERGY-Ottawa (Ed.), University of Ottawa - Graduate Course CHG 8191, Ottawa, ON, 2018: pp. 1–66.

[23] D. Lu, Conventional Coal Combustion II, in: CanmetENERGY-Ottawa (Ed.), University of Ottawa - Graduate Course Lecture CHG 8191, Ottawa, ON, 2018: pp. 1–46.

[24] M. Duchesne, Clean Thermal Conversion Introduction: An Overview, in: CanmetENERGY-Ottawa (Ed.), University of Ottawa - Graduate Course Lecture CHG 8191, Ottawa, ON, 2018: pp. 1–38.

[25] M. Steen, Greenhouse Gas Emissions From Fossil Fuel Fired Power Generation Systems, 2001. http://publications.jrc.ec.europa.eu/repository/handle/JRC21207.

[26] C. Fralick, From Coal to Biomass: Generating a Sustainable Future, in: Ontario Power Generation, Atikokan, ON, 2018: pp. 1–4.

[27] Coal Formation, World Coal Assoc. (n.d.). https://www.worldcoal.org/coal/what-coal (accessed November 19, 2018).

[28] M. Duchesne, Technical Drivers, in: CanmetENERGY-Ottawa (Ed.), University of Ottawa - Graduate Course Lecture CHG 8191, Ottawa, ON, 2018: pp. 1–29.

[29] G. Ökten, O. Kural, E. Algurkaplan, Storage of Coal: Problems and Precautions, Energy Storage

Syst. II (2008) 1–15.

[30] D. Lu, Conventional coal combustion I, in: CanmetENERGY-Ottawa (Ed.), University of Ottawa - Graduate Course Lecture CHG 8191, Ottawa, ON, 2018: pp. 1–41.

[31] M. Duchesne, Coal: An Overview, in: CanmetENERGY-Ottawa (Ed.), University of Ottawa - Graduate Course Lecture CHG 8191, Ottawa, ON, 2018: pp. 1–40.

[32] P.L. Spath, M.K. Mann, D.R. Kerr, Life Cycle Assessment of Coal-fired Power Production, Golden, 1999. https://doi.org/10.2172/12100.

[33] A.A. Khan, W. de Jong, P.J. Jansens, H. Spliethoff, Biomass combustion in fluidized bed boilers: Potential problems and remedies, Fuel Process. Technol. 90 (2009) 21–50. https://doi.org/10.1016/j.fuproc.2008.07.012.

[34] J. Guinée, M. Gorrée, R. Heijungs, G. Huppes, R. Kleijn, A. de Koning, L. van Oers, S.A. Wegener, S. Suh, H. Udo de Haes, H. de Bruijn, R. van Duin, M. Huijbregts, Handbook on Life Cycle Assessment. Operational Guide to the ISO Standards, Dordrecht, 2002.

[35] N. Wrisberg, H. Udo de Haes, U. Triebswetter, P. Eder, R. Clift, Analytical Tools for Environmental Design and Management in a Systems Perspective: The Combined Use of Analytical Tools, Dordrecht, 2002.

[36] G. Berndes, N. Bird, A. Cowie, Bioenergy, land use change and climate change mitigation— background technical report, Rotorua, 2011.

[37] J. Cramer, E. Wissema, M. de Bruijne, E. Lammers, D. Dijk, H. Jager, Testing framework for sustainable biomass (final report), Utrecht, 2007.

[38] G. Berndes, M. Hoogwijk, R. Van Den Broek, The contribution of biomass in the future global energy supply: A review of 17 studies, Biomass and Bioenergy. 25 (2003) 1–28. https://doi.org/10.1016/S0961-9534(02)00185-X.

[39] J.E.G. van Dam, W. Elbersen, R. van Ree, Setting up international biobased commodity trade chains, Utrecht Wageningen, 2014.

[40] R. Samson, M. Drisdelle, L. Mulkins, C. Lapointe, P. Duxbury, The use of switchgrass biofuel pellets as a greenhouse gas offset strategy, in: Bioenergy 2000 Conf., 2016: pp. 1–9. http://scholar.google.com/scholar?hl=en&btnG=Search&q=intitle:The+use+of+switchgrass+biofuel+pellets+as+a+greenhouse+gas+offset+strategy#0.

[41] A. Cook, C. Agnew, Technical Assessment of Grass Pellets as Boiler Fuel in Vermont, in: Vermont Grass Energy Partnersh. Final Rep., 2011: pp. 1–52.

[42] G. Gardbro, K. Åberg, A. Nordin, Techno-economic modeling of the supply chain for torrefied biomass, Umeå University, 2014.

[43] S. V. Vassilev, C.G. Vassileva, V.S. Vassilev, Advantages and disadvantages of composition and properties of biomass in comparison with coal: An overview, Fuel. 158 (2015) 330–350. https://doi.org/10.1016/j.fuel.2015.05.050.

[44] M. Duchesne, Ash and Slag, in: CanmetENERGY-Ottawa (Ed.), University of Ottawa - Graduate

Course Lecture CHG 8191, Ottawa, ON, 2018: pp. 1–52.

[45] M.R. Pelaez-Samaniego, V. Yadama, M. Garcia-Perez, E. Lowell, A.G. McDonald, Effect of temperature during wood torrefaction on the formation of lignin liquid intermediates, J. Anal. Appl. Pyrolysis. 109 (2014) 222–233. https://doi.org/10.1016/j.jaap.2014.06.008.

[46] S. Clarke, F. Preto, Biomass Densification for Energy Production, Minist. Agric. Food Rural Aff. (2017) 1–16. http://www.omafra.gov.on.ca/english/engineer/facts/11-035.htm.

[47] K.J. Moscicki, L. Niedzwiecki, P. Owczarek, M. Wnukowski, Commoditization of biomass: dry torrefaction and pelletization—a review, J. Power Technol. 94 (2014) 233–249. https://doi.org/10.1590/S0100-06832003000600020.

[48] H. Boerrigter, J. Kiel, P.C.A. Bergman, Biomass Pre-treatment by Torrefaction, in: ThermalNET Meeting, 2006: pp. 1–10. https://doi.org/10.1007/s11434-010-4143-y.

[49] R. Fry, S. Day, R. Sakurovs, Moisture-induced swelling of coal, Int. J. Coal Prep. Util. 29 (2009) 298–316. https://doi.org/10.1080/19392690903584575.

[50] H.S. Kambo, A. Dutta, Comparative evaluation of torrefaction and hydrothermal carbonization of lignocellulosic biomass for the production of solid biofuel, Energy Convers. Manag. 105 (2015) 746–755. https://doi.org/10.1016/j.enconman.2015.08.031.

[51] D. Thran, ed., Smart Bioenergy, 1st ed., Springer International, Leipzig, 2015. https://doi.org/10.1007/978-3-319-16193-8.

[52] C.E. Brewer, R.C. Brown, D.A. Laird, Biochar characterization and engineering, Iowa State University, 2012. https://doi.org/12284.

[53] W. Stelte, Steam explosion for biomass pre-treatment Resultat Kontrakt (RK) Report, Gregersensvej, 2013.

[54] A. Funke, F. Ziegler, Hydrothermal carbonization of biomass: A summary and discussion of chemical mecha- nisms for process engineering, Biofuels, Bioprod. Biorefining. 4 (2010) 160–177. https://doi.org/10.1002/bbb.

[55] Arbaflame, Arbacore technology, advantages, and production, 2017. https://doi.org/10.1080/713693392.

[56] D. Kim, K. Yoshikawa, K.Y. Park, Characteristics of biochar obtained by hydrothermal carbonization of cellulose for renewable energy, Energies. 8 (2015) 14040–14048. https://doi.org/10.3390/en81212412.

[57] D. Özçimen, F. Karaosmanoğlu, Production and characterization of bio-oil and biochar from rapeseed cake, Renew. Energy. 29 (2004) 779–787. https://doi.org/10.1016/j.renene.2003.09.006.

[58] S. Kloss, F. Zehetner, A. Dellantonio, R. Hamid, F. Ottner, V. Liedtke, M. Schwanninger, M.H. Gerzabek, G. Soja, Characterization of Slow Pyrolysis Biochars: Effects of Feedstocks and Pyrolysis Temperature on Biochar Properties, J. Environ. Qual. 41 (2012) 990–1000. https://doi.org/10.2134/jeq2011.0070.

[59] X. Chen, G. Chen, L. Chen, Y. Chen, J. Lehmann, M.B. McBride, A.G. Hay, Adsorption of copper and zinc by biochars produced from pyrolysis of hardwood and corn straw in aqueous solution, Bioresour. Technol. 102 (2011) 8877–8884. https://doi.org/10.1016/j.biortech.2011.06.078.

[60] C.E. Brewer, V.J. Chuang, C.A. Masiello, H. Gonnermann, X. Gao, B. Dugan, L.E. Driver, P. Panzacchi, K. Zygourakis, C.A. Davies, New approaches to measuring biochar density and porosity, Biomass and Bioenergy. 66 (2014) 176–185. https://doi.org/10.1016/j.biombioe.2014.03.059.

[61] H.S. Kambo, A. Dutta, Strength, storage, and combustion characteristics of densified lignocellulosic biomass produced via torrefaction and hydrothermal carbonization, Appl. Energy. 135 (2014) 182–191. https://doi.org/10.1016/j.apenergy.2014.08.094.

[62] P.S.W. Lam, Steam Explosion of Biomass To Produce Durable Wood Pellets, University of British Columbia, 2011. https://doi.org/10.14288/1.0059133.

[63] D. Basso, F. Patuzzi, D. Castello, M. Baratieri, E.C. Rada, E. Weiss-Hortala, L. Fiori, Agro-industrial waste to solid biofuel through hydrothermal carbonization, Waste Manag. 47 (2016) 114–121. https://doi.org/10.1016/j.wasman.2015.05.013.

[64] HM3 Energy, Torrefaction Mass and Energy Balance, (2011) 1. https://doi.org/10.1006/icar.1999.6134.

[65] J.S. Tumuluru, C.T. Wright, J.R. Hess, K.L. Kenney, A review of biomass densification systems to develop uniform feedstock commodities for bioenergy application, Biofuels, Bioprod. Biorefining. 5 (2011) 683–707. https://doi.org/10.1002/bbb.

[66] The Pelleting Process, Calif. Pellet Mill Co. (n.d.) 1–33. https://doi.org/10.1016/B978-0-12-151504-1.50005-5.

[67] S.C. Bhattacharya, S. Sett, R.M. Shrestha, State of the art for biomass densification, Energy Sources. 11 (1989) 161–182. https://doi.org/10.1080/00908318908908952.

[68] Solid Biofuels, Nat. Resour. Canada. (n.d.). https://www.nrcan.gc.ca/energy/renewable-electricity/bioenergy-systems/biofuels/7399 (accessed December 12, 2018).

[69] W.H. Chen, J. Peng, X.T. Bi, A state-of-the-art review of biomass torrefaction, densification and applications, Renew. Sustain. Energy Rev. 44 (2015) 847–866. https://doi.org/10.1016/j.rser.2014.12.039.

[70] Q. Hu, H. Yang, D. Yao, D. Zhu, X. Wang, J. Shao, H. Chen, The densification of bio-char: Effect of pyrolysis temperature on the qualities of pellets, Bioresour. Technol. 200 (2016) 521–527. https://doi.org/10.1016/j.biortech.2015.10.077.

[71] S. Matali, N.A. Rahman, S.S. Idris, N. Yaacob, Combustion properties, water absorption and grindability of raw/torrefied biomass pellets and Silantek coal, AIP Conf. Proc. 1901 (2017). https://doi.org/10.1063/1.5010527.

[72] S.M. Vahidhosseini, E. Barati, J.A. Esfahani, Green's function method (GFM) and mathematical solution for coupled equations of transport problem during convective drying, J. Food Eng. 187 (2016) 24–36. https://doi.org/10.1016/j.jfoodeng.2016.04.017.

[73] C. Goebl, The Production of Solid Sustainable Energy Carriers from Biomass by Means of Torrefaction, (n.d.). https://sector-project.eu/ (accessed October 24, 2016).

[74] E. Mousa, C. Wang, J. Riesbeck, M. Larsson, Biomass applications in iron and steel industry: An overview of challenges and opportunities, Renew. Sustain. Energy Rev. 65 (2016) 1247–1266. https://doi.org/10.1016/j.rser.2016.07.061.

[75] A. De Carvalho, Challenges & opportuities for the steel industry in moving towards green growth, in: Green Growth Work., Organisation for Economic Co-operation and Development, Seoul, 2010: pp. 1–16. https://doi.org/10.1021/ef900064c.

[76] C. Wiklund, Optimization of a steel plant utilizing converted biomass, Åbo Akademi University, 2016. http://www.doria.fi/handle/10024/123723.

[77] C.D. The Pembina Institute and Environmental, Holcim, Alternative Fuel Use in Cement Manufacturing - Implications, opportunities and barriers in Ontario, in: Work. Altern. Fuels Cem. Kilns, 2014: pp. 1–38.

[78] A. Rahman, M.G. Rasul, M.M.K. Khan, S. Sharma, Impact of alternative fuels on the cement manufacturing plant performance: An overview, Procedia Eng. 56 (2013) 393–400. https://doi.org/10.1016/j.proeng.2013.03.138.

[79] R.K. Patil, M.P. Khond, Alternative Fuels for Cement Industry: A Review, in: Ind. Eng. Oper. Manag., University of Pune (Department of Mechanical Engineering), Bali, 2014: pp. 298–302.

[80] Cembureau, Cembureau Activity Report, in: European Cement Association, Brussels, 2015: pp. 1–48.

[81] E. Alakangas, M. Junginger, J. Van Dam, J. Hinge, J. Keränen, O. Olsson, C. Porsö, A. Martikainen, J. Rathbauer, L. Sulzbacher, P. Vesterinen, J. Vinterbäck, EUBIONET III - Solutions to biomass trade and market barriers, Renew. Sustain. Energy Rev. 16 (2012) 4277–4290. https://doi.org/10.1016/j.rser.2012.03.051.

[82] International Organization for Standardization, Introduction to Standards, (n.d.). https://www.iso.org/standards.html (accessed April 6, 2019).

[83] M. Duchesne, Biofuels and waste : Overview, in: CanmetENERGY-Ottawa (Ed.), University of Ottawa - Graduate Course Lecture CHG 8191, Ottawa, ON, 2018: pp. 1–54.

[84] T. Wilson, Factors affecting wood pellets durability, Pennsylvania State University, 2010.

[85] Solka-Floc, Specification Sheet for Solka-Floc® 200 MO, North Tonawanda, 2012. http://doc.ccc-group.com/spec/478709.pdf.

[86] W. Jin, K. Singh, J. Zondlo, Pyrolysis Kinetics of Physical Components of Wood and Wood-Polymers Using Isoconversion Method, Agriculture. 3 (2013) 12–32. https://doi.org/10.3390/agriculture3010012.

[87] N.Y. Harun, M.T. Afzal, Chemical and Mechanical Properties of Pellets Made from Agricultural and Woody Biomass Blends, Trans. ASABE. 58 (2015) 1–10. https://doi.org/10.13031/trans.58.11027.

[88] J.H. Peng, X.T. Bi, S. Sokhansanj, C.J. Lim, Torrefaction and densification of different species of softwood residues, Fuel. 111 (2013) 411–421. https://doi.org/10.1016/j.fuel.2013.04.048.

[89] R.D. Tumuluru, Jaya Shankar, Sokhansanji, Shahab, Hess, Richard, Wright, Christopher T., Boradman, A review on biomass torrefaction process and product properties for energy applications, Ind. Biotechnol. 7 (2011) 384–401. https://doi.org/10.1089/ind.2011.0014.

[90] C. Schilling, M. Wöhler, F. Yazdanpanah, X. Bi, A. Lau, C.J. Lim, S. Sokhansanj, S. Pelz, Development of a novel wood pellet durability tester for small samples, Vancouver, 2015.

[91] J. Lufei, T. Robinson, G. Tourigny, P. Gaudet, Solid biofuels - Determination of the effect of water on the mechanical durability of advanced solid biofuel pellets by rain emulation, in: CanmetENERGY-Ottawa (Ed.), Ottawa, ON, 2019: pp. 1–13.

[92] A. Birendra, Torrefied wood pellets biowaste sustainable commodity fuel, BioFuelNet. (n.d.). http://www.biofuelnet.ca/2016/06/09/torrefied-wood-pellets-biowaste-sustainable-commodity-fuel/ (accessed October 24, 2016).

[93] Wikipedia, Knot (papermaking), (n.d.). https://en.wikipedia.org/wiki/Knot_(papermaking) (accessed June 10, 2019).

[94] Process Sensors Corporation, Hog Fuel – What is it? & Why is moisture measurement important?, (n.d.). https://www.processsensors.com/whats-new/blog/hog-fuel-what-is-it-why-is-moisture-measurement-important (accessed June 10, 2019).

[95] J. Gullichsen, C.-J. Fogelholm, eds., Chemical Pulping, in: Tech. Assoc. Pulp Pap. Ind., 1st ed., California, 1999: pp. 1–693.

[96] P. Somboon, On the Application of Grits To Thermomechanical Pulp Refining, Helsinki University of Technology, 2009.

[97] B. Ince, Z. Cetecioglu, O. Ince, Pollution Prevention in the Pulp and Paper Industries, in: Istanbul, 2011. https://doi.org/10.5772/23709.

[98] M.I. Neethi, D. Ravindran, P. Subramanian, Biomass Densification Methods and Mechanism, Cogener. Distrib. Gener. 21 (2006).

[99] S. Kokonya, M. Castro-Díaz, C. Barriocanal, C.E. Snape, An investigation into the effect of fast heating on fluidity development and coke quality for blends of coal and biomass, Biomass and Bioenergy. 56 (2013) 295–306. https://doi.org/10.1016/j.biombioe.2013.05.026.

[100] J. Thibault, J.C. Slattery, Advanced Transport Phenomena, Adv. Transp. Phenom. (2018) 1–306. https://doi.org/10.1017/cbo9780511800238.002.

[101] C. Schilling, J.S. Lee, B. Ghiasi, M. Tajilrou, M. Wöhler, C.J. Lim, X.T. Bi, A. Lau, S. Pelz, L. Tabil, S. Sokhansanj, Towards Manufacturing The “ Ideal Pellet ,” in: Can. Soc. Bioeng., University of British Columbia, Edmonton, 2015: pp. 1–13.

[102] Phoenix Wood Pellet Manufacturing Process, Phoenix Wood Pellets. (2016) 1. https://www.phoenixwoodpellets.co.uk/about-us/manufacturing-process (accessed May 1, 2019).

[103] J.D. Payne, Improving quality of pellet feeds, Natl. Agric. Libr. 162 (1978) 34–41.

[104] N. Kaliyan, R. V Morey, Factors affecting the strength and durability of densified products, in: Annu. Int. Meet. ASABE, Portland, 2006.

[105] M. Shaw, Feedstock and Process Variables Influencing Biomass Densification, Saskatoon, 2008.

[106] Q. Hu, J. Shao, H. Yang, D. Yao, X. Wang, H. Chen, Effects of binders on the properties of bio-char pellets, Appl. Energy. 157 (2015) 508–516. https://doi.org/10.1016/j.apenergy.2015.05.019.

[107] Y. Li, H. Liu, High-pressure densification of wood residues to form an upgraded fuel, Biomass and Bioenergy. 19 (2000) 177–186.

[108] I. Obernberger, G. Thek, Physical characterization and chemical composition of densified biomass fuels with regard to their combustion behavior, Biomass and Bioenergy. 27 (2004) 653–669.

[109] C. Greinöcker, W. Pichler, M. Gosler, Hygroscopicity of wood pellets: Test method development - Influence on pellet quality - Coating of wood pellets, in: Second World Conf. Pellets, Jönköping, Sweden, 2006.

[110] T.B. Reed, G. Trezek, L. Diaz, Biomass Densification Energy Requirements, in: Am. Chem. Soc. Natl. Meet., Washington, 1978.

[111] P.C.A. Bergman, Combined torrefaction and pelletisation - The TOP process, Utrecht, 2005. https://doi.org/ECN-C--05-073.

[112] M. Arshadi, R. Gref, Emission of volatile organic compounds from softwood pellets during storage, For. Prod. 55 (2005) 132–135.

[113] D.F. Arseneau, Competitive Reactions in the Thermal Decomposition of Cellulose, Can. J. Chem. 49 (1971) 632–638. https://doi.org/10.1139/v71-101.

[114] A.J. Williams, Levoglucosan and Cellulose, R. Soc. Chem. (2015). www.chemspider.com/ (accessed February 21, 2017).

[115] C. Karr, ed., Analytical Methods for Coal and Coal Products, III, Academic Press, 1978.

[116] Y. Kadioğlu, M. Varamaz, The effect of moisture content and air-drying on spontaneous combustion characteristics of two Turkish lignites, Fuel. 82 (2003) 1685–1693. https://doi.org/10.1016/S0016-2361(02)00402-7.

[117] T. Robinson, P. Gaudet, G. Tourigny, J. Lufei, Determination of water sorptivity of advanced solid biofuels (Draft Procedure), in: CanmetENERGY-Ottawa (Ed.), Ottawa, ON, 2017.

[118] W.P. da Silva, C.M.D.P.S. e Silva, F.J.A. Gama, J.P. Gomes, Mathematical models to describe thin-layer drying and to determine drying rate of whole bananas, J. Saudi Soc. Agric. Sci. 13 (2014) 67–74. https://doi.org/10.1016/j.jssas.2013.01.003.

[119] T. Miranda, I. Montero, F.J. Sepúlveda, J.I. Arranz, C.V. Rojas, S. Nogales, A review of pellets from different sources, Materials (Basel). 8 (2015) 1413–1427. https://doi.org/10.3390/ma8041413.

[120] I. Kourtchev, S. Hellebust, J.M. Bell, I.P. O'Connor, R.M. Healy, A. Allanic, D. Healy, J.C. Wenger,

J.R. Sodeau, The use of polar organic compounds to estimate the contribution of domestic solid fuel combustion and biogenic sources to ambient levels of organic carbon and PM2.5 in Cork Harbour, Ireland, Sci. Total Environ. 409 (2011) 2143–2155. https://doi.org/10.1016/j.scitotenv.2011.02.027.

[121] F.P. Incropera, D.P. DeWitt, T.L. Bergman, A.S. Lavine, Introduction to heat transfer, 5th ed., J. Wiley, Hoboken, NJ, 2007.

[122] L.D. Gu, J.C. Min, Y.C. Tang, Effects of mass transfer on heat and mass transfer characteristics between water surface and airstream, Int. J. Heat Mass Transf. 122 (2018) 1093–1102. https://doi.org/10.1016/j.ijheatmasstransfer.2018.02.061.

[123] Draft International Standard, Solid Biofuels Durability - Pellets, Int. Organ. Stand. (2014). www.iso.org/iso/home/store/catalogue_tc/ (accessed October 24, 2016).

[124] J. Good, L. Ventress, H. Knoef, B.T. Group, U. Zielke, P.L. Hansen, P. De Wild, B. Coda, S. Van Paasen, J. Kiel, T. Liliedahl, Sampling and analysis of tar and particles in biomass producer gases, 1 (2005) 1–44.

Appendix A. Calibration Data

Thermogravimetric analysis (TGA) is conducted using a refined instrument that monitors the change in solid mass as a function of temperature in isothermal or non-isothermal conditions. The mass is calibrated using specific standards suitable for the order of magnitude (µg) accepted by Discover Model DSCV_TGA: Serial Number TGA1-0168. The temperature calibration is completed by taking advantage of a physicochemical property of metals: the Currie point. The Currie point for some metals and their alloys is given in Table A-1.

Table A-1: Theoretical Currie temperature for some paramagnetic metals and alloys.

Metal (Alloy Composition)	Currie Temperature (°C)
Alumel	152.6
Nickel	354.0
Nickel-Cobalt (63-37)	746.4
Cobalt	1127.0

The Currie point is defined as the temperature for a metal or alloy at which the paramagnetic metal within a magnetic field loses all electromagnetic orientation. The consequence is a fluctuation in apparent weight at the defined Currie temperature. The Nickel-Cobalt (63:37 mass ratio) sample is a weight percentage of a solid mixture designed to calibrate the TGA in the 100-700°C range as opposed to the 100-350 or 100-1100°C ranges.

Appendix B. Protocol Development

B.1. Pellet Durability

A pellet durability protocol was adapted from ISO and scaled down to meet the testing throughput from the single pellet press. The ISO standard (ISO/DIS 17831-1) calls for 500 g of material in a unit with a volume of 11.25 L, which corresponds to 0.044 g of material/mL total volume. To scale down this standard, each bottle was charged with approximately 12 g of material (m_B) in a 300 mL tumbler. The durability protocol was tested using commercial hardwood and steam exploded pellets in the following manner: 1) with and without stainless steel ball bearings, 2) at different residence times, and 3) with two commercial pellets. The durability results are presented in Figure B-1.

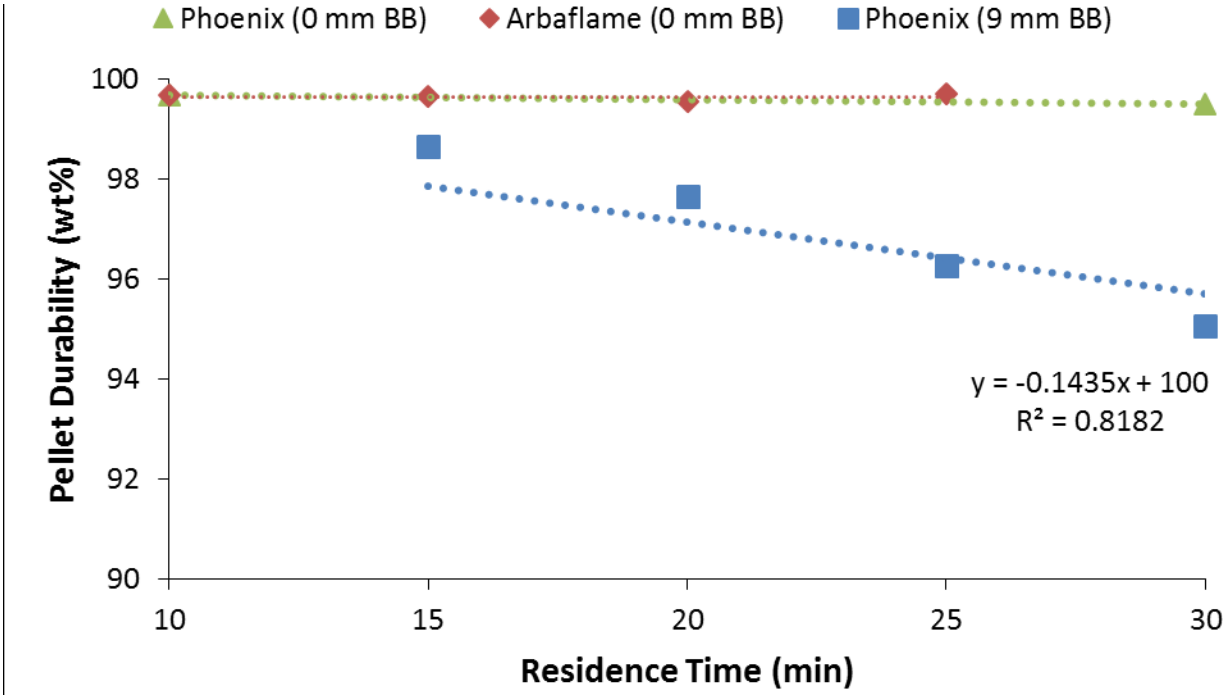

Figure B-1: Pellet durability protocol development with commercial samples in the 300 mL tumbler.

It was expected that the residence time and the source of pellets would be resolved by the durability index. Without the presence of ball bearings in the 300 mL tumbler, the residence time (10-25 minutes) does not influence the pellet durability index (PDI) of the Phoenix or steam explosion (SE) pellets. The p-value for the F-distribution was found to be 0.98 suggesting that the slope of the data is 0 between residence time and PDI ($\alpha = 0.05$). The source (SE pellets or Phoenix pellets) does not influence the PDI without 9 mm stainless steel ball bearings. The conclusion of a hypothesis test comparing sample means from all 13 trials on SE pellets and Phoenix pellets at the same conditions was to fail to reject the null hypothesis and suggest the PDIs are equal. The recommended steps were to install a baffle, add ball bearings or use longer bottles to cause more collisions during the test and yield comparable results to the commercial Seedburo tumbler.

Stainless steel ball bearings (9 mm) were used to increase the severity of the custom bench scale tumbler. This adjustment changed the correlation between residence time and PDI for Phoenix pellets between 15 minutes and 30 minutes ($R^2 = 0.818$). The assumption for this correlation is that a residence time of 0 minutes should give a durability of 100%. Even more importantly, a comparison of sample means between Phoenix pellets tested in the commercial Seedburo tumbler and Phoenix pellets tested in the custom bench scale tumbler (with 9 mm

stainless steel ball bearings) has a p-value of 0.38 and therefore the two protocols are equivalent for this feedstock. The SE pellets were tested for 20 minutes at 50 rpm with 60 g (n = 2) and 100 g (n = 2) of 9 mm stainless steel ball bearings (data not shown). The PDI for SE pellets tested with 60 g and 100 g of 9 mm stainless steel ball bearings does not differ on average with 1 degree of freedom. Ideally, there is some equipment modification that would yield PDI results from SE pellets in the customized tumbler comparable to those generated in commercial Seedburo (PDI = 98.2), but the average durability of SE pellets in the custom bench scale tumbler (n = 8) is 99.5 with a standard deviation of 0.4. Therefore, when the durability of newly generated feedstock is tested, it will be compared along a gradient between the Phoenix pellet durability (97.6) and the SE pellet durability (99.5). The commercial Phoenix pellets and steam exploded pellets were largely recycled during testing and the PDI values appear unaffected (data not shown).

B.2. Briquette Durability

A briquette durability protocol was adapted from ISO and scaled down to meet the testing throughput from the single briquette press. Commercial torrefied briquettes and severely carbonized coal (nutcoke) were tested using the ISO standard (ISO/DIS 17831-2), and compared to adapted briquette durability protocol. The three briquette tumblers (including the ISO standard briquette tumbler) are described in Table B-1.

Table B-1: Dimensions and macroscopic energy calculations experienced during tumbling.

Parameter	Caking Drum	Seedburo	Micum
Volume (L)	2.2	12	390
Shape	Cylinder	Rectangular Prism	Cylinder
Rotation (rpm)	50	50	25
Height (m)	0.20	0.30	1.0
Length (m)	0.07	0.30	0.50
Width (m)	N/A	0.13	N/A
Potential Energy (mJ)	78.5	118	392
Kinetic Energy (mJ)	5.48	12.3	34.3

To calculate the potential and kinetic energy during tumbling, three assumptions were made: 1) the average mass of a briquette was 40 g; 2) all briquettes fall from the maximum height

(Table B-1); and 3) the briquette has a constant speed comparable to the rotational velocity of the tumbler. These assumptions would tend to overestimate the actual potential and kinetic energy experienced by the average briquette. The test results for commercial torrefied briquettes and nutcoke in all three briquette tumblers (Table B-1) are presented in Table B-2.

Table B-2: Protocol development results for coke and torrefied briquette durability.

Briquettes	Nutcoke	Commercial Torrefied
Description	Severe coal carbonization	Unknown biomass torrefaction
Caking Drum	99.5% Durability Sample size 5 Revolution 50 rpm	99.4% Durability Sample size 5 Revolution 50 rpm
Seedburo	94.9% Durability Sample Size 2 Revolution 50 rpm	91.9% Durability Sample Size 3 Revolution 50 rpm
Micum Drum	96.0% Durability Sample size 5 Revolution 25 rpm	91.6% Durability Sample size 5 Revolution 25 rpm

Similar to results from the 300 mL pellet tumbler without stainless steel ball bearings, the briquette caking drum tumbler could not resolve durability differences between coke and torrefied briquettes. When the nutcoke and commercial torrefied briquettes were tested at the ISO scale, the durability is significantly different ($p = 0.004$): 96% compared to 92%, respectively. Therefore, an adopted method was required using the ISO standard pellet tumbler to evaluate briquette durability (Seedburo). In this protocol development, a slight difference was seen between nutcoke and commercial torrefied briquettes as expected from the ISO standard results ($p = 0.22$). Furthermore, the nutcoke ($p = 0.44$) and the commercial torrefied briquette ($p = 0.82$) durability measures are comparable between the ISO standard briquette trials and the scaled protocol using the ISO standard pellet tumbler.

B.3. Control Feedstocks

Five control runs with SE pellets were conducted alongside the PDI tests for the switchgrass stem and hardwood sawdust blends (average = 99.63%). During the protocol development, eight trials with SE pellets and 9 mm stainless steel beads were run with an average PDI of 99.46% and a standard deviation of 0.43. A comparison of means suggests that the two

means are equal. A comparison of means with the second control group (Phoenix pellets) to all historical data from the protocol development suggests a statistical difference. The mean observed during protocol development was 97.62% and the mean from the second control group was 96.8%. However, the ISO standard (ISO/DIS 17831-1) suggests that results are acceptable within 2% for a PDI less than 97.5% [123]. This is sufficient to accept the experimental testing on AAFC feedstock blend PDIs.

Based on the results from Table B-3, the ambient equilibrium moisture content sample means were different for the SE pellets tested on two different days. Assuming the average ambient equilibrium moisture content was 9.5 wt%, the pellets absorbed 11.1 wt% water after the faucet shower test. This result differs significantly from the burette shower test where pellets absorbed between 3.8 wt% and 7.1 wt% water. The immersion test average water absorption was 16.0 wt%. The difference of means for the immersion test and the faucet shower test are statistically significant. Therefore, the flow rate of water (rainfall rate), and the residence time in water (immersion) both impact the water adsorption into pellets. The subsequent effect on pellet durability for SE and Phoenix pellets is discussed below.

The average data generated at the end of protocol development for the Phoenix pellets with the customized bench scale tumbler was 97.65%. A comparison of means for the two separate days suggests the test results obtained from different days were equivalent. The Phoenix pellets had an initial moisture content of 6.0 wt% and absorbed a further 4.7 wt% water. The weathered pellets showed a significant drop in durability (data not shown). The Phoenix pellets were stressed enough after the shower test that moving the pellets from the drying surface on the Buchner funnel to the sieve to test durability resulted in the generation of fines.

The average data generated at the end of protocol development for the SE pellets with the customized bench scale tumbler was 99.71%. The average PDI from this sample and the sample in Figure B-1 does not differ according to a comparison of sample means. The SE pellets had an initial moisture content of 8.8 wt% and absorbed a further 4.2 wt% water. The weathered pellets did not show a significant drop in durability (data not shown). As seen throughout the protocol development stage, the SE pellets are consistently stronger for different tumblers and

different moisture contents. After the shower test, the SE pellets did appear somewhat weaker, but no significant amount of fines was lost before testing durability.

B.4. Pellet Hydrophobicity

The weight percent of water content for SE pellets and commercial Phoenix pellets was assayed using the oven drying method (see Section 2.2.1.1) from two slightly distinct layers within the storage containers. In addition, the immersion test was conducted on SE pellets for two separate dates. A summary of the data is given in Table B-3, where the sequence of three dashes '---' represents no value.

Table B-3: Initial & final moisture content of two sources (4h oven drying method & 1h immersion).

Water content (wt%)		SE Pellets		Phoenix Pellets	
	Test ID	1	2	1	2
Prior to Immersion	Sample size	3	2	1	2
	Average	10.0	8.8	5.8	6.1
	Standard Deviation	0.2	0.1	---	0.1
After Immersion	Sample size	3	3	---	---
	Average	27.1	24.4	---	---
	Standard Deviation	3.4	1.8	---	---

The SE pellets were assayed for water content and a comparison of means between the two trials leads to rejecting the null hypothesis of equal means. The first measurement for water content in commercial Phoenix pellets was 5.8 wt% which is comparable to previous trials (n = 4, $\bar{x} = 5.1$ wt%, standard deviation = 0.1 wt%). In addition, the second moisture content trial is within 0.3 wt% before any testing for hydrophobicity.

A comparison of sample means between the two immersion test data sets on SE pellets suggest the two sample means are equal (statistically) and the test results from the two days are comparable. While no immersion tests were conducted on the Phoenix pellets, it is expected that the pellets would break apart producing large amounts of fines. The durability net change with the less severe shower test was -7.2% (see Section 2.3.7.1).

Two separate shower tests were conducted on SE pellets using the faucet at a flow rate of 50 g/s and a burette at a flow rate of 0.5 g/s. A comparison of the water absorption average

between the immersion test (n = 6), the faucet shower test (n = 3), and the burette shower test (n = 3) is given in Figure B-2.

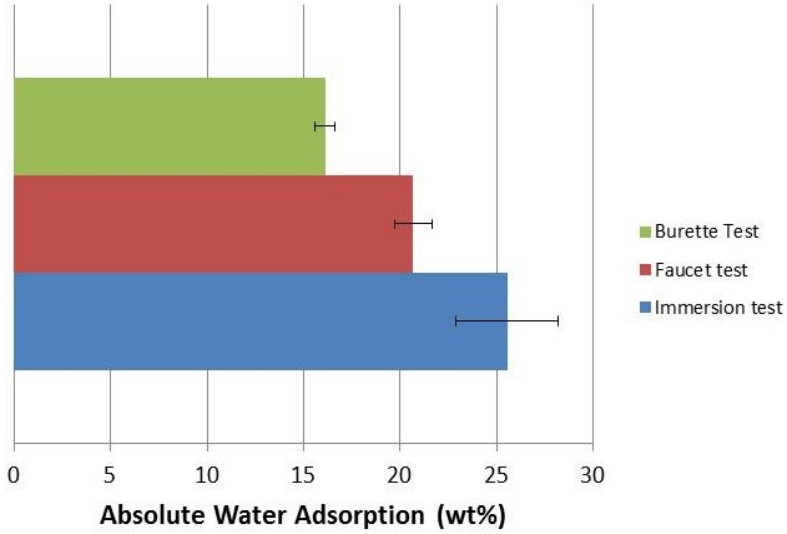

Figure B-2: 1-hour water average adsorption equilibrium for the burette, faucet, & immersion tests.

Qualitatively, a faint yellow leachate from the steam exploded pellets was observed in the pan after the faucet shower test and this colour was more pronounced after the 1 hour immersion test. In addition, a few fines were found in the pan after the shower test which confirms the steam exploded pellets are less durable after exposure to a water shower.

Appendix C. Qualitative Experimental Set-ups

C.1. Durability Equipment

A tumbler with two round plastic bottles permits assaying the mechanical strength of an experimental pellet sample alongside a positive control. Positive controls were taken from commercial materials after a series of protocol development experiments which aided in drawing a link between two scales of tumblers. Briquette durability could not be tested in the custom bench top tumbler because briquette samples are too large. Protocol development testing found that the ISO standard pellet tumbler linked to the ISO standard for briquette durability. The customized small bench top tumbler (a), the commercial pellet tumbler (b), and the custom briquette tumbler (c) at CanmetENERGY-Ottawa are presented in Figure C-1.

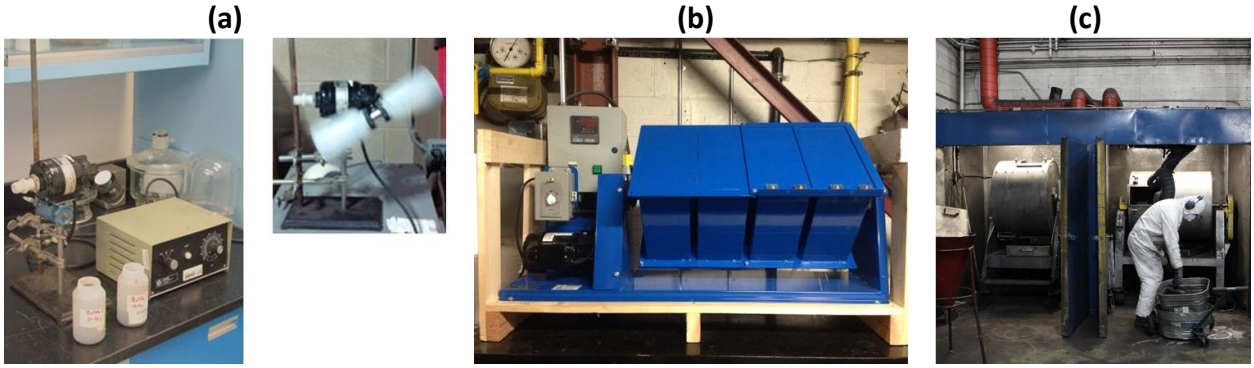

Figure C-1: (a) Custom bench scale pellet, (b) commercial pellet, and (c) custom briquette tumbler.

The volume of each stainless steel compartment (four total) found on the commercial pellet tumbler is 12 L, which is 40 times greater than the customized bench top tumbler. The small scale protocol for the bench top tumbler was used to accommodate small batch sizes derived from the single pellet press, and similar work was done by Schilling *et al*. [90]. The importance of small scale testing comes from the use of the single pellet press which is efficient for producing batches for defined settings like temperature and pressure, but very inefficient at producing batches that meet the quantity used in ISO procedures.

C.2. Hydrophobicity Equipment

Hydrophobicity was assayed using a shower test or an immersion test. The shower test used a burette or a pump and tank in a semi-batch process. The immersion test was scaled depending on the amount of product available. These tests are depicted in Figure C-2.

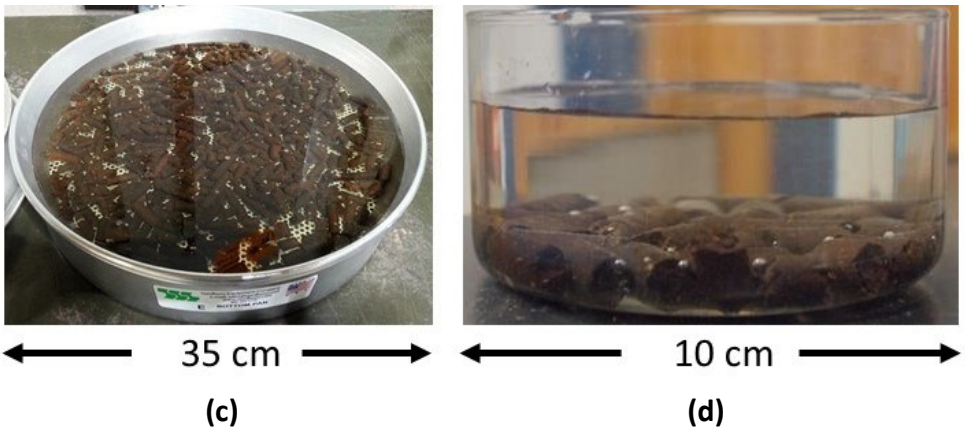

Figure C-2: (a)-(b) Two versions of the semi-batch shower test and (c)-(d) two versions of the batch immersion test for steam exploded pellet hydrophobicity. In (a), a suspended burette above a Buchner funnel to spread the falling water over the cross sectional area of the micro pellet batch being tested. In (b), a feed tank of deionized water, a pump, and the housing container for a packed bed of pellets. The protocols used for immersion from (c) SECTOR and (d) CanmetENERGY.

C.3. Densification Equipment

A series of tests were performed to create pellets/briquettes from the different biomass sources at varying applied temperatures and pressures. The single pellet/briquette press uses a double acting piston powered from pressurized hydraulic oil. The unit surface was wrapped with electrical heating tape and insulation to achieve high temperature environments for densification. The piston is inside a barrel rated for 20.7 MPa (3000 psig), but will be tested at 0.7-3.45 MPa (100-500 psig). The single batch pellet and briquette presses are presented in Figure C-3.

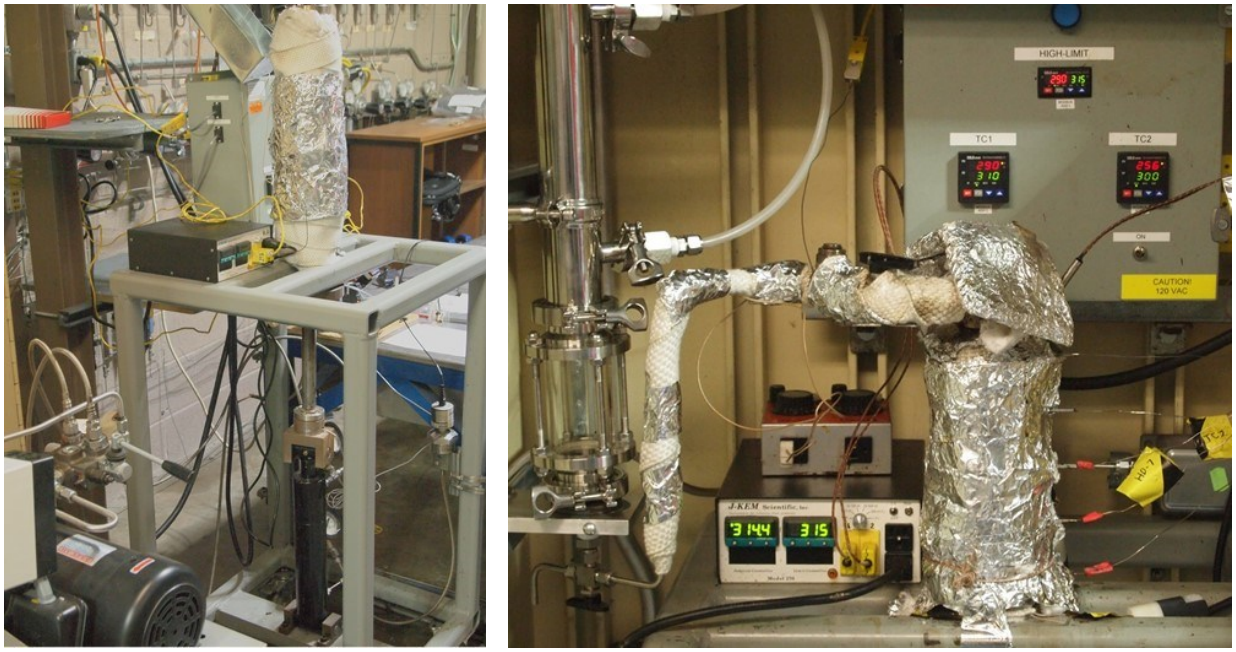

(a) **(b)**

Figure C-3: Installations of (a) the single pellet press and (b) the briquette press with tar trap.

A larger reactor was used in the same way at the low pressure setting to generate larger briquettes for refined applications. The key difference between the single pellet press and the single briquette press is scale. The scale of the briquette press requires additional downstream process units, while some of the operating conditions remain the same. A comparison between pellet production and briquette production by single stage compression is given in Table C-1.

Table C-1: Differences for single pellet and briquette press operating conditions.

Design Characteristic	Units	Pellet Press	Briquette Press
Internal Radius	mm	4.25	40
Piston Pressure Range	psig	100-500	500
Applied Pressure	MPa	40-200	45
Temperature Range	°C	25-350	25-350
Internal Volume	mL	10	300
Solid Load Capacity	g	1.5	40
Torrefaction Gases	g	0.45	12
Ventilation	N/A	Air Duct	Tar Trap + Fumehood

The pellet press set-up allowed a multi-point thermocouple to rest along the surface to obtain a surface temperature reading. It was assumed that the heat transfer from the surface to a 4.25 mm radius was rapid. The briquette press set-up required thermocouples that could directly contact the biomass sample from slots in the side of the reactor. It was assumed that the heat transfer to a 20 mm radius was not rapid. A series of thermocouples at the biomass centre points identified the moment when the internal temperature matched the surface temperature.

The pellet press rested underneath a suction vent to draw condensable and non-condensable gases produced during torrefaction from the laboratory environment. The internal diameter of the pellet press die was 8.5 mm, and so a vent was sufficient to capture 0.3-0.6 g of torrefaction gases. The internal diameter of the briquette press die was 40 mm, and so a vapour trap was necessary to capture 12 g of torrefaction gases. A common scrubbing solution is isopropanol with hydrophobic and hydrophilic surface groups [124]. A single stage separation was observed in-house as sufficient to trap condensable gases. Glycol was used as the cooling fluid. The vapour trap was constructed with Swagelok® fittings and filters and the gas mixture contacted a batch of fresh isopropanol. The vapours were drawn with a slight vacuum pressure (1 in Hg), and the non-condensable gases passed clean and free of tars or liquids into a fumehood. The mixture of isopropanol and condensable gases were extracted with a sampling port, and fresh isopropanol was drawn using a larger vacuum (10 in Hg).

Appendix D. Sample Raw Data

D.1. Material Preparation

The biomass residues used were already relatively dry (2 – 10 wt% moisture). In industry, chipping, sieving and drying are all part of the first steps in the biomass supply chain. These residues are left over from, for example, the forestry, agriculture, and pulp industries. Sample images of these materials are shown in Figure D-1.

Figure D-1: Forestry, agriculture, & pulp industry biomass residues in various degrees of processing. Forestry residues include (a) willow, (b) torrefied willow, and (c) poplar bark. Agricultural residues include (d) switchgrass stem, (e) switchgrass leaf, and (f) hardwood sawdust. Pulp mill residues include (g) knots, (h) hog, and (i) sludge.

Commercial pellets from 5 unique sources were used to develop the in-house standards necessary for further experimental work. In addition, these pellets and briquettes served as experimental controls during subsequent testing of the various in-house samples from the single pellet/briquette press. These sources, any applied thermal treatment, and their corresponding densities are presented in Table D-1.

Table D-1: Densification parameters for commercial biomass materials aimed as fuel sources.

Densified Biomass	Thermal Treatment	Binder (Y/N)	Durability (wt%)	Moisture Content wt% wb	Envelope Density (kg/m^3)	Bulk Density (kg/m^3)[1]
Supplier A1	Torrefaction	Y	97.5	3.5	1211[2]	726.6
Supplier A2	Torrefaction	N	91.4	2.9	1206	674.3
Supplier A4	Torrefaction	Y	96.6	4.6	1224[2]	734.6
Supplier C1	Steam Explosion	N	98.2	9.8	1140	722.5
Supplier D1	None	N	99.1	6.9	1100[2]	715.4
Supplier E1	None	N	97.4	5.5	1080	702.0[2]
Supplier B1	Torrefaction	N	92.2	2.7	1390	682.2

[1]Principle researcher generated these results

[2]Calculated values based on the estimated void fraction and measured density

D.2. Qualitative Densification

Some of the pellets produced had greater charring at their ends compared to the remaining pellet surface area. Frayed ends appeared on some pellets that did not fully compress. In addition, the switchgrass stem pellets showed more frayed ends compared to the hardwood sawdust pellets at either temperature. The pure pellets produced at 300°C (in particular the hardwood sawdust pellets) had a glossy black surface. All results are seen in Figure D-2.

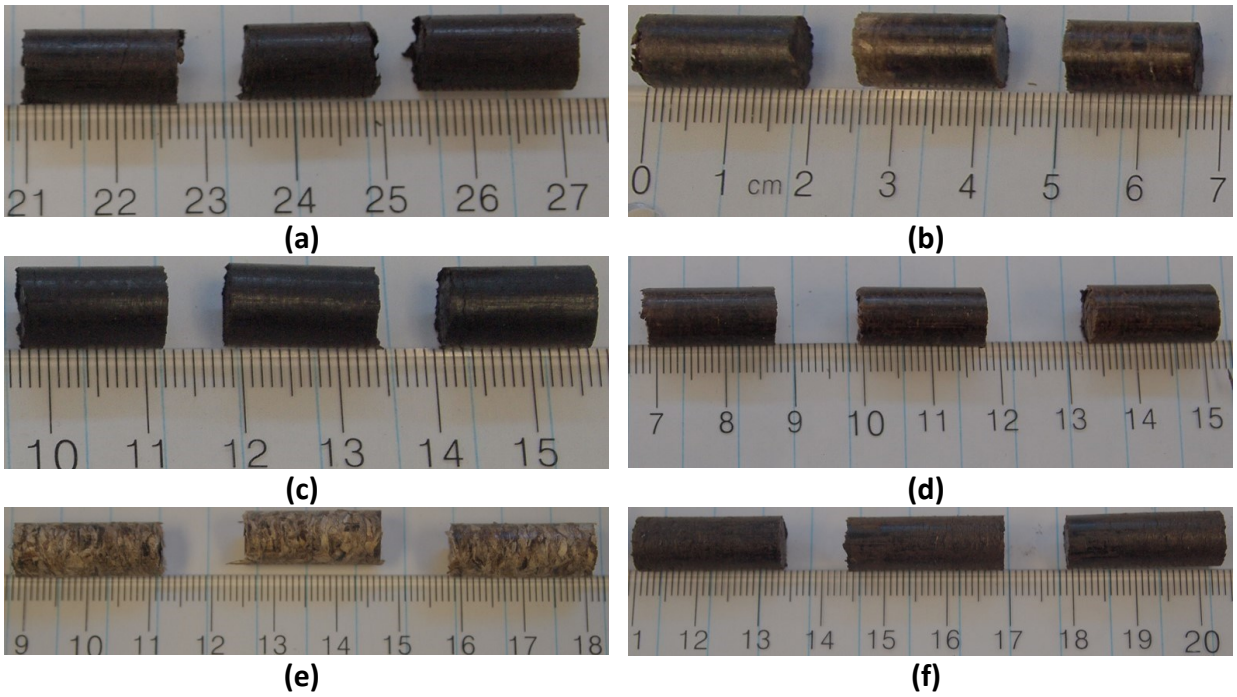

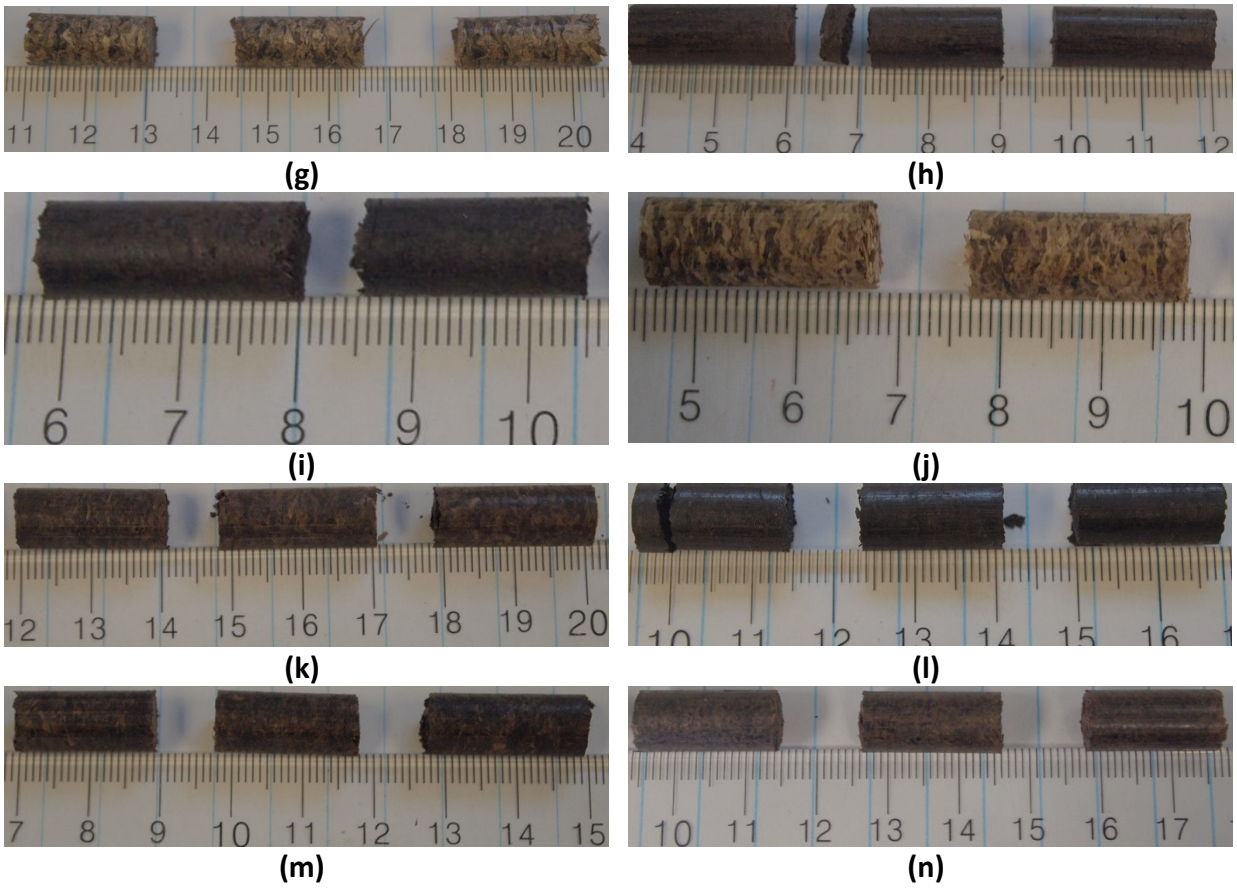

Figure D-2: The AAFC blends of switchgrass stem with hardwood sawdust were produced at a pressure of 215 MPa and at temperatures of 300°C (a), (c) and 250°C (b), (d). The pure switchgrass stem pellets (a)-(b) and the pure hardwood sawdust pellets (c)-(d) are representative images. Representative images of the dry willow (e), (g) and torrefied willow (f), (h) pellets produced at 145 (e)-(f) and 200°C (g)-(h) look the same as pellets produced with added moisture (data not shown). Qualitatively, willow torrefaction followed by cooling and pelletization yields similar looking pellets compared to integrated torrefaction and densification (ITD) of the same willow residue (i). Representative images of the knot fuel at three production temperatures 220°C (j), 260°C (k), and 300°C (l), and hog and sludge fuel pellets are depicted for 260°C (m)-(n) respectively.

The product changed colour from light brown to dark brown to black along the temperature interval of 220°C to 300°C, to more closely resemble a lignite fuel instead of a biomass fuel.

D.3. Quantitative Compression Ratio

Pelletization experiments for 8 materials from Section 2.2.1.4 are presented in Figure D-3.

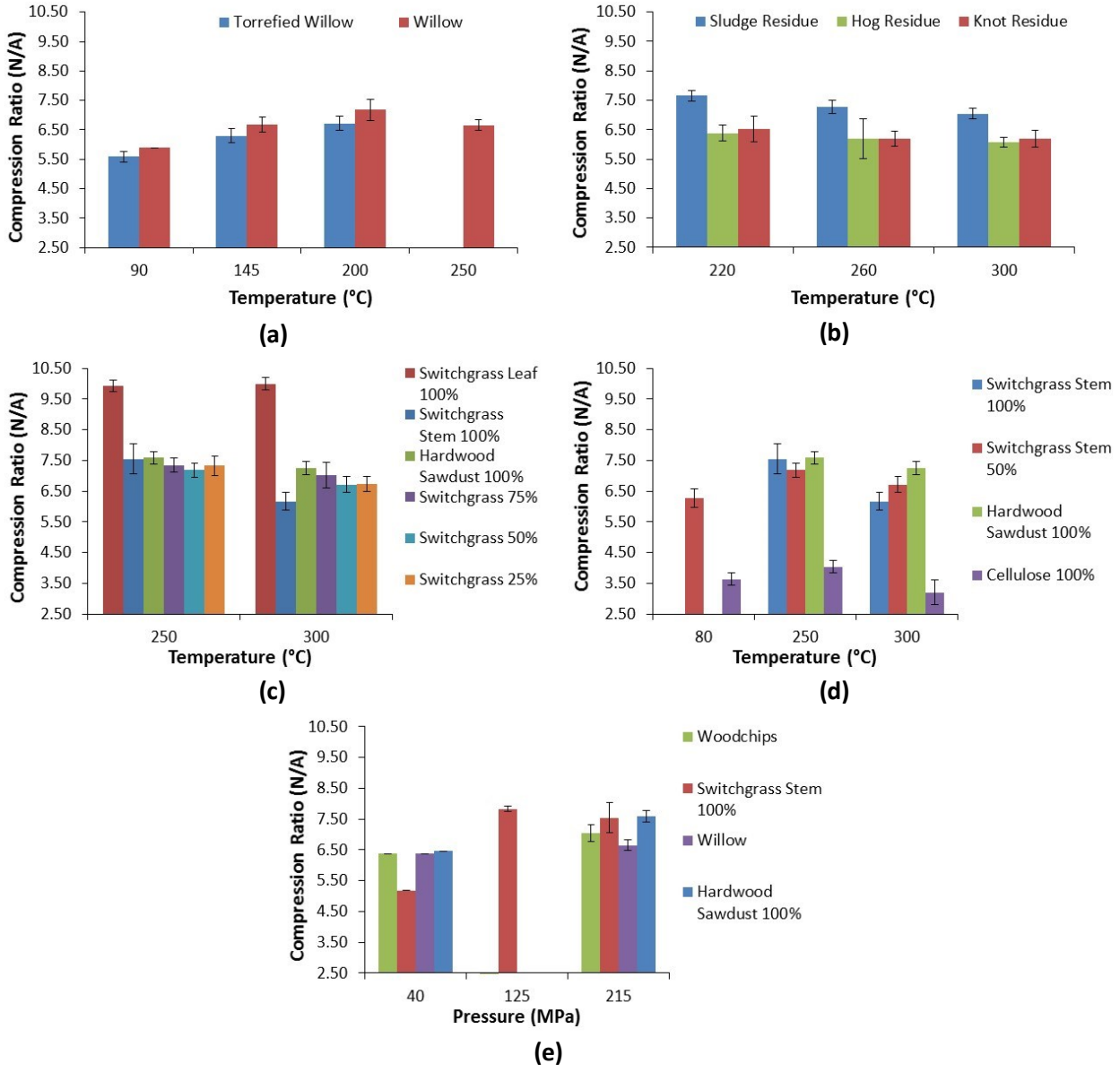

Figure D-3: Pellet compression ratios for 8 biomass residues. Relationships in (a)-(d) for temperature at constant pressure (215 MPa), and (e) for pressure at constant temperature (250°C).

First, untreated willow pellets had a compression ratio of 6.7-7.2 while torrefied willow pellets had a compression ratio of 6.1-6.7 (Figure D-3a). A comparison of means test suggests that the means are not equal; rather compressing untreated biomass is easier compared to previously thermally-treated biomass. Second, the knot and hog residues have statistically similar pellet densities and compression ratios ($p > 0.125$). Sludge residue has the greatest compression ratio and pellet density among pulp mill residues (Figure D-3b). Third, the compression ratio of switchgrass leaves was 1.5 fold greater than that of stems, while the pellet density and bulk

density of leaves were 1.1 fold and 1.7 fold lower respectively (Figure D-3c). The switchgrass stem was hammer-milled while the leaves were cut with a blender which could explain this apparent difference. The pellet density and compression ratio decreased with increasing ITD temperature (Figure D-3c, d). However, neither trend is statistically significant. The compression ratio of cellulose pellets (Figure D-3d) was approximately two fold lower because the bulk density of the laboratory cellulose (100-200 mesh) was 2.4 fold higher than the AAFC biomass feedstocks (14-28 mesh). Finally, the compression ratio is not a strong function of pressure for a given biomass source as seen in Figure D-3e. By definition, the compression ratio normalizes out the effect of the starting bulk density which varied by ± 0.05 g/mL (50 kg/m^3).

D.4. Thermogravimetric Analysis

The severity factor (see Equation (2-4)) is a function of the temperature and the time at each temperature. For five minute pelletization experiments via ITD, it is assumed that the material reached a constant temperature within 20 seconds based on some heat transfer calculations. The severity factor at constant temperature for five minutes varies according to Figure D-4.

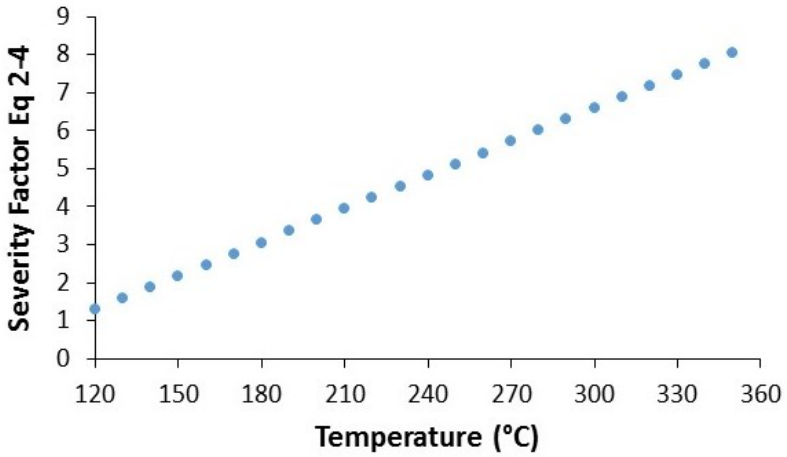

Figure D-4: Severity factor as a function of temperature assuming 5 minutes at constant T.

Historical data of switchgrass thermogravimetric analysis supports the yields obtained by ITD as seen in Figure D-5.

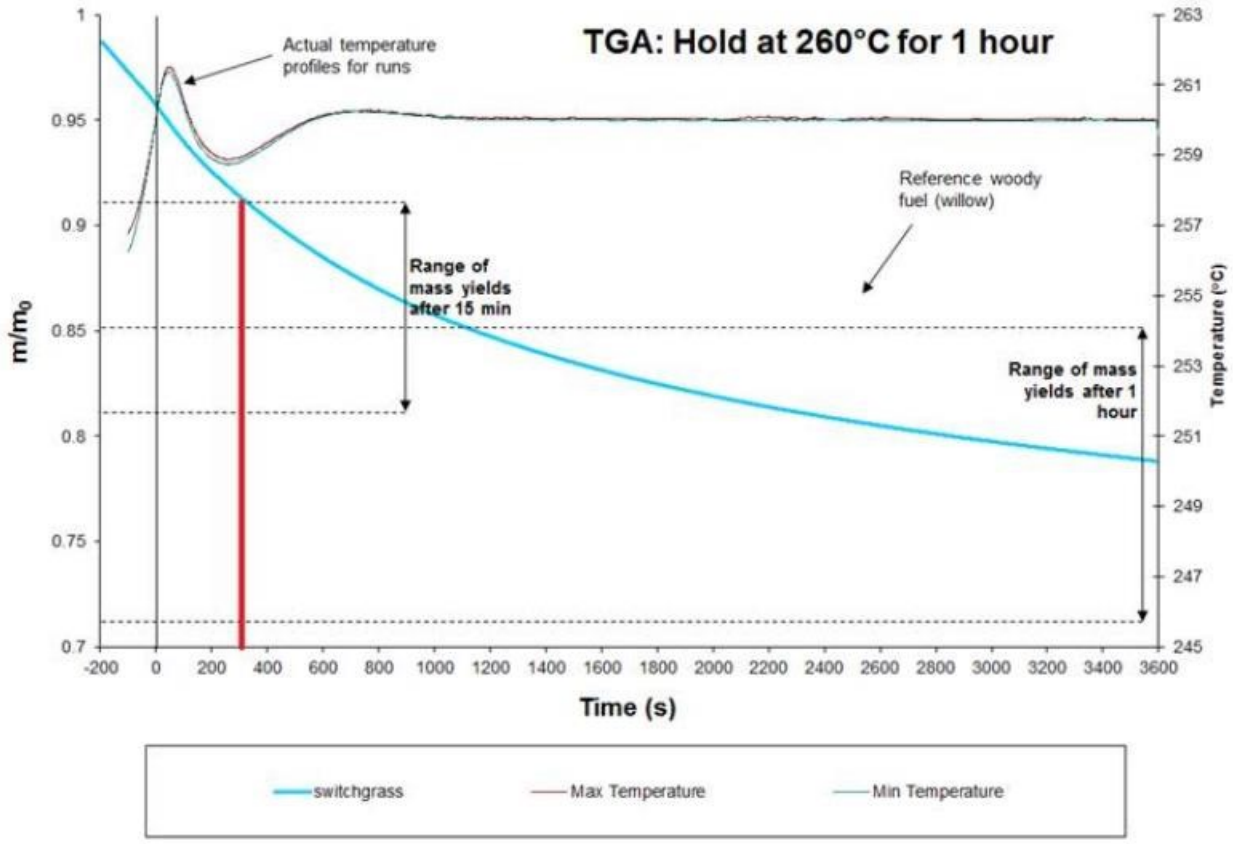

Figure D-5: Switchgrass torrefaction simulation at 260°C for 1 hour.

D.5. Transport Phenomena Data

A random sample of 10 pellets (or briquettes) was taken from the stock of commercial torrefied pellets, steam exploded pellets, and torrefied briquettes to assay the average dimensions and density. The results are presented in Table D-2.

Table D-2: Physical properties of pellets and briquettes used for the Industry Evaluation Program of advanced solid biofuels for direct coal substitution.

Source	Average Length (mm)	Average Diameter (mm)	Average Density (g/mL)
Poplar ITD	36	40	1.10
Poplar + Pyrolysis Tar	31	40	1.11
Supplier A1	30	6	1.21[1]
Supplier A2	5	6	1.21
Supplier A3	20	6	1.24[1]
Supplier A4	10	6	1.22[1]
Supplier A5	10	6	1.20[1]
Supplier B1	50	30	1.39
Supplier C1	18	8	1.14

[1]Calculated values based on the estimated void fraction and measured bulk density

Typical simulated thermal profiles for different pellets and briquettes is given in Figure D-6. The temperature point was taken at a midpoint in the finite difference mesh so as to approximate the average temperature.

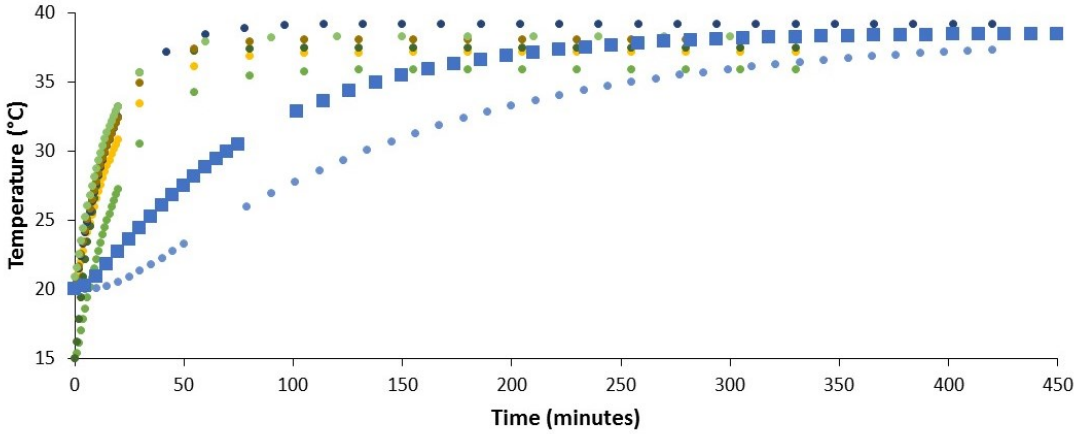

Figure D-6: Unsteady state energy balance for eight different pellets and briquettes during drying after immersion. Pellet temperatures rose quickly because of their smaller size whereas briquettes took longer to approach 0 unaccomplished change.

Steam exploded pellets, torrefied pellets, and torrefied briquettes were dried using conditions described above (see Chapter 3). When the initial moisture content is greater than the critical moisture content (constant drying rate portion), the heat transfer is limiting. The initial rate data after t_0 (wt%/min) represents the linear portion of the curve. Samples are also

compared for the amount of final dry basis biomass after oven drying and the mass flux during the initial heating period (approximately 30 minutes for pellets). This data is given in Table D-3.

Table D-3: Unsteady state heat transfer during convective drying of biomass pellets/briquettes.

Private Sector Producer	Constant evaporation rate min^{-1} (db wt%)	Final dry biomass (g)	Average Mass flux during heating (g/m^2s)
Supplier A1	0.0041	569.7	0.407
Supplier A2	0.0040	576.3	0.394
Supplier A3	0.0028	562.0	0.295
Supplier A4	0.0029	553.8	0.290
Supplier A5	0.0036	544.4	0.386
Supplier B1	0.0051	546.3	0.488
Supplier C1	0.0059	493.6	0.445

Other drying profiles were measured in the laboratory for pellet samples (Figure D-7).

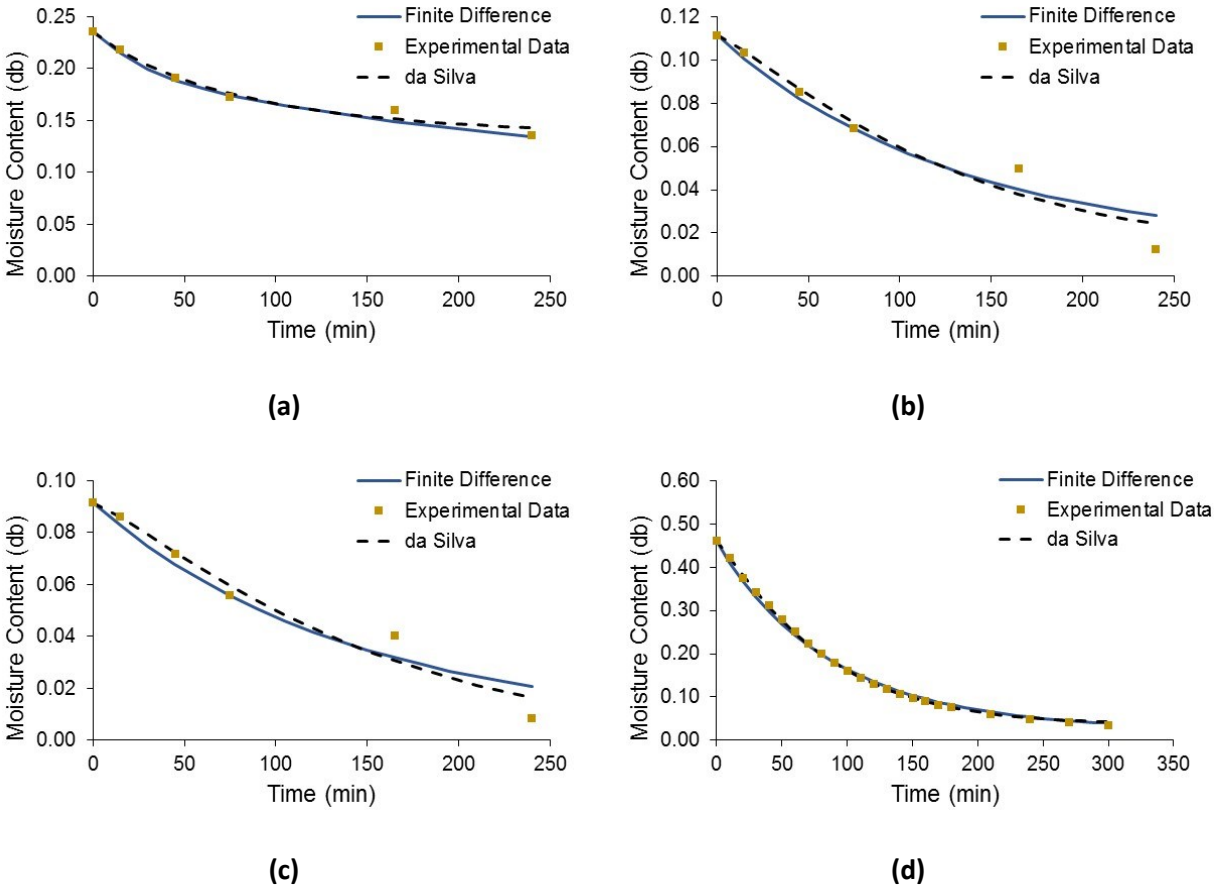

Figure D-7: (a)-(c) Pellet drying at room temperature after immersion for 1 hour in 125 mL of deionized water. (d) Pellet drying in a convection oven at 40°C after immersion for 48 hours in 4.5 L of deionized water. Results for (a) Supplier C2, (b) Supplier A1, (c) pulp Hog ITD (260°C and 215 MPa), and (d) Supplier A5 (drying without any other samples).

Appendix E. Numerical Solutions

The mass transfer finite difference solutions are given as:

$$\omega'^{n+1}_{ij} = \lambda\left(1 - \frac{1}{2(i-1)}\right)\omega'^{n}_{i-1j} + \lambda\omega'^{n}_{ij-1} + (1-4\lambda)\omega'^{n}_{ij} + \lambda\left(1 + \frac{1}{2(i-1)}\right)\omega'^{n}_{i+1j} + \lambda\omega'^{n}_{ij+1}$$

When both ‘z’ and ‘r’ are equal to 0:

$$\omega'^{n+1}_{ij} = 2\lambda\omega'^{n}_{i+1j} + 2\lambda\omega'^{n}_{ij+1} + (1-4\lambda)\omega'^{n}_{ij}$$

And when ‘z’ is equal to 0 while ‘r’ is equal to R:

$$\omega'^{n+1}_{ij} = 2\lambda\omega'^{n}_{i-1j} + 2\lambda\omega'^{n}_{ij+1} + \left(1 - 4\lambda - \left(\frac{2\lambda\Delta s k_c}{D_{AB}}\right)\left(1 + \frac{1}{2(i-1)}\right)\right)\omega'^{n}_{ij} + \left(\frac{2\lambda\Delta s k_c}{D_{AB}}\right)\left(1 + \frac{1}{2(i-1)}\right)\omega'_{\infty}$$

At the corner where when ‘z’ is equal to L and ‘r’ is equal to R:

$$\omega'^{n+1}_{ij} = 2\lambda\omega'^{n}_{i-1j} + 2\lambda\omega'^{n}_{ij-1} + \left(1 - 4\lambda - \left(\frac{2\lambda\Delta s k_c}{D_{AB}}\right)\left(2 + \frac{1}{2(i-1)}\right)\right)\omega'^{n}_{ij} + \left(\frac{2\lambda\Delta s k_c}{D_{AB}}\right)\left(2 + \frac{1}{2(i-1)}\right)\omega'_{\infty}$$

The last corner is at ‘z’ equal to L and ‘r’ equal to 0:

$$\omega'^{n+1}_{ij} = 2\lambda\omega'^{n}_{i+1j} + 2\lambda\omega'^{n}_{ij-1} + \left(1 - 4\lambda - \left(\frac{2\lambda\Delta s k_c}{D_{AB}}\right)\right)\omega'^{n}_{ij} + \left(\frac{2\lambda\Delta s k_c}{D_{AB}}\right)\omega'_{\infty}$$

Apart from the four corners, there are four equations that describe the boundaries between the corners. At ‘r’ equal to 0 along the ‘z’ axis:

$$\omega'^{n+1}_{ij} = 2\lambda\omega'^{n}_{i+1j} + (1-4\lambda)\omega'^{n}_{ij} + \lambda\omega'^{n}_{ij-1} + \lambda\omega'^{n}_{ij+1}$$

At ‘r’ equal to R along the ‘z’ axis:

$$\omega'^{n+1}_{ij} = 2\lambda\omega'^{n}_{i-1j} + \lambda\omega'^{n}_{ij-1} + \lambda\omega'^{n}_{ij+1} + \left(1 - 4\lambda - \left(\frac{2\lambda\Delta sk_c}{D_{AB}}\right)\left(1 + \frac{1}{2(i-1)}\right)\right)\omega'^{n}_{ij} + \left(\frac{2\lambda\Delta sk_c}{D_{AB}}\right)\left(1 + \frac{1}{2(i-1)}\right)\omega'_{\infty}$$

At 'z' equal to 0 along the 'r' axis:

$$\omega'^{n+1}_{ij} = \lambda\left(1 - \frac{1}{2(i-1)}\right)\omega'^{n}_{i-1j} + (1 - 4\lambda)\omega'^{n}_{ij} + \lambda\left(1 + \frac{1}{2(i-1)}\right)\omega'^{n}_{i+1j} + 2\lambda\omega'^{n}_{ij+1}$$

Finally, at 'z' equal to L along the 'r' axis:

$$\omega'^{n+1}_{ij} = \lambda\left(1 - \frac{1}{2(i-1)}\right)\omega'^{n}_{i-1j} + 2\lambda\omega'^{n}_{ij-1} + \left(1 - 4\lambda - \left(\frac{2\lambda\Delta sk_c}{D_{AB}}\right)\right)\omega'^{n}_{ij} + \lambda\left(1 + \frac{1}{2(i-1)}\right)\omega'^{n}_{i+1j} + \left(\frac{2\lambda\Delta sk_c}{D_{AB}}\right)\omega'_{\infty}$$

The heat transfer finite difference solutions are given as:

$$T^{n+1}_{ij} = \lambda\left(1 - \frac{1}{2(i-1)}\right)T^{n}_{i-1j} + \lambda T^{n}_{ij-1} + (1 - 4\lambda)T^{n}_{ij} + \lambda\left(1 + \frac{1}{2(i-1)}\right)T^{n}_{i+1j} + \lambda T^{n}_{ij+1}$$

When both 'z' and 'r' are equal to 0:

$$T^{n+1}_{ij} = 2\lambda T^{n}_{i+1j} + 2\lambda T^{n}_{ij+1} + (1 - 4\lambda)T^{n}_{ij}$$

And when 'z' is equal to 0 while 'r' is equal to R:

$$T^{n+1}_{ij} = 2\lambda T^{n}_{i-1j} + 2\lambda T^{n}_{ij+1} + \left(1 - 4\lambda - \left(\frac{2\lambda\Delta sh}{k}\right)\left(1 + \frac{1}{2(i-1)}\right)\right)T^{n}_{ij} + \left(\frac{2\lambda\Delta sh}{k}\right)\left(1 + \frac{1}{2(i-1)}\right)T_{\infty} + \left(1 + \frac{1}{2(i-1)}\right)\left(\frac{2\lambda\Delta H_v\rho_s\Delta sk_c}{k}\right)(\omega'_{\infty} - \omega'_{*})$$

At the corner where when 'z' is equal to L and 'r' is equal to R:

$$T^{n+1}_{ij} = 2\lambda T^{n}_{i-1j} + 2\lambda T^{n}_{ij-1} + \left(1 - 4\lambda - \left(\frac{2\lambda\Delta sh}{k}\right)\left(2 + \frac{1}{2(i-1)}\right)\right)T^{n}_{ij} + \left(\frac{2\lambda\Delta sh}{k}\right)\left(2 + \frac{1}{2(i-1)}\right)T_{\infty} + \left(2 + \frac{1}{2(i-1)}\right)\left(\frac{2\lambda\Delta H_v\rho_s\Delta sk_c}{k}\right)(\omega'_{\infty} - \omega'_{*})$$

The last corner is at 'z' equal to L and 'r' equal to 0:

$$T^{n+1}_{ij} = 2\lambda T^{n}_{i+1j} + 2\lambda T^{n}_{ij-1} + \left(1 - 4\lambda - \left(\frac{2\lambda\Delta sh}{k}\right)\right)T^{n}_{ij} + \left(\frac{2\lambda\Delta sh}{k}\right)T_{\infty} + \left(\frac{2\lambda\Delta H_v\rho_s\Delta sk_c}{k}\right)(\omega'_{\infty} - \omega'_{*})$$

Apart from the four corners, there are four equations that describe the boundaries between the corners. At 'r' equal to 0 along the 'z' axis:

$$T_{ij}^{n+1} = 2\lambda T_{i+1j}^{n} + (1-4\lambda)T_{ij}^{n} + \lambda T_{ij-1}^{n} + \lambda T_{ij+1}^{n}$$

At 'r' equal to R along the 'z' axis:

$$T_{ij}^{n+1} = 2\lambda T_{i-1j}^{n} + \lambda T_{ij-1}^{n} + \lambda T_{ij+1}^{n} + \left(1 - 4\lambda - \left(\frac{2\lambda\Delta sh}{k}\right)\left(1 + \frac{1}{2(i-1)}\right)\right)T_{ij}^{n} + \left(\frac{2\lambda\Delta sh}{k}\right)\left(1 + \frac{1}{2(i-1)}\right)T_{\infty} + \left(1 + \frac{1}{2(i-1)}\right)\left(\frac{2\lambda\Delta H_v \rho_s \Delta s k_c}{k}\right)(\omega'_{\infty} - \omega'_{*})$$

At 'z' equal to 0 along the 'r' axis:

$$T_{ij}^{n+1} = \lambda\left(1 - \frac{1}{2(i-1)}\right)T_{i-1j}^{n} + (1-4\lambda)T_{ij}^{n} + \lambda\left(1 + \frac{1}{2(i-1)}\right)T_{i+1j}^{n} + 2\lambda T_{ij+1}^{n}$$

Finally, at 'z' equal to L along the 'r' axis:

$$T_{ij}^{n+1} = \lambda\left(1 - \frac{1}{2(i-1)}\right)T_{i-1j}^{n} + 2\lambda T_{ij-1}^{n} + \left(1 - 4\lambda - \left(\frac{2\lambda\Delta sh}{k}\right)\right)T_{ij}^{n} + \lambda\left(1 + \frac{1}{2(i-1)}\right)T_{i+1j}^{n} + \left(\frac{2\lambda\Delta sh}{k}\right)T_{\infty} + \left(\frac{2\lambda\Delta H_v \rho_s \Delta s k_c}{k}\right)(\omega'_{\infty} - \omega'_{*})$$

E.1. VBA Finite Difference Code

E.1.1. Nomenclature

```
Option Explicit 'Forces the declaration of variables in order for program execution
'Declaration of global variables used in Sub routine and all functions in order to avoid declaring them each time
Private lambda_m As Double, Dab As Double, kc As Double, M_infinite As Double, time_step As Double, space_step As Double
Private lambda_h As Double, h As Double, k As Double, T_infinite As Double, Delta_H As Double, density As Double
'Beginning of Sub routine
```

E.2.1. Subroutine

E.2.1.1. Declarations

```
Sub Finite_Difference_Sol()

'Defininining the physical properties of the system and the numerical method parameters
Dim Nr As Integer, Nl As Integer, Nt As Integer, alpha As Double

'Defining the initial conditions and process dimensions
Dim M_initial As Double, T_initial As Double

'Defining the array used to hold the solutions to the numerical method
Dim Unsteady_Mass() As Variant, Unsteady_Temp() As Variant, Average_Mass() As Variant

'Defining temporary variables used to initiate loops and counters
Dim x1 As Double, x2 As Integer, x3 As Integer
```

E.2.1.2 Initializations

```
'Initial calculations before beginning the mass transfer system
Dab = (10000#) * Worksheets("Numerical Mass").Cells(2, 3) 'cm2/s
kc = (100#) * Worksheets("Numerical Mass").Cells(3, 3) 'cm/s
M_infinite = Worksheets("Numerical Mass").Cells(10, 3) 'N/A
M_initial = Worksheets("Summary").Cells(2, 6) 'N/A
space_step = 1 / 10 'cm
time_step = 1 's
Nr = 1 + 100 * Worksheets("Numerical Mass").Cells(4, 3) / (2 * space_step)
Nl = 1 + 100 * Worksheets("Numerical Mass").Cells(5, 3) / (2 * space_step)
Nt = 1 + Worksheets("Numerical Mass").Cells(8, 3) / time_step
lambda_m = Dab * time_step / (space_step) ^ 2
ReDim Unsteady_Mass(1 To Nt, 1 To Nr, 1 To Nl)
ReDim Average_Mass(1 To ((Nt + 599) / 600), 1 To Nr - 1, 1 To Nl - 1)

'Initial calculations before beginning the heat transfer system
alpha = (10000#) * Worksheets("Numerical Heat").Cells(6, 3) 'cm2/s
h = (0.0001) * Worksheets("Numerical Heat").Cells(2, 3) 'W/cm2/K
k = (0.01) * Worksheets("Numerical Heat").Cells(3, 3) 'W/cm/K
T_infinite = 40 'C
T_initial = 20 'C
space_step = 1 / 10 'cm
time_step = 1 's
Nr = 1 + 100 * Worksheets("Numerical Heat").Cells(7, 3) / (2 * space_step)
Nl = 1 + 100 * Worksheets("Numerical Heat").Cells(8, 3) / (2 * space_step)
Nt = 1 + Worksheets("Numerical Heat").Cells(10, 3) / time_step
lambda_h = alpha * time_step / (space_step) ^ 2
ReDim Unsteady_Temp(1 To Nt, 1 To Nr, 1 To Nl)

'Defining an array and variables needed to track change in water and the heat of vaporization
density = Worksheets("Numerical Heat").Cells(5, 3) 'kg/m3
Delta_H = Worksheets("Summary").Cells(5, 3) / Worksheets("Summary").Cells(6, 3) 'kJ/g
```

E.3.1. Calculations

E.3.1.1. Numerical Stability

```
'Checking a condition of numerical stability for both heat and mass transfer problems
If lambda_m > 0.25 Or lambda_h > 0.25 Then

    MsgBox ("Numerical solution error - infinite instability")
    MsgBox ("Mass transfer lambda_m = " & lambda_m)
    MsgBox ("Mass transfer lambda_h =  " & lambda_h)

Else
```

E.3.1.2. Filling Arrays

```
'Establishing the initial condition in the unsteady state mass and temperature matrix
For x1 = 1 To Nt 'Moving the finite difference solution through time
    For x2 = 1 To Nr 'Moving the finite difference solution through radial space
        For x3 = 1 To Nl 'Moving the finite difference solution through Cartesian space
            Unsteady_Mass(x1, x2, x3) = M_initial
            Unsteady_Temp(x1, x2, x3) = T_initial
        Next x3
    Next x2
Next x1
```

E.4.1. Finite Differences

```
'Meat of the code.

For x1 = 1 To Nt - 1 'Moving the finite difference solution through time
    For x2 = 1 To Nr 'Moving the finite difference solution through radial space
        For x3 = 1 To Nl 'Moving the finite difference solution through Cartesian space

        If x2 = 1 And x3 = 1 Then 'First code executed while analyzing the corner point at r = 0, z = 0
            Unsteady_Mass(x1 + 1, x2, x3) = PelletCentre(lambda_m, Unsteady_Mass(x1, x2 + 1, x3), Unsteady_Mass(x1, x2, x3
 + 1), Unsteady_Mass(x1, x2, x3))
            Unsteady_Temp(x1 + 1, x2, x3) = PelletCentre(lambda_h, Unsteady_Temp(x1, x2 + 1, x3), Unsteady_Temp(x1, x2, x3
 + 1), Unsteady_Temp(x1, x2, x3))

        ElseIf x2 = 1 And x3 > 1 And x3 < Nl Then 'Second code executed while analyzing the centre axis (r = 0) along z sp
ace
            Unsteady_Mass(x1 + 1, x2, x3) = HorizonCentre(lambda_m, Unsteady_Mass(x1, x2 + 1, x3), Unsteady_Mass(x1, x2, x
3), Unsteady_Mass(x1, x2, x3 - 1), Unsteady_Mass(x1, x2, x3 + 1))
            Unsteady_Temp(x1 + 1, x2, x3) = HorizonCentre(lambda_h, Unsteady_Temp(x1, x2 + 1, x3), Unsteady_Temp(x1, x2, x
3), Unsteady_Temp(x1, x2, x3 - 1), Unsteady_Temp(x1, x2, x3 + 1))

        ElseIf x2 = 1 And x3 = Nl Then 'Third code excuted while analyzing the corner point at r = 0, z = Nl
            Unsteady_Mass(x1 + 1, x2, x3) = CentreSurface_m(Unsteady_Mass(x1, x2 + 1, x3), Unsteady_Mass(x1, x2, x3 - 1),
Unsteady_Mass(x1, x2, x3))
            'Energy balance depends on the vapour moisture content at the surface (saturated vapour pressure)
            Unsteady_Temp(x1 + 1, x2, x3) = CentreSurface_h(Unsteady_Temp(x1, x2 + 1, x3), Unsteady_Temp(x1, x2, x3 - 1),
Unsteady_Temp(x1, x2, x3), SurfaceVapour(Unsteady_Temp(x1, x2, x3)))

        ElseIf x3 = 1 And x2 > 1 And x2 < Nr Then 'Fourth code executed while analyzing the axis perpendicular to the cent
re axis (z = 0) along the r space
            Unsteady_Mass(x1 + 1, x2, x3) = VerticCentre(lambda_m, x2, Unsteady_Mass(x1, x2 - 1, x3), Unsteady_Mass(x1, x2
, x3), Unsteady_Mass(x1, x2 + 1, x3), Unsteady_Mass(x1, x2, x3 + 1))
            Unsteady_Temp(x1 + 1, x2, x3) = VerticCentre(lambda_h, x2, Unsteady_Temp(x1, x2 - 1, x3), Unsteady_Temp(x1, x2
, x3), Unsteady_Temp(x1, x2 + 1, x3), Unsteady_Temp(x1, x2, x3 + 1))

        ElseIf x3 = Nl And x2 > 1 And x2 < Nr Then 'Fifth code executed while analyzing the axis perpendicular to the cent
re axis (z = Nl) along the r space
            Unsteady_Mass(x1 + 1, x2, x3) = VerticSurface_m(x2, Unsteady_Mass(x1, x2 - 1, x3), Unsteady_Mass(x1, x2, x3 -
1), Unsteady_Mass(x1, x2, x3), Unsteady_Mass(x1, x2 + 1, x3))
            'Energy balance depends on the vapour moisture content at the surface (saturated vapour pressure)
            Unsteady_Temp(x1 + 1, x2, x3) = VerticSurface_h(x2, Unsteady_Temp(x1, x2 - 1, x3), Unsteady_Temp(x1, x2, x3 -
1), Unsteady_Temp(x1, x2, x3), Unsteady_Temp(x1, x2 + 1, x3), SurfaceVapour(Unsteady_Temp(x1, x2, x3)))

        ElseIf x2 = Nr And x3 = 1 Then 'Sixth code executed while anlayzing the corner point at r = Nr, z = 0
            Unsteady_Mass(x1 + 1, x2, x3) = CentreCorner_m(x2, Unsteady_Mass(x1, x2 - 1, x3), Unsteady_Mass(x1, x2, x3 + 1
), Unsteady_Mass(x1, x2, x3))
            'Energy balance depends on the vapour moisture content at the surface (saturated vapour pressure)
            Unsteady_Temp(x1 + 1, x2, x3) = CentreCorner_h(x2, Unsteady_Temp(x1, x2 - 1, x3), Unsteady_Temp(x1, x2, x3 + 1
), Unsteady_Temp(x1, x2, x3), SurfaceVapour(Unsteady_Temp(x1, x2, x3)))

        ElseIf x2 = Nr And x3 > 1 And x3 < Nl Then 'Seventh code executed while analyzing the centre axis (r = Nr) along z
 space
            Unsteady_Mass(x1 + 1, x2, x3) = HorizonSurface_m(x2, Unsteady_Mass(x1, x2 - 1, x3), Unsteady_Mass(x1, x2, x3 -

 1), Unsteady_Mass(x1, x2, x3), Unsteady_Mass(x1, x2, x3 + 1))
            'Energy balance depends on the vapour moisture content at the surface (saturated vapour pressure)
            Unsteady_Temp(x1 + 1, x2, x3) = HorizonSurface_h(x2, Unsteady_Temp(x1, x2 - 1, x3), Unsteady_Temp(x1, x2, x3 -
 1), Unsteady_Temp(x1, x2, x3), Unsteady_Temp(x1, x2, x3 + 1), SurfaceVapour(Unsteady_Temp(x1, x2, x3)))

        ElseIf x2 = Nr And x3 = Nl Then 'Eighth code executed while anlayzing the corner point at r = Nr, z = Nl
            Unsteady_Mass(x1 + 1, x2, x3) = CornerSurface_m(x2, Unsteady_Mass(x1, x2 - 1, x3), Unsteady_Mass(x1, x2, x3 -
1), Unsteady_Mass(x1, x2, x3))
            'Energy balance depends on the vapour moisture content at the surface (saturated vapour pressure)
            Unsteady_Temp(x1 + 1, x2, x3) = CornerSurface_h(x2, Unsteady_Temp(x1, x2 - 1, x3), Unsteady_Temp(x1, x2, x3 -
1), Unsteady_Temp(x1, x2, x3), SurfaceVapour(Unsteady_Temp(x1, x2, x3)))

        ElseIf x2 > 1 And x2 < Nr And x3 > 1 And x3 < Nl Then 'Ninth code executed while analyzing all the intermediate po
ints between the surface and the centre
            Unsteady_Mass(x1 + 1, x2, x3) = PelletInterior(lambda_m, x2, Unsteady_Mass(x1, x2 - 1, x3), Unsteady_Mass(x1,
x2, x3 - 1), Unsteady_Mass(x1, x2, x3), Unsteady_Mass(x1, x2 + 1, x3), Unsteady_Mass(x1, x2, x3 + 1))
            Unsteady_Temp(x1 + 1, x2, x3) = PelletInterior(lambda_h, x2, Unsteady_Temp(x1, x2 - 1, x3), Unsteady_Temp(x1,
x2, x3 - 1), Unsteady_Temp(x1, x2, x3), Unsteady_Temp(x1, x2 + 1, x3), Unsteady_Temp(x1, x2, x3 + 1))

        End If

        Next x3
    Next x2

'   Used to print the quarter cylinder data for Temperature or Mass Changes
'    For x3 = 1 To Nl
'        For x2 = 1 To Nr
'            Worksheets("Data Print").Cells(x2, x3) = Unsteady_Temp(x1, x2, x3)
'        Next x2
'    Next x3

Next x1

'End of the condition for chekcing for stability
End If
```

E.5.1. Print Unsteady State

E.5.1.1. Midpoint Method for Numerical Integration

```
'Code to calculate the median values in cylindrical coordinates for a select number of data points
For x1 = 1 To ((Nt + 599) / 600) '2 s interval uses 299, 300
    For x2 = 1 To Nr - 1
        For x3 = 1 To Nl - 1

            If x1 = 22 Then
                Average_Mass(x1, x2, x3) = WorksheetFunction.Median(Unsteady_Mass(12661, x2, x3), Unsteady_Mass(12661, x2,
 x3 + 1), Unsteady_Mass(12661, x2 + 1, x3), Unsteady_Mass(12661, x2 + 1, x3 + 1))
            ElseIf x1 = 40 Then
                Average_Mass(x1, x2, x3) = WorksheetFunction.Median(Unsteady_Mass(23521, x2, x3), Unsteady_Mass(23521, x2,
 x3 + 1), Unsteady_Mass(23521, x2 + 1, x3), Unsteady_Mass(23521, x2 + 1, x3 + 1))
            Else
                Average_Mass(x1, x2, x3) = WorksheetFunction.Median(Unsteady_Mass(600 * x1 - 599, x2, x3), Unsteady_Mass(6
00 * x1 - 599, x2, x3 + 1), Unsteady_Mass(600 * x1 - 599, x2 + 1, x3), Unsteady_Mass(600 * x1 - 599, x2 + 1, x3 + 1))
            End If

        Next x3
    Next x2
Next x1
```

E.5.1.2. Cylindrical Coordinate Average

```
'Code to calculate the average in cylindrical coordinates for a select number of data points
Dim midpoint As Double, temp_sum As Double

For x1 = 1 To ((Nt + 599) / 600) '2 s interval uses 299, 300

    midpoint = 0
    temp_sum = 0

    For x2 = 1 To Nr - 1
        For x3 = 1 To Nl - 1

            midpoint = space_step * WorksheetFunction.Average(x2 - 1, x2)
            temp_sum = temp_sum + Average_Mass(x1, x2, x3) * midpoint * (space_step) ^ 2

        Next x3
    Next x2

    'Code to print a select number of data points to manage against the experimental data
    If x1 = 22 Then
        Worksheets("Data Print").Cells(x1 + 1, 1) = 211
    ElseIf x1 = 40 Then
        Worksheets("Data Print").Cells(x1 + 1, 1) = 392
    Else
        Worksheets("Data Print").Cells(x1 + 1, 1) = 10 * (x1 - 1)
    End If

    Worksheets("Data Print").Cells(x1 + 1, 2) = 2 * temp_sum / ((100 * Worksheets("Numerical Mass").Cells(4, 3) / 2) ^ 2 *
 (100 * Worksheets("Numerical Mass").Cells(5, 3) / 2))

Next x1
```

E.5.1.3 Printing the Temperature Data

```
'Worksheets("Data Print").Cells(1, 1) = Unsteady_Mass(Nt, 1, 1)

'Code to print a select number of temperature data points to manage against the experimental data
For x1 = 1 To ((Nt + 599) / 600) '2 s interval uses 299, 300

    If x1 < 22 Then '2 s interval uses 29, 30

    Worksheets("Data Print").Cells(x1 + 1, 3) = (x1 - 1)
    Worksheets("Data Print").Cells(x1 + 1, 4) = Unsteady_Temp(60 * x1 - 59, 2, 3)

    ElseIf x1 < 44 Then '2 s interval uses 540, 10619

    Worksheets("Data Print").Cells(x1 + 1, 3) = 18 * x1 - 354
    Worksheets("Data Print").Cells(x1 + 1, 4) = Unsteady_Temp(1080 * x1 - 21239, 2, 3)

    End If

Next x1

End Sub
```

E.6.1. User Defined Functions

E.6.1.1. Antoine Equation Solver

```
'Development of the heat balance that accounts for temperature drop on evaporation
Function SurfaceVapour(ow1 As Variant) As Double

    'Parameters used for the Antoine Equation for Water Vapour
    Dim A_h2o As Double, B_h2o As Double, C_h2o As Double, Ts As Double, Psat As Double

    'Converting solid surface temperature to Kelvin
    Ts = ow1 + 273.15 'K

    'Initializing variables for the Antoine equation with water as the fluid
    A_h2o = 6.20963
    B_h2o = 2354.731
    C_h2o = 7.559

    Psat = 10 ^ (A_h2o - (B_h2o / (Ts + C_h2o))) 'Calculating the vapour pressure at the surface
    C_h2o = (Worksheets("Summary").Cells(6, 3) * Psat) / (Worksheets("Summary").Cells(9, 3) * 0.083144598 * Ts) 'kg/kg
    SurfaceVapour = C_h2o / (1 - C_h2o) 'kg/kg

End Function
```

E.6.1.2. Pellet Centre

```
'All of the mass and heat transfer functions
Function PelletCentre(lambda As Double, ow1 As Variant, ow2 As Variant, ow3 As Variant) As Double

    PelletCentre = (2 * lambda * ow1) + (2 * lambda * ow2) + ((1 - 4 * lambda) * ow3)

        'M_north = 2 * lambda * Unsteady_Mass(x1, x2 + 1, x3)
        'M_east = 2 * lambda * Unsteady_Mass(x1, x2, x3 + 1)
        'M_cent = (1 - 4 * lambda) * Unsteady_Mass(x1, x2, x3)

End Function
```

E.6.1.3. Horizon Centre

```
Function HorizonCentre(lambda As Double, ow1 As Variant, ow2 As Variant, ow3 As Variant, ow4 As Variant) As Double

    HorizonCentre = (2 * lambda * ow1) + ((1 - 4 * lambda) * ow2) + (lambda * ow3) + (lambda * ow4)

        'M_north = 2 * lambda * Unsteady_Mass(x1, x2 + 1, x3)
        'M_cent = (1 - 4 * lambda) * Unsteady_Mass(x1, x2, x3)
        'M_west = lambda * Unsteady_Mass(x1, x2, x3 - 1)
        'M_east = lambda * Unsteady_Mass(x1, x2, x3 + 1)

End Function
```

E.6.1.4. Centre Surface M

```
'Has two definitions
Function CentreSurface_m(ow1 As Variant, ow2 As Variant, ow3 As Variant) As Double

    Dim DMT As Double
    DMT = 2 * lambda_m * space_step * kc / Dab
    CentreSurface_m = (2 * lambda_m * ow1) + (2 * lambda_m * ow2) + ((1 - (4 * lambda_m) - DMT) * ow3) + (DMT * M_infinite
)

        'M_north = 2 * lambda_m * Unsteady_Mass(x1, x2 + 1, x3)
        'M_west = 2 * lambda_m * Unsteady_Mass(x1, x2, x3 - 1)
        'M_cent = (1 - (4 * lambda_m) - (2 * lambda_m * space_step * kc / Dab)) * Unsteady_Mass(x1, x2, x3)
        'M_east = (2 * lambda_m * space_step * kc / Dab) * M_infinite

End Function
```

E.6.1.5. Vertic Centre

```
Function VerticCentre(lambda As Double, x2 As Integer, ow1 As Variant, ow2 As Variant, ow3 As Variant, ow4 As Variant) As
Double

    Dim space_x1 As Double, space_x2 As Double
    space_x1 = 1 - (1 / (2 * (x2 - 1)))
    space_x2 = 1 + (1 / (2 * (x2 - 1)))
    VerticCentre = (lambda * space_x1 * ow1) + ((1 - 4 * lambda) * ow2) + (lambda * space_x2 * ow3) + (2 * lambda * ow4)

        'M_south = lambda * (1 - (1 / (2 * (x2 - 1)))) * Unsteady_Mass(x1, x2 - 1, x3)
        'M_cent = (1 - 4 * lambda) * Unsteady_Mass(x1, x2, x3)
        'M_north = lambda * (1 + (1 / (2 * (x2 - 1)))) * Unsteady_Mass(x1, x2 + 1, x3)
        'M_east = 2 * lambda * Unsteady_Mass(x1, x2, x3 + 1)

End Function
```

E.6.1.6. Vertic Surface M

```
'Has two definitions
Function VerticSurface_m(x2 As Integer, ow1 As Variant, ow2 As Variant, ow3 As Variant, ow4 As Variant) As Double

    Dim space_x1 As Double, space_x2 As Double, DMT As Double
    space_x1 = 1 - (1 / (2 * (x2 - 1)))
    space_x2 = 1 + (1 / (2 * (x2 - 1)))
    DMT = 2 * lambda_m * space_step * kc / Dab
    VerticSurface_m = (lambda_m * space_x1 * ow1) + (2 * lambda_m * ow2) + ((1 - (4 * lambda_m) - DMT) * ow3) + (lambda_m
* space_x2 * ow4) + (DMT * M_infinite)

        'M_south = lambda_m * (1 - (1 / (2 * (x2 - 1)))) * Unsteady_Mass(x1, x2 - 1, x3)
        'M_west = 2 * lambda_m * Unsteady_Mass(x1, x2, x3 - 1)
        'M_cent = (1 - (4 * lambda_m) - (2 * lambda_m * space_step * kc / Dab)) * Unsteady_Mass(x1, x2, x3)
        'M_east = (2 * lambda_m * space_step * kc / Dab) * M_infinite
        'M_north = lambda_m * (1 + (1 / (2 * (x2 - 1)))) * Unsteady_Mass(x1, x2 + 1, x3)

End Function
```

E.6.1.7. Centre Corner M

```
'Has two definitions
Function CentreCorner_m(x2 As Integer, ow1 As Variant, ow2 As Variant, ow3 As Variant) As Double

    Dim space_x2 As Double, DMT As Double
    space_x2 = 1 + (1 / (2 * (x2 - 1)))
    DMT = 2 * lambda_m * space_step * kc / Dab
    CentreCorner_m = (2 * lambda_m * ow1) + (2 * lambda_m * ow2) + ((1 - (4 * lambda_m) - (space_x2 * DMT)) * ow3) + (spac
e_x2 * DMT * M_infinite)

        'M_south = 2 * lambda_m * Unsteady_Mass(x1, x2 - 1, x3)
        'M_east = 2 * lambda_m * Unsteady_Mass(x1, x2, x3 + 1)
        'M_cent = (1 - (4 * lambda_m) - (1 + (1 / (2 * (x2 - 1)))) * (2 * lambda_m * space_step * kc / Dab)) * Unsteady_Ma
ss(x1, x2, x3)
        'M_north = lambda_m * ((1 + 1 / (2 * (x2 - 1))) * 2 * space_step * kc / Dab) * M_infinite

End Function
```

E.6.1.8. Horizon Surface M

```
'Has two definitions
Function HorizonSurface_m(x2 As Integer, ow1 As Variant, ow2 As Variant, ow3 As Variant, ow4 As Variant) As Double

    Dim space_x2 As Double, DMT As Double
    space_x2 = 1 + (1 / (2 * (x2 - 1)))
    DMT = 2 * lambda_m * space_step * kc / Dab
    HorizonSurface_m = (2 * lambda_m * ow1) + (lambda_m * ow2) + ((1 - (4 * lambda_m) - (space_x2 * DMT)) * ow3) + (space_
x2 * DMT * M_infinite) + (lambda_m * ow4)

        'M_south = 2 * lambda_m * Unsteady_Mass(x1, x2 - 1, x3)
        'M_west = lambda_m * Unsteady_Mass(x1, x2, x3 - 1)
        'M_cent = (1 - (4 * lambda_m) - (1 + (1 / (2 * (x2 - 1)))) * (2 * lambda_m * space_step * kc / Dab)) * Unsteady_Ma
ss(x1, x2, x3)
        'M_north = (2 * lambda_m * space_step * kc / Dab) * (1 + (1 / (2 * (x2 - 1)))) * M_infinite
        'M_east = lambda_m * Unsteady_Mass(x1, x2, x3 + 1)

End Function
```

E.6.1.9. Corner Surface M

```
'Has two definitions
Function CornerSurface_m(x2 As Integer, ow1 As Variant, ow2 As Variant, ow3 As Variant) As Double

    Dim space_x3 As Double, DMT As Double
    space_x3 = 2 + (1 / (2 * (x2 - 1)))
    DMT = 2 * lambda_m * space_step * kc / Dab
    CornerSurface_m = (2 * lambda_m * ow1) + (2 * lambda_m * ow2) + (space_x3 * DMT * M_infinite) + ((1 - (4 * lambda_m) -
 (space_x3 * DMT)) * ow3)

        'M_south = 2 * lambda_m * Unsteady_Mass(x1, x2 - 1, x3)
        'M_west = 2 * lambda_m * Unsteady_Mass(x1, x2, x3 - 1)
        'M_north = (2 * lambda_m * space_step * kc / Dab) * (2 + (1 / (2 * (x2 - 1)))) * M_infinite
        'M_cent = (1 - 4 * lambda_m - (2 * lambda_m * space_step * kc / Dab) * (2 + 1 / (2 * (x2 - 1)))) * Unsteady_Mass(x
1, x2, x3)

End Function
```

E.6.1.10. Pellet Interior

```
Function PelletInterior(lambda As Double, x2 As Integer, ow1 As Variant, ow2 As Variant, ow3 As Variant, ow4 As Variant, o
w5 As Variant) As Double

    Dim space_x1 As Double, space_x2 As Double
    space_x1 = 1 - (1 / (2 * (x2 - 1)))
    space_x2 = 1 + (1 / (2 * (x2 - 1)))
    PelletInterior = (space_x1 * lambda * ow1) + (lambda * ow2) + ((1 - 4 * lambda) * ow3) + (space_x2 * lambda * ow4) + (
lambda * ow5)

        'M_south = lambda * (1 - (1 / (2 * (x2 - 1)))) * Unsteady_Mass(x1, x2 - 1, x3)
        'M_west = lambda * Unsteady_Mass(x1, x2, x3 - 1)
        'M_cent = (1 - 4 * lambda) * Unsteady_Mass(x1, x2, x3)
        'M_north = lambda * (1 + (1 / (2 * (x2 - 1)))) * Unsteady_Mass(x1, x2 + 1, x3)
        'M_east = lambda * Unsteady_Mass(x1, x2, x3 + 1)

End Function
```

E.6.1.11. Centre Surface H

```
'Has two definitions
'Function CentreSurface_h(ow1 As Variant, ow2 As Variant, ow3 As Variant) As Double
Function CentreSurface_h(ow1 As Variant, ow2 As Variant, ow3 As Variant, ow4 As Variant) As Double

    Dim DMT As Double, evap As Double
    DMT = 2 * lambda_h * space_step * h / k
    evap = 2 * lambda_h * Delta_H * density * space_step * kc / k
    CentreSurface_h = (2 * lambda_h * ow1) + (2 * lambda_h * ow2) + ((1 - (4 * lambda_h) - DMT) * ow3) + (DMT * T_infinite
) + (evap * (M_infinite - ow4))

        'T_north = 2 * lambda_h * Unsteady_Temp(x1, x2 + 1, x3)
        'T_west = 2 * lambda_h * Unsteady_Temp(x1, x2, x3 - 1)
        'T_cent = (1 - (4 * lambda_h) - (2 * lambda_h * space_step * h / k)) * Unsteady_Temp(x1, x2, x3)
        'T_east = (2 * lambda_h * space_step * h / k) * T_infinite

End Function
```

E.6.1.12. Vertic Surface H

```
'Has two definitions
'Function VerticSurface_h(x2 As Integer, ow1 As Variant, ow2 As Variant, ow3 As Variant, ow4 As Variant) As Double
Function VerticSurface_h(x2 As Integer, ow1 As Variant, ow2 As Variant, ow3 As Variant, ow4 As Variant, ow5 As Variant) As
 Double

    Dim space_x1 As Double, space_x2 As Double, DMT As Double, evap As Double
    space_x1 = 1 - (1 / (2 * (x2 - 1)))
    space_x2 = 1 + (1 / (2 * (x2 - 1)))
    DMT = 2 * lambda_h * space_step * h / k
    evap = 2 * lambda_h * Delta_H * density * space_step * kc / k
    VerticSurface_h = (lambda_h * space_x1 * ow1) + (2 * lambda_h * ow2) + ((1 - (4 * lambda_h) - DMT) * ow3) + (lambda_h
* space_x2 * ow4) + (DMT * T_infinite) + (evap * (M_infinite - ow5))

        'T_south = lambda_h * (1 - (1 / (2 * (x2 - 1)))) * Unsteady_Temp(x1, x2 - 1, x3)
        'T_west = 2 * lambda_h * Unsteady_Temp(x1, x2, x3 - 1)
        'T_cent = (1 - (4 * lambda_h) - (2 * lambda_h * space_step * h / k)) * Unsteady_Temp(x1, x2, x3)
        'T_east = (2 * lambda_h * space_step * h / k) * T_infinite
        'T_north = lambda_h * (1 + (1 / (2 * (x2 - 1)))) * Unsteady_Temp(x1, x2 + 1, x3)

End Function
```

E.6.1.13. Centre Corner H

```
'Has two definitions
'Function CentreCorner_h(x2 As Integer, ow1 As Variant, ow2 As Variant, ow3 As Variant) As Double
Function CentreCorner_h(x2 As Integer, ow1 As Variant, ow2 As Variant, ow3 As Variant, ow4 As Variant) As Double

    Dim space_x2 As Double, DMT As Double, evap As Double
    space_x2 = 1 + (1 / (2 * (x2 - 1)))
    DMT = 2 * lambda_h * space_step * h / k
    evap = 2 * lambda_h * Delta_H * density * space_step * kc / k
    CentreCorner_h = (2 * lambda_h * ow1) + (2 * lambda_h * ow2) + ((1 - (4 * lambda_h) - (space_x2 * DMT)) * ow3) + (spac
e_x2 * DMT * T_infinite) + (space_x2 * evap * (M_infinite - ow4))

        'T_south = 2 * lambda_h * Unsteady_Temp(x1, x2 - 1, x3)
        'T_east = 2 * lambda_h * Unsteady_Temp(x1, x2, x3 + 1)
        'T_cent = (1 - (4 * lambda_h) - (1 + (1 / (2 * (x2 - 1)))) * (2 * lambda_h * space_step * h / k)) * Unsteady_Temp(
x1, x2, x3)
        'T_north = lambda_h * ((1 + 1 / (2 * (x2 - 1))) * 2 * space_step * h / k) * T_infinite

End Function
```

E.6.1.14. Horizon Surface H

```
'Has two definitions
'Function HorizonSurface_h(x2 As Integer, ow1 As Variant, ow2 As Variant, ow3 As Variant, ow4 As Variant) As Double
Function HorizonSurface_h(x2 As Integer, ow1 As Variant, ow2 As Variant, ow3 As Variant, ow4 As Variant, ow5 As Variant) A
s Double

    Dim space_x2 As Double, DMT As Double, evap As Double
    space_x2 = 1 + (1 / (2 * (x2 - 1)))
    DMT = 2 * lambda_h * space_step * h / k
    evap = 2 * lambda_h * Delta_H * density * space_step * kc / k
    HorizonSurface_h = (2 * lambda_h * ow1) + (lambda_h * ow2) + ((1 - (4 * lambda_h) - (space_x2 * DMT)) * ow3) + (space_
x2 * DMT * T_infinite) + (lambda_h * ow4) + (space_x2 * evap * (M_infinite - ow5))

        'T_south = 2 * lambda_h * Unsteady_Temp(x1, x2 - 1, x3)
        'T_west = lambda_h * Unsteady_Temp(x1, x2, x3 - 1)
        'T_cent = (1 - (4 * lambda_h) - (1 + (1 / (2 * (x2 - 1)))) * (2 * lambda_h * space_step * h / k)) * Unsteady_Temp(
x1, x2, x3)
        'T_north = (2 * lambda_h * space_step * kc / Dab) * (1 + (1 / (2 * (x2 - 1)))) * T_infinite
        'T_east = lambda_h * Unsteady_Temp(x1, x2, x3 + 1)

End Function
```

E.6.1.15. Corner Surface H

```
'Has two definitions
'Function CornerSurface_h(x2 As Integer, ow1 As Variant, ow2 As Variant, ow3 As Variant) As Double
Function CornerSurface_h(x2 As Integer, ow1 As Variant, ow2 As Variant, ow3 As Variant, ow4 As Variant) As Double

    Dim space_x3 As Double, DMT As Double, evap As Double
    space_x3 = 2 + (1 / (2 * (x2 - 1)))
    DMT = 2 * lambda_h * space_step * h / k
    evap = 2 * lambda_h * Delta_H * density * space_step * kc / k
    CornerSurface_h = (2 * lambda_h * ow1) + (2 * lambda_h * ow2) + (space_x3 * DMT * T_infinite) + ((1 - (4 * lambda_h) -
 (space_x3 * DMT)) * ow3) + (space_x3 * evap * (M_infinite - ow4))

        'T_south = 2 * lambda_h * Unsteady_Temp(x1, x2 - 1, x3)
        'T_west = 2 * lambda_h * Unsteady_Temp(x1, x2, x3 - 1)
        'T_north = (2 * lambda_h * space_step * kc / Dab) * (2 + (1 / (2 * (x2 - 1)))) * T_infinite
        'T_cent = (1 - 4 * lambda_h - (2 * lambda_h * space_step * h / k) * (2 + 1 / (2 * (x2 - 1)))) * Unsteady_Temp(x1,
x2, x3)

End Function
```